Nanoscale Horizons

ROYAL SOCIETY OF CHEMISTRY

REVIEW

View Article Online
View Journal | View Issue

Cite this: *Nanoscale Horiz.*, 2024, **9**, 1432

Multi-metallic MOF based composites for environmental applications: synergizing metal centers and interactions

Wei Wang,[a] Bergoi Ibarlucea,[ab] Chuanhui Huang,[c] Renhao Dong,[c] Muhannad Al Aiti,*[ad] Shirong Huang*[a] and Gianaurelio Cuniberti*[a]

The escalating threat of environmental issues to both nature and humanity over the past two decades underscores the urgency of addressing environmental pollutants. Metal–organic frameworks (MOFs) have emerged as highly promising materials for tackling these challenges. Since their rise in popularity, extensive research has been conducted on MOFs, spanning from design and synthesis to a wide array of applications, such as environmental remediation, gas storage and separation, catalysis, sensors, biomedical and drug delivery systems, energy storage and conversion, and optoelectronic devices, *etc.* MOFs possess a multitude of advantageous properties such as large specific surface area, tunable porosity, diverse pore structures, multi-channel design, and molecular sieve capabilities, *etc.*, making them particularly attractive for environmental applications. MOF-based composites inherit the excellent properties of MOFs and also exhibit unique physicochemical properties and structures. The tailoring of central coordinated metal ions in MOFs is critical for their adaptability in environmental applications. Although many reviews on monometallic, bimetallic, and polymetallic MOFs have been published, few reviews focusing on MOF-based composites with monometallic, bimetallic, and multi-metallic centers in the context of environmental pollutant treatment have been reported. This review addresses this gap by providing an in-depth overview of the recent progress in MOF-based composites, emphasizing their applications in hazardous gas sensing, electromagnetic wave absorption (EMWA), and pollutant degradation in both aqueous and atmospheric environments and highlighting the importance of the number and type of metal centers present. Additionally, the various categories of MOFs are summarized. MOF-based composites demonstrate significant promise in addressing environmental challenges, and this review provides a clear and valuable perspective on their potential in environmental applications.

Received 1st April 2024,
Accepted 3rd July 2024

DOI: 10.1039/d4nh00140k

rsc.li/nanoscale-horizons

1. Introduction

Environmental issues, including massive emissions of hazardous gases and sewage, harmful electromagnetic wave pollution, as well as water pollution issues have become increasingly severe, with advancing human activity. One of the most effective and reliable solutions for the disposal of environmental pollutants at present is materials technology. In the past decades, various types of nanomaterials have been explored and applied. However, an unsatisfying fact is that new materials are obtained after a long period of exploration, although it is undeniable that they can effectively solve some problems. However, as the problems become more complicated, the material obviously encounters its own bottleneck. This result leads to prolongation of the materials research. Repeatedly, the efficiency of solving problems has been greatly reduced. Therefore, multifunctional, versatile materials attracted a great deal of interests in addressing environmental issues.

The materials in question for detection, absorption and degradation of pollutants in both aqueous and atmospheric environments will provide a platform, where pollutant molecules can be detected and they will interact with each other on the surface activated sites to be further absorbed and degraded. The abundant activated sites originated from a large specific surface area, and extra electrons and holes come from

[a] *Institute for Materials Science and Max Bergmann Center for Biomaterials, TUD Dresden University of Technology, Dresden, 01062, Germany. E-mail: muhannad.al_aiti@tu-dresden.de, shirong.huang@tu-dresden.de, gianaurelio.cuniberti@tu-dresden.de*
[b] *TECNALIA, Basque Research and Technology Alliance (BRTA), Donostia-San Sebastian, 20009, Spain*
[c] *Center for Advancing Electronics Dresden & Faculty of Chemistry and Food Chemistry, TUD Dresden University of Technology, Mommsenstrasse 4, 01062 Dresden, Germany*
[d] *Dresden Center for Nanoanalysis, Technische Universität Dresden, 01062 Dresden, Germany*

heterogeneous atoms, heterogeneous interfaces and defects. Additionally, the porous structure of the material, good electrical conductivity, magnetic properties and the matching characteristics of the two are critical for dealing with electromagnetic pollution. Among other electromagnetic wave absorbing (EMWA) materials that are still widely applied so far carbonyl iron and graphene may be found. The former shows high magnetic permeability, but the disadvantages such as single loss mechanism, narrow absorption frequency band, and weak absorption performance limit its further value. Moreover, the latter exhibits excellent conductivity characteristics, its poor impedance matching characteristics and high filling degree also limit its application.[1,2] TiO_2 was first used in photocatalysis to degrade refractory organic pollutants and heavy metal ions,[3,4] but TiO_2 itself has an extremely low utilization rate of sunlight, that is, it can only absorb and utilize UV which accounts for only 5% of sunlight. It is powerless to nearly 45% of visible light. Until the multifunctional materials with multiple unique advantages emerge, metal organic frameworks (MOFs), as potential multifunctional materials, greatly improve the efficiency of material exploration and shows endless possibilities.

MOFs are a class of crystalline porous coordination polymers consisting of metal ions or clusters and organic ligands. However, in the past, there has been a lack of generally accepted definition of the hybrid assembly of anionic polymers and cationic clusters.[5–14] A consensus was reached when the work of Hoskins and Robson on MOFs was reported in 1990, which marks a new beginning in their study.[15] Yaghi's group[16] synthesized and characterized MOF-5 in a groundbreaking work, in which 1,4-benzenedicarboxylate (BDC) as a ligand and Zn^{2+} as a metallic ion were used being to date the most investigated MOF material. This work is groundbreaking in terms of MOF. MOFs play an important role and value as a new functional material system in many fields.[17–27] Due to their structural assembly, they show unique structural advantages, such as being multi-space, multi-components, multi-morphological and tailorable, which endow MOFs many characteristics, including high specific surface area, open metal site, high porosity and structural diversity. Consequentially, MOF-based composites inherit the excellent properties of MOFs, but also exhibit different physicochemical properties and structures.

Over the last two decades, MOF-based composites have shown continuous popularity in environmental applications (Fig. 1). A substantial body of research on MOF-based composites has yielded promising outcomes in addressing environmental concerns.[28–46] MOF-based composites possess promising porosity, pore size, specific surface area, microstructure, redox properties, and polarity to exhibit excellent hazardous gas sensing.[47–65] Large specific surface area from MOF-based composites provides rich reaction sites and strong light absorption and utilization rate, leading to remarkable effects in photocatalytic degradation of hazardous gases[66–70] and water remediation.[71–75] In the meantime, the porous structure derived from organic linkers, the good electrical conductivity,

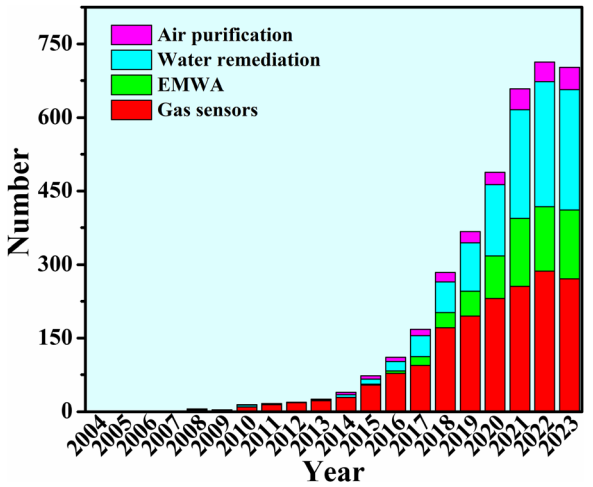

Fig. 1 Number of published papers of MOF-based composites from 2004 to 2023 for gas sensing (red), EMWA (green), water remediation (blue) and air purification (pink) (Web of science, search keywords: metal organic framework, electromagnetic wave absorption, microwave absorption; gas sensor; water remediation; air purification.).

the magnetic properties provided by the magnetic metal from the metal center, and the electromagnetic matching properties that can be tailored, have become the advantages of MOF-based composites in EMWA.[18,76–79] So far, there have been various reviews in terms of environmental applications.[80–90]

Bimetallic MOFs and their derivatives with special emphases on their preparation and applications were reported.[91,92] These works focused on synthetic strategies, and the development of bimetallic MOFs and their derivatives for a variety of applications, summarizing the findings on the influence of polymetallic ions on MOFs, highlighting the challenges associated with their compatibility, and focusing on the techniques employed for the synthesis and characterization of polymetallic MOFs. Additionally, the review about the state-of-the-art on bimetallic MOFs and derived composites for the main current types of electro- and photoelectroncatalytic applications was reported.[93] Uniquely, the review about mixed-metal metal–organic frameworks was reported to focus on synthetic approaches, characterization techniques, computational techniques, catalysis, and gas adsorption and separation applications.[94] Furthermore, numerous related reviews have been published, each summarizing the development and various applications of MOF-based materials from diverse perspectives. These reviews are integral to advancing the field.[95,96] However, few reviews provide a comprehensive overview in treatment of environmental pollutants: (a) monometallic, bimetallic, and multi-metallic MOF-based composites; (b) focusing on various effects on different central metal types for MOF-based composites; (c) as sensing materials for hazardous gas detection, as absorber deals with EMW pollution, as photocatalysts degrade pollutant molecules both in aqueous and atmospheric environments.

In this review, we aim to comb the recent progress in MOF-based composites characterized by monometallic, bimetallic,

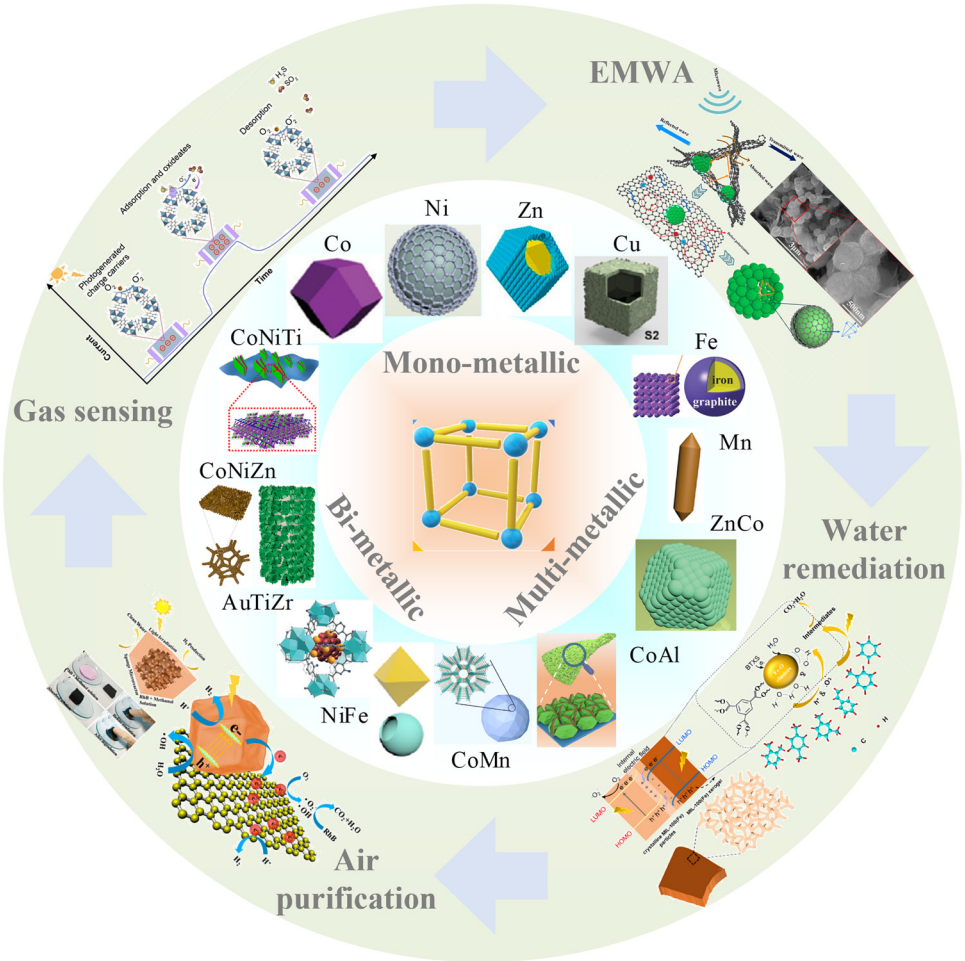

Scheme 1 Schematic diagram of the applications of mono-, bi- and multi-metallic MOF-based materials in Environmental Applications. Parts of them are reproduced with permission from ref. 22, Copyright (2021) Elsevier B.V.,[70] Copyright (2021) Elsevier, Copyright (2018) American Chemical Society.[97] Copyright (2023) Wiley-VCH GmbH.

and multi-metallic centers, emphasizing their applications in the detection, absorption, and degradation of environmental pollutants. Specifically, the discussion centers on their efficacy in hazardous gases sensing, EMWA, and degradation of pollutants in both aqueous and atmospheric environments, as shown in Scheme 1. Moreover, categories of MOFs are summarized. Finally, this work systematically summarizes the effect of different metal ions centers on the characteristics of MOF-based composites, the relationship between advantages and disadvantages, and the further impact of different applications, current challenges, future opportunities, and directions in the design strategies of MOFs with different metal ions centers in the environmental fields.

2. MOF-based composites for environmental applications

In recent years, there has been a surge of interest in surrounding MOFs owing to their remarkable array of properties and versatile functionalities. MOFs are composed of two essential components: metal nodes and organic linkers. A comprehensive examination of MOFs underscores the imperative for enhancing their environmental sustainability, necessitating modifications to both metallic and organic constituents. Such enhancements may entail substitution or hybridization of these components, which means that the emergence of MOF-based composites. MOF-based composites inherit the excellent properties of MOFs, but also exhibit different physicochemical properties and structures. The structural diversity inherent in organic linkers endows MOF-based composites with a high degree of tunability, enabling the manifestation of diverse architectures with enhanced performance characteristics. Concurrently, the metal nodes play a pivotal role in applications such as hazardous gas sensing, EMWA, and photocatalysis, by facilitating customizable porous structures, favorable electrical conductivity, and serving as a source of magnetism to effectively attenuate electromagnetic waves. Furthermore, the integration of catalytically active centers within MOF-based composites serves to augment electron transfer rates and catalytic efficiency, thus bolstering their efficacy in environmental protection applications. Consequently, a thorough

exploration of strategies for enhancing the environmental compatibility of MOF-based composites, predicated upon varying central metal species, is warranted.

Presently, a myriad of environmental pollutants, both of natural origin and anthropogenic, pervade the atmosphere, infiltrate the soil, and permeate water reservoirs, posing significant risks to human health. The primary objective in mitigating these pollutants lies in their detection at ultra-low concentrations, subsequent efficient absorption, and ultimate degradation. Specifically, this following work focuses on three typical applications: the sensing of hazardous gases, the EMWA, and the degradation of pollutants within aqueous and atmospheric domains.

2.1 Sensing of hazardous gases

The pervasive presence of polluting and hazardous gases emanating from diverse sources poses a constant threat to the well-being of living organisms. These gases include ammonia (NH_3), nitrogen dioxide (NO_2), nitric oxide (NO), hydrogen sulphide (H_2S), sulphur dioxide (SO_2), carbon dioxide (CO_2), carbon monoxide (CO), and others. Beyond specific concentration thresholds in the environment, these gases are deemed lethal. For instance, an excess of 25 parts per million (ppm) of ammonia in the air can jeopardize human skin, respiratory systems, and overall health.[98] In addition, H_2S up 5 ppm has a harmful impact on the human respiratory system.[97] Concentrations of these gases ranging from 100 to 150 ppm, these gases can lead to a loss of smell. In the range of 200 to 300 ppm, the risk escalates to pulmonary edema. Further, exposure to concentrations between 500 and 700 ppm may result in loss of consciousness, while levels surpassing 700 ppm can swiftly lead to death within minutes.[99] Excess NO in air can lead to asthma and cancer.[100] Therefore, there is a need for monitoring of these gases by designed highly sensitive gas sensors.

2.1.1 Gas sensing mechanisms. Gas sensors refer to a class of devices that are used to detect the concentration of specific gases in the environment. Gas sensors typically consist of two main components: the sensing material and the transducer. The interaction of the sensing material with the target gas results in dielectric fluctuation, magnetic, optical, thermal, acoustic, colourimetric and/or gravitational properties, which can be converted into detectable signals by the transducer. Specifically, the interactions between the sensing materials and the target can be classified into two types. The first is non-covalent interactions, such as van der Waals forces, hydrogen bonding, coordination and π–π interactions. The second is covalent bonding that arises between the sensing materials and the target. The former tends to be a reversible or partially reversible process, while the latter is an irreversible process of action, but the latter offers high sensitivity and selectivity.[85] Different gas sensors work on different principles. Semiconductor gas sensors operate by leveraging the interaction between sensing materials and target gases, inducing changes in the resistance of the semiconductor material. This alteration in resistance allows for the measurement of gas concentration.[44,48,97,101,102] Electrochemical sensors, on the other hand, utilize gas-induced redox reactions within an electrochemical cell to generate a current signal, facilitating the detection of gas concentration;[103–105] optical sensors represent another category, where gases either absorb or scatter light at specific wavelengths, leading to changes in light intensity. For instance, infrared sensors utilize infrared wavelengths to detect the interaction between light and target gas molecules, providing a means to measure gas concentration.[106–109] Additionally, there are alternative sensor types such as acoustic wave sensors and electromagnetic induction sensors.[110,111]

2.1.2 As sensing materials for hazardous gas sensors. MOF-based composites stand out as an innovative class of crystalline nano-porous materials endowed with customized physical and chemical characteristics. These properties include, but are not limited to, porosity, pore size, specific surface area, microstructure, redox properties, and polarity.[49,50,56,59,61,65] MOF-based composites excel in integrating precisely tailored host–guest interactions within their porous scaffolds, making them highly promising candidate materials for gas sensing applications. While MOF materials inherently possess insulating properties owing to the regular arrangement of organic ligands obstructing the conducting path,[53–55] post-processing of MOFs results in the formation of materials with characteristics resembling graphene or metal oxide composites. This alteration significantly modifies their conductive properties, showcasing distinct structural features and surface chemistry. Importantly, this post-processing ensures the preservation of the MOFs' porous structure or may even create additional porosity. Consequently, it generates a substantial number of active sites for interactions between the target gas and MOF-based composites. Defect-like graphite or other doped variants of composites can be obtained from organic linkers, which can lead to large and electron-rich π surfaces that can interact with the target gas through van der Waals forces, charge transfer and π–π interactions. Metal oxides can be derived from metal centers featuring chemisorbed oxygen molecules on their surfaces, enabling interactions with target gases through chemical reactions associated with oxygen. Subsequently, researchers have uncovered a novel category of conductive MOF materials. Furthermore, the controllable introduction of defects, doping and functionalization adds active sites with stronger affinity and specificity to the sensing materials, which plays an invaluable role in enhancing gas selectivity and sensitivity of sensors.

Metal centers play a crucial role within MOF-based composites, attributed to the following points: (1) varied metals incorporated into MOFs result in distinct pore structures and surface properties, influencing their selectivity towards gases. (2) Parts of MOFs (such as, Fe, Co, Ni, Cu and Cr-based) exhibit commendable electrical conductivity. The selection of a specific metal profoundly impacts the electronic conductivity of MOFs, consequently influencing the sensitivity and response time of gas sensors. (3) Metals within MOFs can play a role in the adsorption and catalytic reactions of gases, a factor of significance in gas sensor applications. The selection of a specific metal can finely tune the catalytic activity of the MOF,

rendering it suitable for various gas sensing applications. (4) The stability of MOFs is influenced by the choice of metals. The formation of parts of metals with specific organic ligands enhances the stability of the MOF, enabling its utilization under more severe environmental conditions, such as high temperature or high humidity. This not only expands the range of applications but also prolongs the lifetime of the MOF.

2.1.2.1 Monometallic MOF-based composites. Monometallic MOFs are relatively simple to design and synthesize, involving only one type of metal ion, which also tends to mean that they exhibit higher stability in sensor applications. In the work of Liu *et al.*,[48] they prepared monometallic Co-MOF and monometallic Zn-MOF sensors for the accurate detection of the hazardous gas H_2S. 500 ppb of H_2S gas were detected at around 190 °C and 200 °C, respectively, and the results showed that the response was only 1.2%. Similarly another Co-based MOF, Co-PBA with a BET of only 4.0 $m^2 g^{-1}$, and a Ni-based MOF showed 3.2% and 5.9% response results for 100 ppm H_2S gas at 200 °C operation temperature.[112] Moreover, Cu-based monometallic MOFs,[64] Fe-based MOFs,[97] Zn-based MOFs[47] and In-based MOFs[57] have been investigated to deal with H_2S (as shown in Fig. 2a–f). Furthermore, Zn, Cu, Ba and Ni-based monometallic MOFs have been applied to cope with N-containing hazardous gases (NH_3, NO_2 and NO),[47,52,58,60,62,63] and it has been investigated that the sensors can be operated at room temperature to show good responsiveness. For example, CuO NPs and CuO TNFs prepared by Liu *et al.*[60] showed good response to NO_2, respectively. Especially, CuO TNFs showed a response result of 391.0% in 500 ppb concentration of NO_2. The limit of detection (LOD) was 50 ppb. attributed to its higher BET of 11.47 $m^2 g^{-1}$ compared to CuO NPs (3.64 $m^2 g^{-1}$), which is undoubtedly an attractive highlight for a wide range of applications. In contrast, Zn based MOF exhibited 51.41% response exposed to a concentration of 1 ppm at 200 °C operating temperature (Fig. 2g–i).[47] Additionally, Zr and Zn based monometallic MOFs have also been applied to detect CO_2 and SO_2 hazardous gases.[113–115] Although the Fe-based MOF, MIL-88B was tailored to modulate the structure of the MOF by the large pore (lp) phase/narrow pore (np) phase ratio by Gang Xu *et al.*,[97] and the optimized MIL-88B-20% exhibited the best sensing performance among all the reported MOF based H_2S-sensing materials (Fig. 2j–l), there are still significant limitations to achieve a breakthrough in the field of gas sensing using monometallic MOFs.

2.1.2.2 Bimetallic MOF-based composites. The design and synthesis of bimetallic MOF-based composites clearly demonstrated enhanced sensing performance in terms of improved gas uptake and selectivity as well as more precise modulation of physical properties such as porosity, surface area, *etc.* This is inextricably linked to the fact that two different metals can act synergistically to enhance the performance of MOFs. In contrast to the results observed with Zn and Co monometallic MOFs, the utilization of ZnO/Co_3O_4 as sensing materials through Zn/Co bimetallic MOFs, a structure acquired by Zn doping in Co MOF, demonstrated superior sensing performance for H_2S gas (Fig. 3a and b). Notably, it exhibited exceptional sensitivity, detecting 10 ppb H_2S gas at 120 °C. This heightened performance extended to outstanding selectivity and long-term stability, with a remarkable 95% response retention even after 45 days. The remarkable sensing capabilities of this bimetallic MOF structure are primarily ascribed to regular morphology, abundant oxygen vacancies (52.8%) and high specific surface area (96.5 $m^2 g^{-1}$).[48] The introduction of additional metal centers appears to play a crucial role in modifying the microstructure of the MOF, leading to an increase in defects and specific surface area. This, in turn, effectively enhances the efficiency of electrical signal transmission. In a parallel fashion, the strategic design of the Cu/Ni bimetallic MOF has propelled the detection of H_2S gas to new heights, notably achieving operability at room temperature. The sensor exhibits a substantial advancement, boasting a response range of 64–98% at a gas concentration of 80 ppm. Furthermore, it demonstrates an impressive sensitivity with a LOD ranging from 19–32 ppb, signifying its potential for highly sensitive gas detection applications.[64]

Tan *et al.*[117] synthesized a CoNi bimetallic MOF, from which they derived distinctive double-shelled $Co_3O_4/NiCo_2O_4$ nanocages designed for H_2S gas detection. The engineered nanocages exhibited a notable surface-to-volume ratio and a high surface area of 103 $m^2 g^{-1}$. The results demonstrated both high selectivity and a robust gas response, particularly evident in the detection of 100 ppm H_2S at the optimal temperature of 250 °C. This underscores the promising potential of the CoNi bimetallic MOF-derived nanocages for effective and sensitive H_2S gas sensing applications. Although Hussain *et al.*[118] obtained Cu/Zn bimetallic MOF sensors operating at 250 °C instead of room temperature, the response at lower gas concentrations is very high compared to the corresponding monometallic MOFs sensors[64,119] with 425%, while having a ppb level of sensitivity with LOD of 500 ppb. A parallel enhancement in performance is evident in NO_2 gas sensing, as demonstrated by Li *et al.*,[120] who employed In/Zn bimetallic MOF sensors. These sensors exhibited remarkably low LOD with results as impressive as 0.2 ppb, coupled with a substantial 185.8% response when exposed to a 1 ppm concentration of NO_2 gas. In comparison to the performance of Zn monometallic MOFs,[47] this significant improvement can be attributed to the unique molecular characteristics of In, with a diameter of 9.9 Å. Remarkably, this diameter aligns with the cavity size (11.6 Å) and pore size (3.4 Å) of ZIF-8. Consequently, the In atoms can be *in situ* trapped within the cavities of Zn MOF. The intrinsic gas permeability of the resulting hollow structure, coupled with the electronic sensitization of In metals, collectively contribute to the observed enhancement in gas sensing performance. Furthermore, bimetallic MOF sensors have found application in detecting various hazardous gases, including H_2.[65]

2.1.2.3 Multi-metallic MOF-based composites. Multi-metallic MOFs have higher structural tunability and can be powerful in gas sensing applications by selecting multiple metal ions to achieve more complex properties and enhanced metal

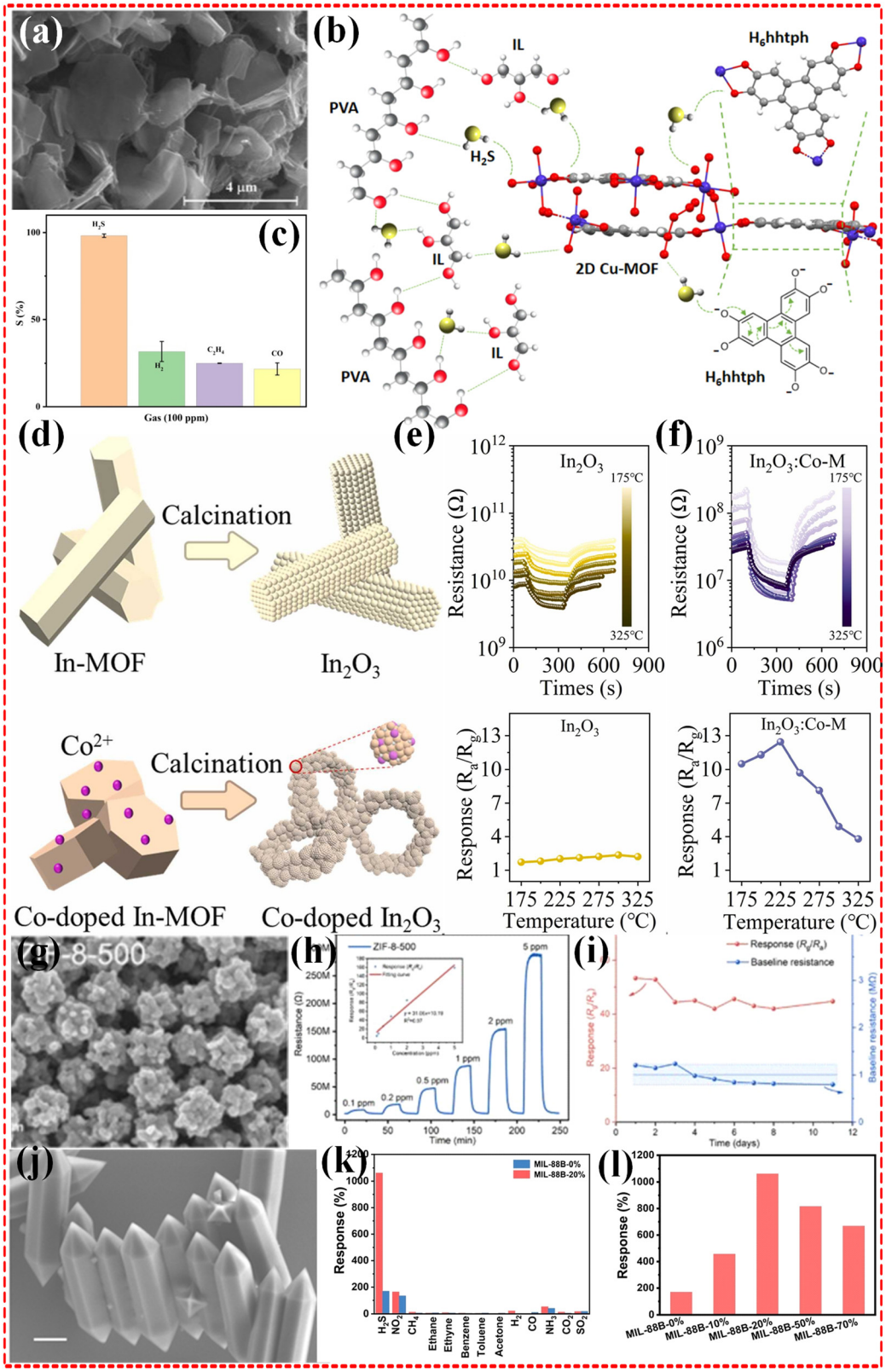

Fig. 2 (a)–(c) SEM image, selectivity and illustration of the suggested H_2S gas sensing mechanism of Cu MOF sensor. Reproduced with permission from ref. 64, Copyright (2022) the authors. (d)–(f) The schematic formation procedure of In MOF and Co/In MOF (e), transient resistance and gas responses to 2 ppm H_2S at different temperatures for In MOF (e) and Co/In MOF (f). Reproduced with permission from ref. 57, Copyright (2023) Elsevier B.V. (g)–(i) Schematic representation (g) and stability performance (h)–(i) of the as-prepared sensors. Reproduced with permission from ref. 47, Copyright (2022) Elsevier B.V. (j)–(l) SEM image (j), selectivity (k) and response (l) of as-prepared Fe-MOF. Reproduced with permission from ref. 97, Copyright (2023) Wiley-VCH GmbH.

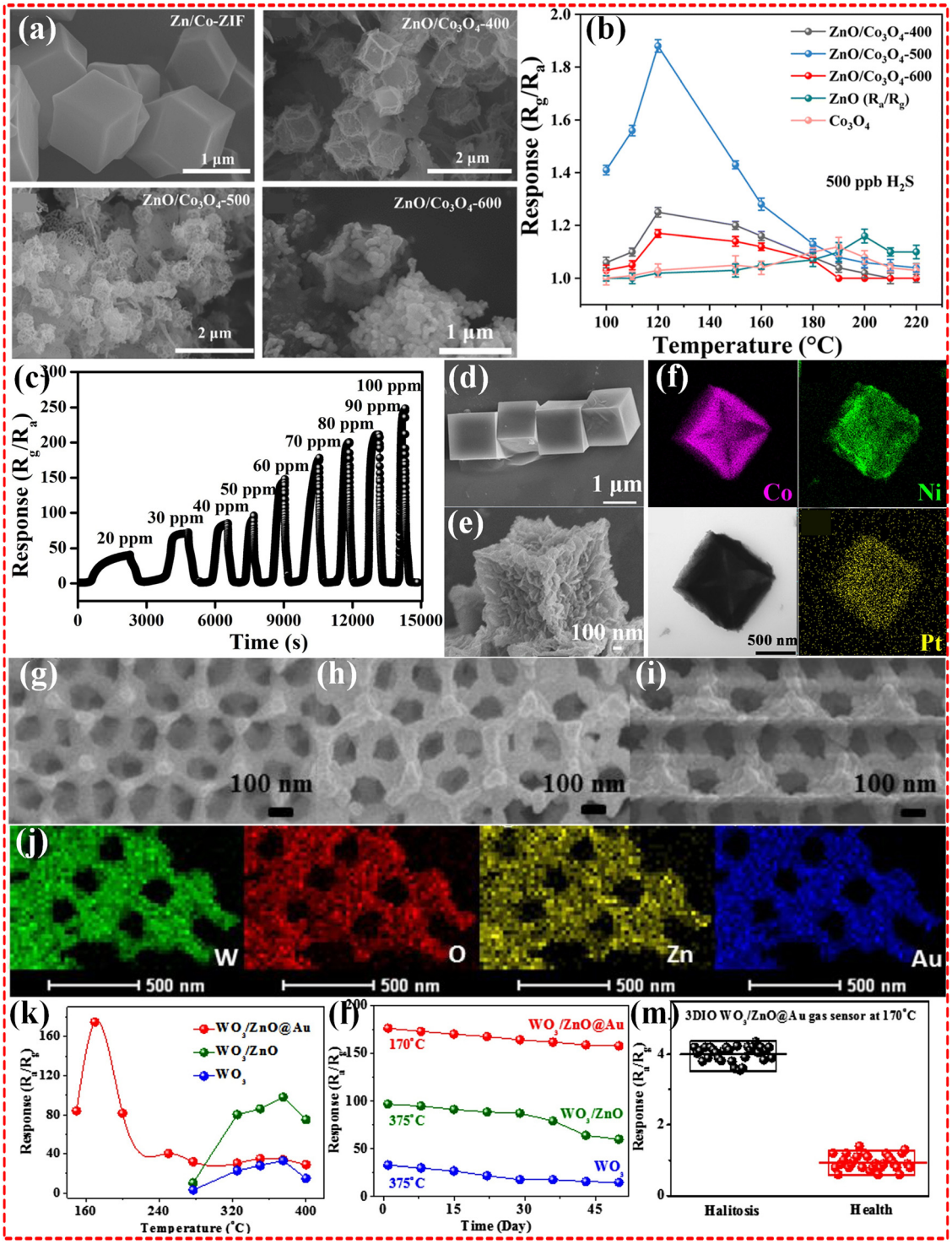

Fig. 3 (a) SEM images of the prepared all samples; (b) responses of the sensors to 500 ppb H_2S at different working temperatures. Reproduced with permission from ref. 48, Copyright (2023) Royal Society of Chemistry (RSC). (c) The concentration-dependent response curves of the sensors based on Co_3O_4@NiO-2.0@Pt3.0 microcubes towards H_2S at 200 °C; SEM images of pure Co-PBA (d), Co_3O_4@NiO-2.0 microcubes (e), elemental mapping images (f) of Co_3O_4@NiO-2.0@Pt3.0 microcubes. Reproduced with permission from ref. 112, Copyright (2021) Elsevier B.V. SEM images of W MOF (g), W/Zn MOF (h), and W/Zn/Au MOF samples (i). And the elemental mapping images of W/Zn/Au MOF sample (j). The relationship of the operating temperature and response to 10 ppm H_2S (k), the long-term stability (l) of samples. The responses to simulated H_2S abnormal breath samples and healthy breath samples of W/Zn/Au MOF sample (m). Reproduced with permission from ref. 116, Copyright (2020) Elsevier B.V.

synergies. Wang *et al.* improved the H_2S sensing performance of monometallic Co-PBA by introducing Ni metal based on their previous work,[112] but the effect is undeniably limited. Further additional introduction of Pt metal improved the response to H_2S gas by several tens of times (Fig. 3c–f). Yang *et al.*[116] synthesized Zn based MOF derived WO_3/ZnO@Au composites and employed them for H_2S gas sensing (Fig. 3g–m). The results showed that Zn/Au/W multi-metallic MOFs composites perform an outstanding gas sensing with 175% response to 10 ppm H_2S. The LOD of the sensor is 50 ppb level, and it still exhibits 8.5% response to such a low concentration of H_2S. Furthermore, the selectivity and long-term stability of Zn MOFs were validated through experimental confirmation. Notably, the incorporation of multi-heterojunctions and small-sized gold nanoparticles (NPs) efficiently encapsulated within the channels of Zn MOFs plays a crucial role in enhancing the overall sensing performance. The presence of Au or Zn atoms induces electron localization, bringing s-orbital electrons closer to O atoms. This process facilitates their combination into p-orbitals, leading to an increased negative charge on the O atoms and, consequently, enhanced absorption of H_2S gas. The introduction of small-sized Au nanoparticles serves a dual purpose: firstly, it augments surface oxygen deficiency through the ''spillover effect,'' and secondly, it effectively enhances the electrical conductivity of the MOF-derived 3DIO WO_3/ZnO@Au sensor. This dual mechanism not only improves gas absorption but also ensures superior electrical properties, collectively contributing to the heightened sensitivity and overall performance of the sensor.

A brief overview of sensing performance of mono-metallic, bi-metallic, and multi-metallic MOFs and its derivatives is reported in Table 1. It includes sensing materials, target gas, sensor condition, LOD, and response. The research work on the use of mono-metallic MOFs for the sensing of hazardous gases is widespread and promising. However, employing only one type of metal may result in relatively low selectivity, limiting the material's capability to discern and detect specific gases.

The metal ions within monometallic MOFs establish robust interactions with specific gas molecules, enhancing selectivity towards target gases. For instance, Cu-based MOFs demonstrate high sensitivity to NH_3, while Zn-based MOFs exhibit strong adsorption capacities for CO_2. The homogeneous distribution of monometallic centers within MOFs ensures consistent active sites, thereby promoting sensor repeatability and reliability. Tailoring MOFs with different monometallic ions allow for flexible adjustment of their physical and chemical properties to meet diverse gas sensing requirements. For example, Fe- and Ni-based MOFs are utilized for detecting oxygen and hydrogen, respectively.

Table 1 MOF-based composites with mono-, bi- and multi-metallic centers for hazardous gases sensing

Categories	Center metals	Sensing materials	Target gas	Sensor condition (°C)	LOD (ppm)	Response (%/ppm)	Ref.
Mono-	Zn	ZIF-8	CO_2	RT	3130	0.7 mLn min^{-1}	115
				4.85	774		
		MOF-5-NH_2	SO_2	RT	0.05	—	114
		ZIF-8/ZnO nanorod	H_2S	RT	0.05	52/10	119
		ZIF-8–500	NO_2	200	0.1	51.41/1	47
	Cu	Cu_3(HHTP)(THQ)	NH_3	RT	0.2	~15/100	52
		Cu-MOF/PVA/IL	H_2S	RT	1	99/100	64
		CuO tube-like nanofibers	NO_2	RT	0.05	391/0.5	60
		CuO NPs				12.5/0.5	
		SiO_2CuOF-graphene-PAni	NH_3	RT	0.6	—	63
	Ni	NiPc-MOF NiNPc-MOF	NH_3	RT	0.31	~50/40	58
			H_2S		0.02	100/40	
			NO		0.001	700/40	
	Y	Fum-fcu-MOF	H_2S	RT	0.1	13/10	51
	Fe	MIL-88B-20%	H_2S	RT	0.17	1061/100	97
	In	In_2O_3	H_2S	225	2	2.04	57
	Ba	Ba-MOF	NH_3	30	1	243/25	62
	Zr	UiO-66-NH_2	SO_2	RT	0.005	88.73/50	113
Bi-	Zn/Pd	ZnO/Pd	H_2	200	—	8.5/50	65
	Zn/In	In/ZnO-10	NO_2	300	0.0002	24.6/0.1	120
						185.8/1	
	Cu/Zn	CuO/ZnO	H_2S	250	0.5	425/50	118
	Cu/In	CuO/In_2O_3	H_2S	70	0.2	229.3/5	121
	Cu/Ni	NiPc-Cu	H_2S	RT	0.019–0.032	64–98/80	58
	Co/Ni	Co_3O_4/$NiCo_2O_4$	H_2S	250	30	~8/100	
	Co/In	In_2O_3:Co–M	H_2S	225	0.1	175.5/50	57
	Co/Pd	SWCNT/PdO-Co_3O_4 HNCs	NO_2	100	1	44.11/20	122
	Pt/Zn	Pt/ZnO-1 wt% 3DIO NPs	H_2S	320	0.025	11.2/1	123
	In/Mo	In_2O_3/MoS_2	NO_2	RT	0.0088	209/50	124
	Ag/Zr	(Ag_2O@UiO-66IJZr)-NO_2	H_2S	RT	1	90/100	125
Multi-	Co/Ni/Pt	Co_3O_4@NiO-2.0@Pt3.0	H_2S	200	—	250/100	112
	Zn/Au/W	WO_3/ZnO@Au	H_2S	170	0.05	175/10	116

Many monometallic MOFs possess excellent structural stability and maintain consistent sensing performance across a broad range of temperature and humidity conditions. However, their high selectivity can sometimes pose limitations by exhibiting strong responsiveness to specific gases while showing weaker responses to others, which restricts their applicability in complex gas environments. The incorporation of additional metal ions into MOFs evidently enhances their performance in sensing hazardous gases. Bimetallic MOFs harness the synergistic benefits of two distinct metal ions, enabling enhanced interactions with a diverse array of gas molecules. This synergy significantly boosts both selectivity and sensitivity towards specific gases. For instance, a combination such as Pt and Cu can offer high selectivity for gases, like CO and NH_3. The incorporation of bimetallic centers within MOFs provides multiple active sites, thereby broadening their applicability across a wide spectrum of gas detection needs. This versatility makes bimetallic MOFs particularly advantageous for use in complex gas environments. However, it is essential to acknowledge that certain bimetallic MOFs may face challenges related to structural instability arising from mismatches between the incorporated metals. This instability can impact the long-term stability of the materials, influencing their practical applications.

The synthesis of bi-metallic MOFs can be relatively intricate, demanding precise control over synthesis conditions. This complexity may, in turn, result in higher production costs. While bi-metallic MOFs offer enhanced performance through synergistic interactions between two metal ions, there are instances where these interactions may lead to interference, affecting overall MOF performance. For example, specific gas molecules may preferentially bind to one metal ion, potentially diminishing the activity of the other metal ion within the MOF structure. Although bimetallic centers generally improve structural stability, certain combinations may still encounter stability challenges under extreme conditions, impacting the long-term durability and reliability of the sensor. Therefore, careful consideration and optimization of bimetallic combinations are crucial to mitigate these potential issues and ensure consistent sensor performance over extended periods.

While we found out that there are many studies on the design and synthesis of multi-metallic MOFs,[126–139] they are very limited in hazardous gases sensing applications, which may be due to several reasons as the following: the synthesis of multi-metallic MOFs is usually more difficult than that of monometallic and bimetallic MOFs, which is mainly considered for the stability of multi-metallic MOFs, especially in high temperature or high humidity environments for gas sensing, the structural damage or inactivation of the active sites of multi-metallic MOFs will limit their sensor applications; more importantly, no study has yet been able to demonstrate that the polymetallic MOFs exhibit obvious advantages in terms of hazardous gas sensing compared to mono- and bimetallic MOFs. In consequence, easier to synthesize and structurally stable mono- and bimetallic MOFs are highly favored in the field of hazardous gas sensors.

In the context of hazardous gas sensing applications, the composition of metal ions within MOFs plays a pivotal role. The nature and quantity of these metal ions significantly influence the sensor's efficacy in detecting various hazardous gas molecules, each characterized by distinct structural and chemical properties. Consequently, it becomes imperative to carefully choose metal centers that are amenable to modification by additional metals, fostering synergistic effects. It is crucial to note that the selection of metal centers directly impacts the sensing performance of the MOF. Therefore, a judicious approach should be taken when introducing additional metal centers, aiming to achieve optimal synergies without compromising the sensor's effectiveness. In practice, efforts should be directed towards avoiding excessive introduction of extra metal centers, focusing instead on precision to ensure a substantial enhancement in sensing capabilities.

2.2 Electromagnetic wave absorbing

2.2.1 Electromagnetic pollution. Electromagnetic pollution arises from both natural and man-made sources. Natural electromagnetic pollution is typically caused by natural phenomena, such as lightning, which can result in direct damage to equipment and objects. In severe cases, lighting can generate electromagnetic interference over a broad area in the frequency range of several thousand Hz to several hundred MHz. Natural electromagnetic pollution poses a significant challenge to shortwave communications, as it can cause severe interference. While natural electromagnetic pollution is limited in its occurrence and scope, the rapid advancements in technology have led to widespread and continuous exposure to anthropogenic electromagnetic pollution. Modern technologies such as smartphones, tablets, electric cars, power converters, and navigation systems, communication networks, and electricity transmission systems emit electromagnetic radiation that exposes people to various frequencies of electromagnetic interference on a daily basis.[140–143] Anthropogenic sources of electromagnetic pollution are more extensive, stronger, more harmful, and longer-lasting than natural sources.

2.2.2 Electromagnetic waves absorption

2.2.2.1 Monometallic MOF-based composites. Metals such as Fe, Co and Ni are commonly used as metal centers for MOF materials due to their excellent magnetic and electronic properties. A classical Co-based MOF material (ZIF-67) was successfully prepared by Qin Kuang's group using 2-methylimidazole as organic linkers. The morphological structure obtained (shown in Fig. 4a and b) exhibited a wrinkled surface after annealing treatment, but the dodecahedral structure remained almost unchanged. The material showed excellent EMWA performance with a reflection loss (RL) of −35.3 dB and a thickness of 2.5 mm. The effective absorption bandwidth (EAB) (RL $\leq$ −10 dB) was 5.80 GHz (8.40–14.20 GHz).[78] The excellent EMWA performance is attributed to the synergetic effects among magnetic Co metals, the highly porous structure, and the electrical conductivity of carbon materials. However, the magnetic loss was limited due to the conversion of the surface of the strongly magnetic Co particles to CoO during exposed to

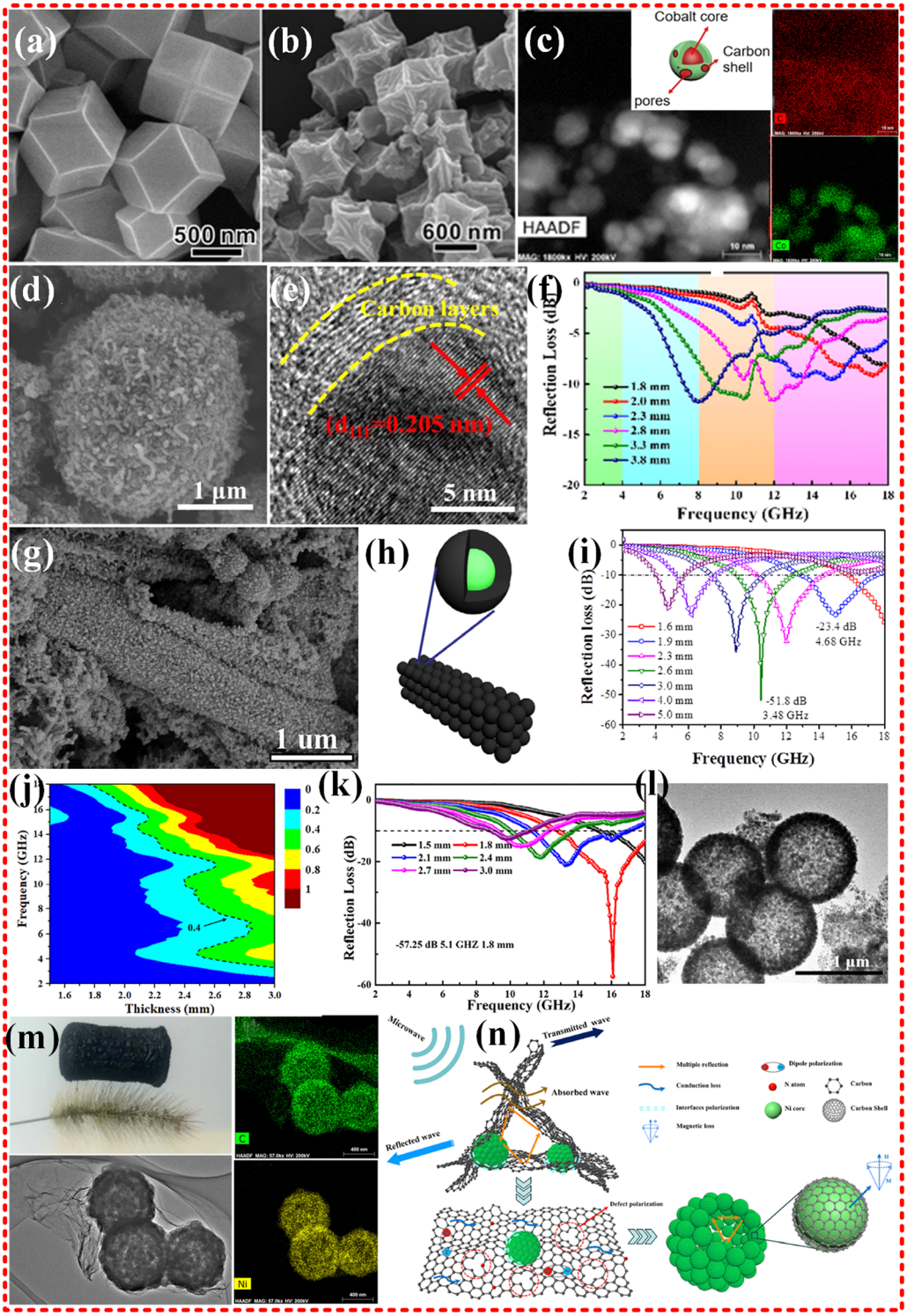

Fig. 4 (a) and (b) High-magnification SEM images of Co-MOF (ZIF-67) precursors, and low-magnification SEM of Co/C-600. Reproduced with permission from ref. 78, Copyright (2015) American Chemical Society. (c) Schematic illustration of porous core–shell Co–C samples. HAADF image, and elemental mapping of Co–C-800. Reproduced with permission from ref. 77, Copyright (2018) American Chemical Society. (d)–(f) SEM images and HRTEM images of the core–shell Co@CNTs-1 composite. RL values of Co@CNTs-1. Reproduced with permission from ref. 144, Copyright (2021) Elsevier Inc. (g)–(i) SEM images of S500. Schematic illustration of porous carbon-wrapped Ni composites. frequency dependence of microwave absorption performance of S500 with different thickness. Reproduced with permission from ref. 150, Copyright (2016) Elsevier B.V. (j)–(l) TEM images of Ni/C-20, calculated delta maps and reflection loss curves of Ni/C-20. Reproduced with permission from ref. 151, Copyright (2019) Elsevier B.V. (m) and (n) TEM images and elemental mapping of C and Ni of NCGF-4. Schematic illustration on microwave absorption mechanism of NCGF. Reproduced with permission from ref. 22, Copyright (2021) Elsevier B.V.

air. To address this issue, Yujie Chen and Hua Li developed a monometallic Co source with 2,5-dihydroxyterephthalic acid as organic linkers to obtain another Co-based MOF 74 (shown in Fig. 4c).[77] The study showed that the absorbing properties of the material improved to some extent, with an RL of −62.12 dB, a thickness of 2.4 mm and an EAB of 4.6 GHz. This improvement was attributed to the ferromagnetism of the cobalt cores and dielectric properties of the carbon shell. The magnetic properties of the samples were comparable to those of the other studies. However, when the authors replaced the Co source with a Ni source to obtain a monometallic Ni-MOF 74, the material exhibited very limited EMW absorption properties. In our previous research,[18] we attempted to enhance the impedance matching of ZIF67 based on cobalt by loading it into rGO, but the results were not as expected. We found that the performance could be improved by incorporating new metal components. While the Co-based MOF modified with carbon nanotubes did not exhibit excellent wave absorption properties (as shown in Fig. 4d–f).[144] This may be due to the relatively low or high complex permittivity, or the relatively complex permeability, which leads to poor impedance matching and limits the EMWA performance. However, research on Co-based monometallic MOFs are ongoing due to strongly magnetic nature of cobalt.[79,145–149]

Ni and Co are commonly used as metal centers in MOF materials due to their similar chemical properties. Guangbin Ji's group synthesized Ni-MOFs and utilized the more positive reduction potential of Ni^{2+} ions (−0.25 V) compared to Co^{2+} ions (−0.28 V) to obtain carbon-coated Ni metals, while preserving the MOF structure (refer to Fig. 4g–i).[150] which exhibits excellent absorption performance with an RL value of −51.8 dB and an EAB of 3.48 GHz for a thickness of 2.6 mm. Dielectric loss resulted from conductivity losses among conductive Ni@C nanospheres, as well as multiple reflection induced by porous structure. Magnetic loss originated from planes of cubic Ni (FCC) instead of hexagonal Ni (HCP), influenced by the content of non-magnetic carbon and the particle size. Compared to Co-MOF, the Ni-MOF synthesized in this study demonstrated poor magnetic properties. Yanhong Zou's group obtained Ni@C composites that exhibit excellent EMWA performance, with an RL of −55.7 dB and an EAB of 6.4 GHz with a thickness of 1.85 mm.[152] It is believed that natural loss, rather than the eddy current effect, is responsible for the magnetic loss observed in this composite. Haibo Yang's group synthesized hollow Ni/C microsphere derived from Ni-MOF (refer to Fig. 4j–l),[151] which demonstrated remarkable performance with an RL of −57.25 dB with thickness of only 1.8 mm and an EAB of 5.1 GHz. This superior performance is attributed to the hollow structure and the synergistic effect between carbon and nickel nanoparticles. The results highlight the crucial role of Ni particles in magnetic loss mechanism, leading to better impedance matching performance. Our group attempted to improve the electrical conductivity and impedance matching properties of Ni microsphere-like MOFs by implanting them into a graphene foam framework.[22] This was achieved by optimizing the GO framework, as illustrated in Fig. 4m and n. The results show that the desired improvement was obtained, with an RL of −63 dB at a loading of only 15 wt%, a thickness of just 1.76 mm, and an EAB of 5.4 GHz. The magnetic properties of the composite were further enhanced by increasing the Ni content in the graphene foam, albeit at the cost of attenuating some of its capability to improve impedance matching. Additionally, many monometallic Ni applications are available in pure MOFs and composites.[153–158]

Metallic iron and ferrite have been used in EMWA to focus on magnetic loss, thanks to their superior chemical stability and high saturation magnetization strength. However, pure Fe materials have limited electromagnetic wave absorption capabilities, and dielectric loss materials are often in combination with Fe-based materials to achieve impedance matching and boost EMWA performance. A classical Fe based MOF is Prussian blue, which can be heat-treated to produce Fe/C nanocubes (as illustrated in Fig. 5a and b). These nanocubes exhibit ultrawide band EMWA performance with an EAB of 7.2 GHz (range from 10.8 to 18.0 GHz), but their RL falls short of expectations. In addition to the magnetic loss contributed by Fe, the graphitized carbon provides dielectric loss, and multiple dielectric resonances are believed to improve EMWA performance. The natural ferromagnetic resonance is considered the main mode of magnetic loss, and there is no hysteresis loss, domain wall resonance loss, or eddy current effect.[159] Further, in addition to Fe particles, Fe_3C/Fe and Fe_3C/Fe/C composites were derived from other Fe-based MOFs, such as MIL-101.[160] Although the EMWA performance generally results in an RL of −39.43 dB, an effective absorption bandwidth of 14.32 GHz (ranging from 3.68 to 18.00 GHz) is mentioned in the literature. It should be noted that another relevant way to evaluate practical applications is to determine the effective absorption bandwidth at a particular thickness, which in this study is approximately 6 GHz with a thickness of 2 mm. Recently, similar research has yielded Fe/Fe_3C@NC composites from Fe-MOFs, which exhibit strong RL of −70.8 dB at a thickness of 2.5 mm and an EAB of 5.15 GHz at a matching thickness of 1.7 mm.[161] Notably, novel Fe/Fe_3O_4/FeN/NC composites were obtained from Fe-MOFs (as shown in Fig. 5c and d), exhibiting exceptional EMWA performance, with an RL of −60.08 dB at thickness of merely 1.44 mm and an EAB of 5.06 GHz at 1.64 mm, surpassing many similar researches. This is attributed to the multiple scattering and reflection, interfacial polarization, dipole polarization contributing to dielectric loss, eddy current effects and multiple resonance effects contributing to magnetic loss.[162] For monometallic Fe-based MOF materials with strong magnetic properties, achieving good impedance matching and maximizing magnetic loss without excessive loss of dielectric loss both are crucial, and the discovery of complementary materials and content control are indispensable.[163–168]

In addition to the commonly used magnetic metals, such as Fe, Co, and Ni, other metal centers, including Zn, Zr, Cu, Mn, and Ti, have also been utilized in MOFs materials to achieve efficient EMWA performance. Mn-MOF was employed as a precursor to derive MnO_2@C composites by Chongbo Liu's

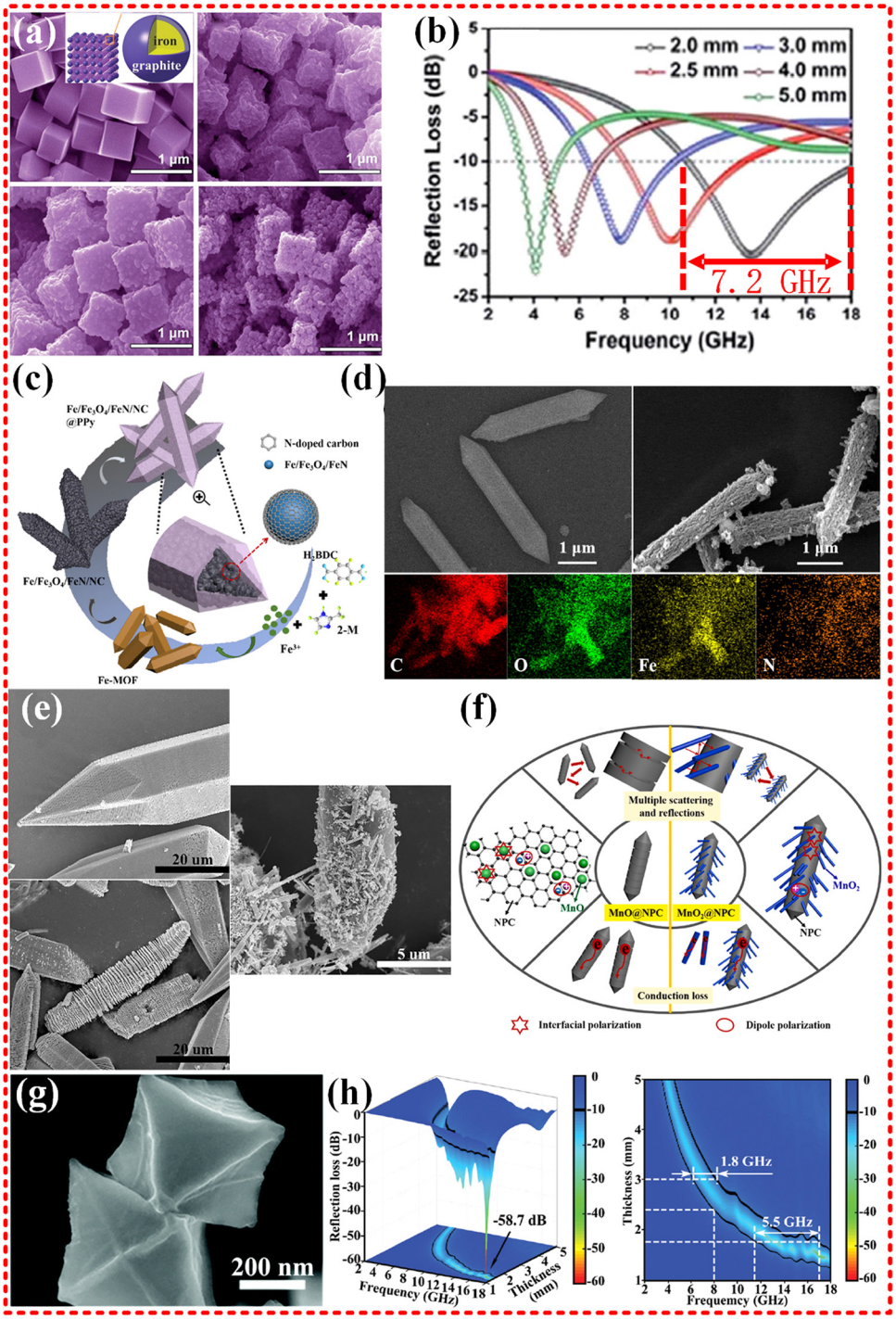

Fig. 5 (a) and (b) SEM images of the as-prepared PB nanocubes, the reflection losses curves of S2, reproduced with permission from ref. 159, Copyright (2015) Royal Society of Chemistry. (c) and (d) The illustration of formation process of FON/NC@PPy composites, SEM images of Fe-MOF, FON/NC, Elemental mappings of FON/NC@PPy composites, reproduced with permission from ref. 162, Copyright (2021) Elsevier Inc. (e) and (f) SEM micrographs of Mn-MOF-74, MnO@NPC-800 and MnO_2@NPC-800 sample, schematics of the MA mechanisms of the MnO@NPC and MnO_2@NPC composite materials, reproduced with permission from ref. 169, Copyright (2020) Elsevier B.V. (g) and (h) The FE-SEM images of ZrO_2/C-800, three-dimensional RL representations and two-dimensional RL projection maps of ZrO_2/C-800, reproduced with permission from ref. 170, Copyright (2020) Royal Society of Chemistry.

group, resulting in ultra-strong EMWA performance with maximum RL in S, C, X, Ku bands exceeding −50 dB, as shown in Fig. 5e and f.[169] The MnO@NPC-800 composite exhibited a RL of is −54.38 dB at 5.12 GHz, demonstrating its superior low-frequency characteristics. Moreover, the MnO_2@NPC-800 composites show a maximum RL value −63.21 dB at 12.48 GHz with

a thickness of 2.05 mm. It is noteworthy that the composites exhibited good impedance matching with stable and high permittivity and polarization, and relaxation from the 3D caterpillar-like structure, resulting in good reflection loss value in all bands (S, C, X, Ku bands).

The ZrO_2/C octahedra derived from Zr-based MOFs (UiO-66) prepared by Jiurong Liu's group focus on EMWA with an RL −58.7 dB at a frequency of 16.8 GHz and a thickness of 1.5 mm. Additionally, the maximum EAB of 5.5 GHz was achieved at a thickness of 1.7 mm (as shown in Fig. 5g and h).[170] The results indicate that the dielectric losses are mainly attributed to the derived carbon material, and the degree of carbonization, which depends on the annealing temperature (ZrO_2/C-700, 800, 900), determines the material's attenuation capability and impedance matching properties. Proper carbonization leads to excellent EMWA performance.

Zn-based MOFs have also been extensively studied for EMWA. For instance, ZIF-8 MOFs have been employed to prepare ZnO/NC nanocomplexes with two different structures, namely yolk–shell and hollow structures, as depicted in Fig. 6a and b.[171] These nanocomplexes exhibited EMWA with different RL value of −51.2 dB and −52.4 dB, respectively, depending on the heat treatment temperature, and an EAB over 4 GHz. The absorption mechanism of these nanocomplexes was attributed to the multiple reflections caused by the hollow structure and the polarization loss of the defect as a center. However, due to the lack of magnetic metal centers, the magnetic component of the electromagnetic wave was not effectively absorbed. Similarly, a core–shell structured ZnO/C@PPy composite was also obtained from ZIF-8 (Zn-based MOF) with a RL of −76.31 dB and an EAB of 6.38 GHz, covering the whole Ku-band, as shown in Fig. 6c–f.[172] Nonetheless, this is also shown by the lack of attention to the magnetic component and the problem of impedance mismatch, despite the fact that some wave absorption performance was achieved.

Guangbin Ji's group synthesized CuO/C composites using the ZIF-67 MOF as a template (shown in Fig. 6g), which exhibit high impedance matching properties, a rarity for non-magnetic monometallics used in EMWA applications. Impedance matching depends on both dielectric and magnetic permeability

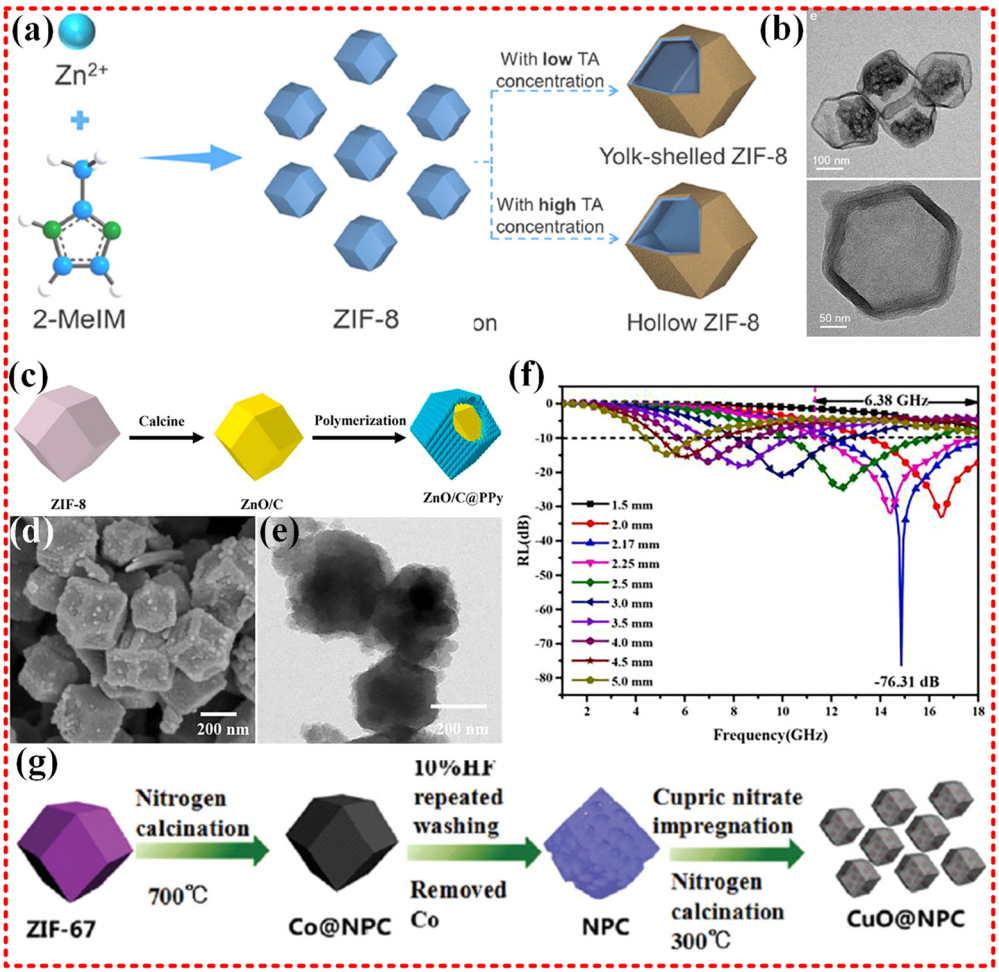

Fig. 6 (a) and (b) Schematic routes of synthesis of yolk–shell ZIF-8 and hollow ZIF-8 structures, TEM images of YS-ZnO/NC-800 and H-ZnO/NC-700, reproduced with permission from ref. 171, Copyright (2022) Elsevier Ltd. (c)–(f) Scheme for the synthesis of ZnOC@PPy, the SEM and TEM of Z700@P4, RL of Z700@P4, reproduced with permission from ref. 172, Copyright (2022) Elsevier B.V. (g) Schematic diagram of the synthesis process of CuO@NPC, reproduced with permission from ref. 173, Copyright (2016) The Royal Society of Chemistry.

properties. The obtained CuO/C composites demonstrated an RL −57.5 dB at 14.9 GHz with a thickness of 1.55 mm, and an EAB of 4.7 GHz (13–17.7 GHz) due to the porous carbon material derived from the MOF and high impedance match obtained with Cu embedded in the MOF.[173] Additionally, Jun Chen's group synthesized hollow copper-based sulfides with various morphologies, derived from Cu-based MOF (Cu-MOF-74).[174] These hollow copper-based sulfides demonstrated low reflection losses, with an RL of only −15 dB, and an EAB of 6.2 GHz at a fill of 20%. The absorption properties are attributed to the synergistic effect of multiple reflections and scattering from the hollow cavity structure, and the conductivity loss from the 3D conductive network. However, the magnetic loss component is lacking and may lead to poor impedance matching, resulting in a smaller RL.

The novel TiO_2/C composite has been synthesized, using Ti-based MOF (MIL-125 (Ti)) and exhibited excellent EMWA performance with a minimum RL of −49.6 dB and an effective EAB of 4.6 GHz (13.4–18 GHz) with thickness of 1.6 mm. The EMWA performance is strongly influenced by dielectric losses, including relaxation scheme losses.[175] Ti is a space metal known for its light weight, high strength, chemical stability and good corrosion resistance. Although Ti-based MOFs can meet the light weight requirements for wave absorbers, it is important to note that the results of current studies do not demonstrate the potential of monometallic Ti-based MOFs EMW absorption. Relying solely on dielectric losses would be unwise, but combination of magnetic and dielectric-based MOFs could potentially overcome the limitations of a lack of magnetism and make it the best option in the EMWA field.

2.2.2.2 Bimetallic MOF-based composites. Bimetallic MOFs can be divided into two categories: monometallic MOFs lacking magnetic dielectric properties and combined with magnetic dielectric metals (such as Fe, Co and Ni), and MOFs consisting of two strong magnetic metals with strong dielectric properties that complement each other, leading to better impedance matching. Generally, bimetallic MOFs exhibit better EMWA performance than monometallic MOFs. Our research suggests that metals such as Cr, Mn, and Cd, which do not perform well as metal centers alone in MOF materials, can be combined with Co, Fe, or Ni bimetals in MOFs to achieve strong EMWA performance.

As previously mentioned, monometallic Co@C composites have exhibited poor EMWA performance. However, Yang's group was able to improve the performance of Co@C composites by synthesizing Co–Cd- and Co–Zn-based bimetallic-MOFs. Monometallic Co-based MOFs exhibit good magnetic permeability, but weak conductivity leads to an imbalance in impedance matching. To address this issue, Cd and Zn were used to increase the surface area of the material, enhancing the interfacial polarization loss and the multiple reflections, thus contributing to EMWA performance.[144] Moreover, the Zn-based MOF has lower dielectric properties, which reduces permittivity to achieve better impedance matching. Renchao Che's group has also synthesized Co@NC–ZnO composites based on Co–Zn-MOF, which demonstrated the strongest RL value of −69.6 dB at only 1.9 mm thickness, with wideband absorption covering 6.8 GHz at 2.4 mm (as shown in Fig. 7). The authors have controlled the Co/Zn mass ratio and adjusted the MOF framework to make the electronic conduction network and magnetic

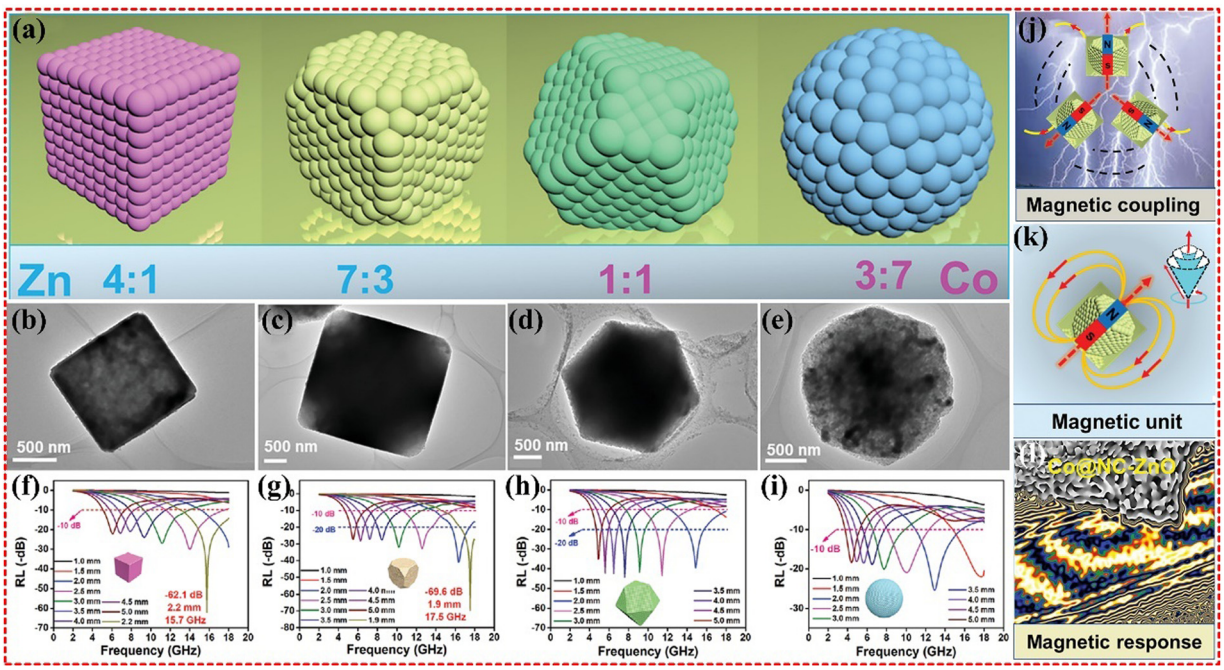

Fig. 7 (a) Morphology evolution, (b–e) TEM images, and (f–i) the reflection loss curves of Co@NC-ZnO-1, Co@NC-ZnO-2, Co@NC-ZnO-3, and Co@NC-ZnO-4, (j) the magnetic coupling, (k) magnetic response unit, and (l) magnetic response scale. Reproduced with permission from ref. 176, Copyright (2021) Wiley-VCH GmbH.

coupling network compatible each other. The unique magnetic coupling and boosted magnetic responding ability were verified using the off-axis electronic holography.[176]

The CoAl-LDH nanoarray was obtained by liquid metal synthesis method using Co-based MOF as a precursor (as shown in Fig. 8a), and it preformed excellent EMWA performance with an ultra-wideband of 8.48 GHz at a thickness of 2.6 mm. The presence of heterogeneous atoms and interfaces provided interfacial polarization centers and defective polarization centers, driving polarization losses into action, resulting in enhancing impedance matching properties. The homogeneous dispersion of Co in the MOF contributed to magnetic loss.[177] MnO/Co/C heterogeneous nanocomposites were synthesized by Jiurong Liu's group derived from MnCo-MOF-74 (as shown in Fig. 8b–d), and good performance was achieved with an RL of −68.89 dB, and an EAB of 5.3 GHz. The EMWA performance is mainly attributed to optimized impedance matching, polarization loss (interface polarization, dipole polarization, *etc.*), natural resonance loss, conductivity loss and multiple scattering.[178] Additionally, Jiurong Liu's group synthesized Co/ZrO_2/C using Co–Zr-MOF (UIO-66), which showed remarkable EMWA performance with an RL of −57.2 dB, and EAB of 11.9 GHz covering 74.4% of the whole measured bandwidth.[179] The introduction of dielectric Co brought new magnetic loss to the already good dielectric loss of the ZrO_2/C material, significantly improving the impedance matching performance. Strong

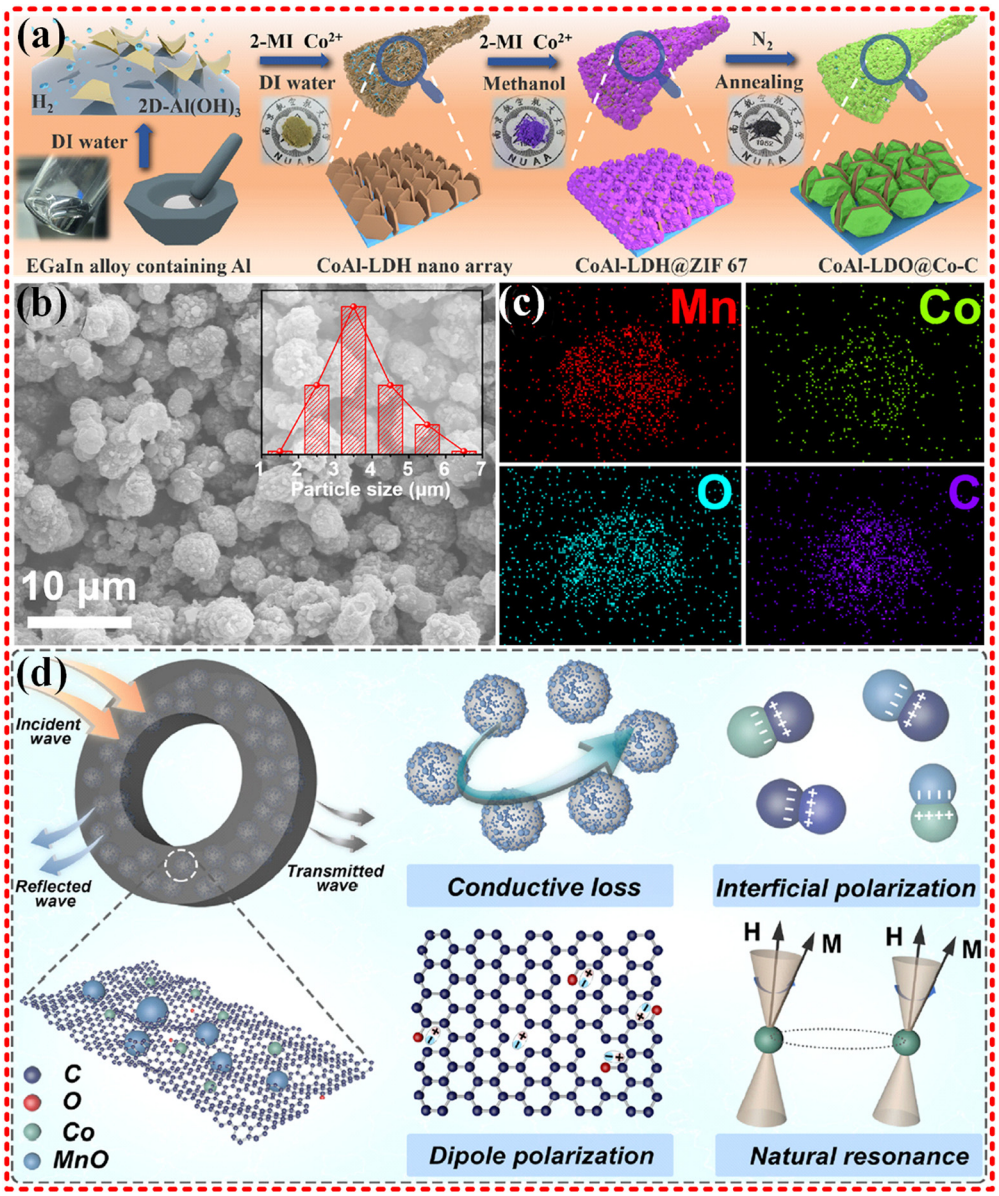

Fig. 8 (a) Schematic diagram of the synthesis process of CoAl-LDO@Co-C, reproduced with permission from ref. 177, Copyright (2021) Elsevier Inc. (b)–(d) SEM images (insets showed the particle size distributions), elemental distribution mapping, and the proposed EMW absorption mechanism of the MOF-derived MnO/Co/C nanocomposites, reproduced with permission from ref. 178, Copyright (2022) Elsevier Ltd.

interface polarization and the synergistic effect between the multiple components together also contributed to the excellent EMWA performance. Moreover, the Ni/NiO/Cu@C composites derived from Ni–Cu-MOF[180] was synthesized, exhibiting a RL of −38.1 dB with only 10 wt% filler loading. The low density of the filler loading can guarantee enhanced conduction loss and impedance matching. Similarly, the introduction of the magnetic dielectric Ni into the monometallic Cu MOF contributes to magnetic loss, while the improved impedance matching, strong interface polarization and the synergistic effect between the multiple components lead to improved EMWA performance. Furthermore, $TiO_2/ZrTiO_4$/C composites derived from PCN-415 (TiZr-MOFs)[181] has been designed and synthesized, qualified with a RL of −67.8 dB (2.16 mm, 13.0 GHz), and an EAB of 5.9 GHz (2.70 mm). The synergy of enhanced interfacial polarization and other attenuation mechanisms in the composites is revealed.

Dual magnetic metal MOFs, such as CoNi-MOF, CoFe-MOF and NiFe-MOF, have been found to exhibit high impedance matching and excellent EMWA performance. In our previous research, a monometallic Co-MOF was found to have limited EMWA performance. However, by introducing Ni metal to form CoNi alloys, strong magnetic properties were obtained, resulting in enhanced wave absorption performance with an RL of −58.2 dB at 10.62 GHz, and EAB of up to 4.03 GHz (8.80–12.83 GHz).[18] In a recent study conducted by Zhai *et al.*, a similar strategy was employed for the synthesis of the Co@NC/Ni nanocomposite. The researchers utilized ZIF67 and $Ni(OH)_2$ precursors, which were subsequently subjected to carbonization at 600 °C (as illustrated in Fig. 9a–g). Notably, the Ni component was sourced from $Ni(OH)_2$, while ZIF67 played a dual role in preventing Ni agglomeration and undergoing natural pyrolysis to yield Ni nanoparticles protected by graphitized carbon. Furthermore, the interface between ZIF67 and $Ni(OH)_2$ imposed constraints on the formation of Co@NC post-ZIF67 pyrolysis. This limitation was attributed to the magnetic nanoparticles' propensity to contribute significantly to the attenuation of the magnetic component in electromagnetic waves.[19] Jinxiao Wang's group synthesized a CNT/CoO/Ni_2O_3 composite derived from a Ni–Co bimetallic MOF, as shown in Fig. 9h–j. The composites exhibited an RL of −49.6 dB and an EAB of 3.87 GHz, which was attributed to the dual electric network formed by Ni^{3+} and Co^{2+} energy splitting, and d–d orbital electron transfer.[182] Additionally, Zirui Jia's group also obtained a Ni–Co/PC composite derived from a Ni–Co bimetal MOF. The composites exhibited significantly improved EMWA performance with an RL of −67.81 dB and an EAB of 6.16 GHz. This enhancement was attributed to the excellent electrical conductivity, rich surface, high attenuation capability, and the eddy current loss-dominated magnetic loss, all of which contributed to its EMWA performance.[183]

Hollow $CoFe_2O_4$/CoFe@C microspheres were synthesized from Co–Fe MOF, with a focus on crystal transformation, heterogeneous structures, and magnetic exchange coupling, as shown in Fig. 10a–e. The microspheres exhibited strong magnetic saturation (Ms) of 152.4 emu g^{-1} and optimized RL of −51 dB, with an EAB of 6.0 GHz. These properties were attributed to the synergistic effects of enhancing impedance matching, polarization relaxation, and multi-interfaces.[184] Recently, the NiFe@N–C/rGO was synthesized from NiFe-MOF, as shown in Fig. 10f–i. This novel material presents tunable wideband properties and an RL of 72.28 dB, with an EAB of 7.14 GHz, almost covering the whole X and Ku bands. The EWM absorption mechanism was revealed theoretically based on formation energy and dipole moment.[185]

2.2.2.3 Multi-metallic MOF-based composites. Multi-metallic MOFs offer several advantages over monometallic and bimetallic MOFs by combining the benefits of more than two materials, which enable the construction of multiple topologies that can benefit the EMWA mechanism. In particular, these materials can enhance impedance matching, multiple reflections and scattering, and the presence of interfaces and defect sites that provide polarization losses. The caterpillar-like Co/MnO/CNTs composites derived from Co–Mn–Zn multi-metallic MOF was synthesized by Junying Zhang group, as shown in Fig. 11a–e, which showed strong RL of −58.0 dB and an EAB from 13.52 GHz to 18 GHz, with a thickness of only 1.32 mm, exceeding that of monometallic Co-based MOF materials.[186] This improvement was attributed to the integration of electromagnetic dielectric materials to improve permeability, as well as the multi-scale response ability with caterpillar-like structure, and well impedance matching.[187] The Lei Wang group has synthesized a novel double-shell-structured $MnFe_2O_4$@FeO/C derived from Mn–Fe–Zn multi-metallic MOFs (as shown in Fig. 11f–j). The resulting material exhibits an RL of −53.75 dB with a thickness of 1.8 mm, and the corresponding EAB is 4.74 GHz ranging from 10.27 to 13.90 GHz and 16.89 to 18.0 GHz. By adjusting the Zn-MOF content, the thickness of the carbon layer can be controlled to obtain desirable electromagnetic parameters. The unique construction, expected impedance matching, polarization loss, and strong magnetic loss all contribute to the excellent EMWA performance.[188] Furthermore, the Zirui Jia group has synthesized $NiCo_{2-0.5x}Cr_2O_3$@C nanoparticles based on Ni–Co–Cr multi-metallic MOFs (as shown in Fig. 11k–s). The introduction of additional $NiCo_2$–Cr_2O_3 has resulted in excellent EMWA performance with an RL of −52.71 dB at 1.6 mm and an EAB of 5.28 GHz at 1.89 mm. The synergistic effect between the appropriate ratio of Cr_2O_3, NiCo alloy, and good impedance matching optimized by carbon materials contributes to the improved performance.[189] More research works are being conducted on multifunctional MOFs that combine the properties of multiple structures and metals.[190–193]

The metallic component within MOF-based composites plays a pivotal role in the realm of EMWA. Researchers have been actively exploring the use of MOF-based composites to create novel heterogeneous interfaces and augment electrical conductivity. The aim is to achieve optimal alignment between the conductive and magnetic properties of the materials and the energy of electromagnetic waves. However, upon a thorough examination of related studies, it becomes evident that

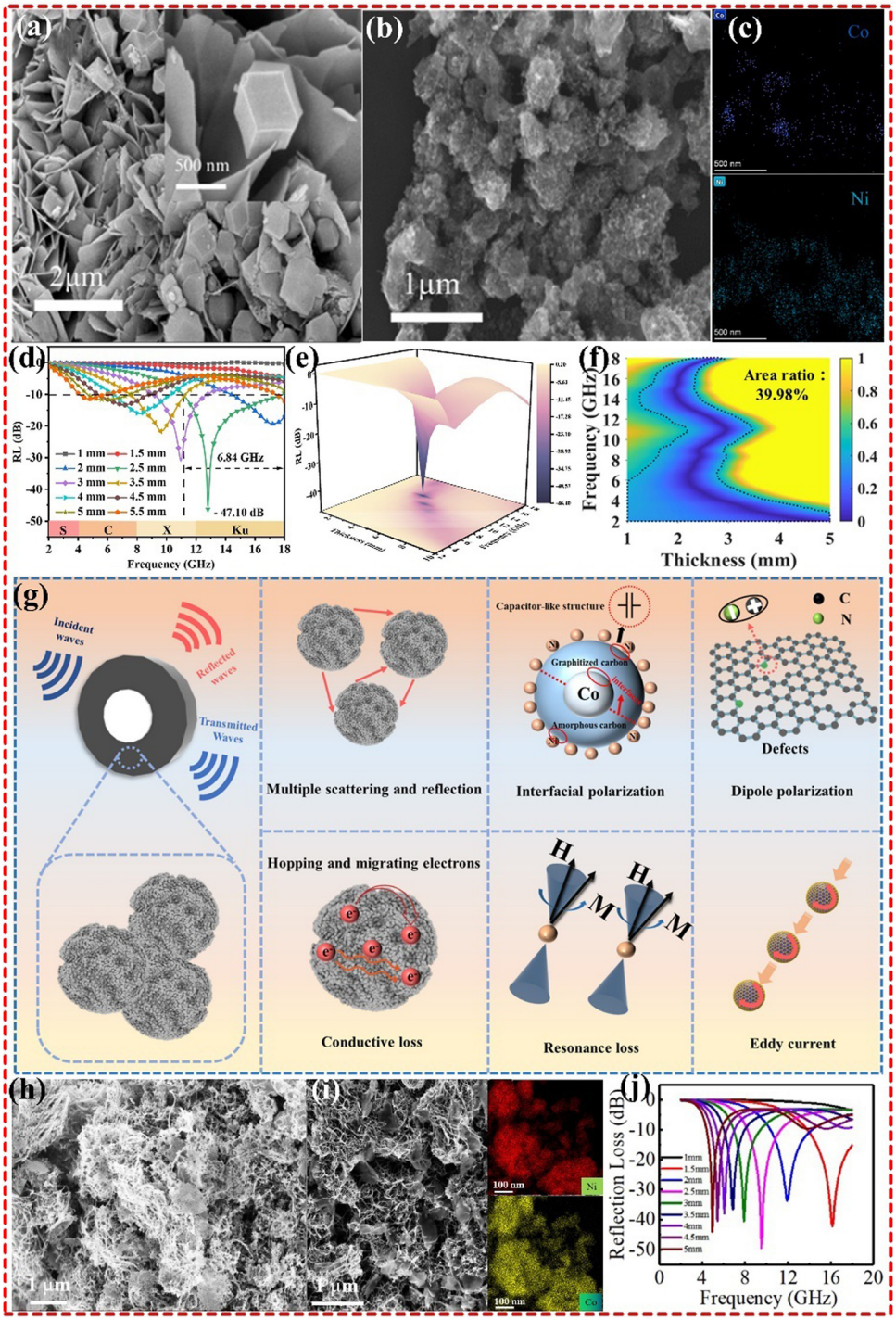

Fig. 9 (a)–(g) SEM images of (a) $Ni(OH)_2$, and (b) S-2, (c) TEM-EDS mapping images of S-2, (d) and (e) 2D and 3D RL plots of S-2, (f) calculated delta value maps of S-2, (g) schematic illustration of the EMWA mechanism for Co@NC/Ni composite. Reproduced with permission from ref. 19, Copyright (2023) Elsevier. (h)–(j) SEM images of CNT/NiCo-600 and CNT/NiCo-MOF-74, EDS results of CNT/NiCo-MOF-74, RL values of CNT/NiCo-600. Reproduced with permission from ref. 182, Copyright (2021) Elsevier B.V.

MOF-based composites exhibit varying types and quantities of metal centers, resulting in distinctive EMWA performance. A brief overview of EMWA performance of mono-, bi-, and multi-metallic MOF-based composites is reported in Table 2, which includes details such as varying loading amounts, minimum reflection loss, effective absorption bandwidth, and matching thickness. An EMWs is characterized by the simultaneous propagation of electric and magnetic fields. In the context of MOFs, various metals exhibit distinct electronegativity and electronic structures, giving rise to diverse energy band

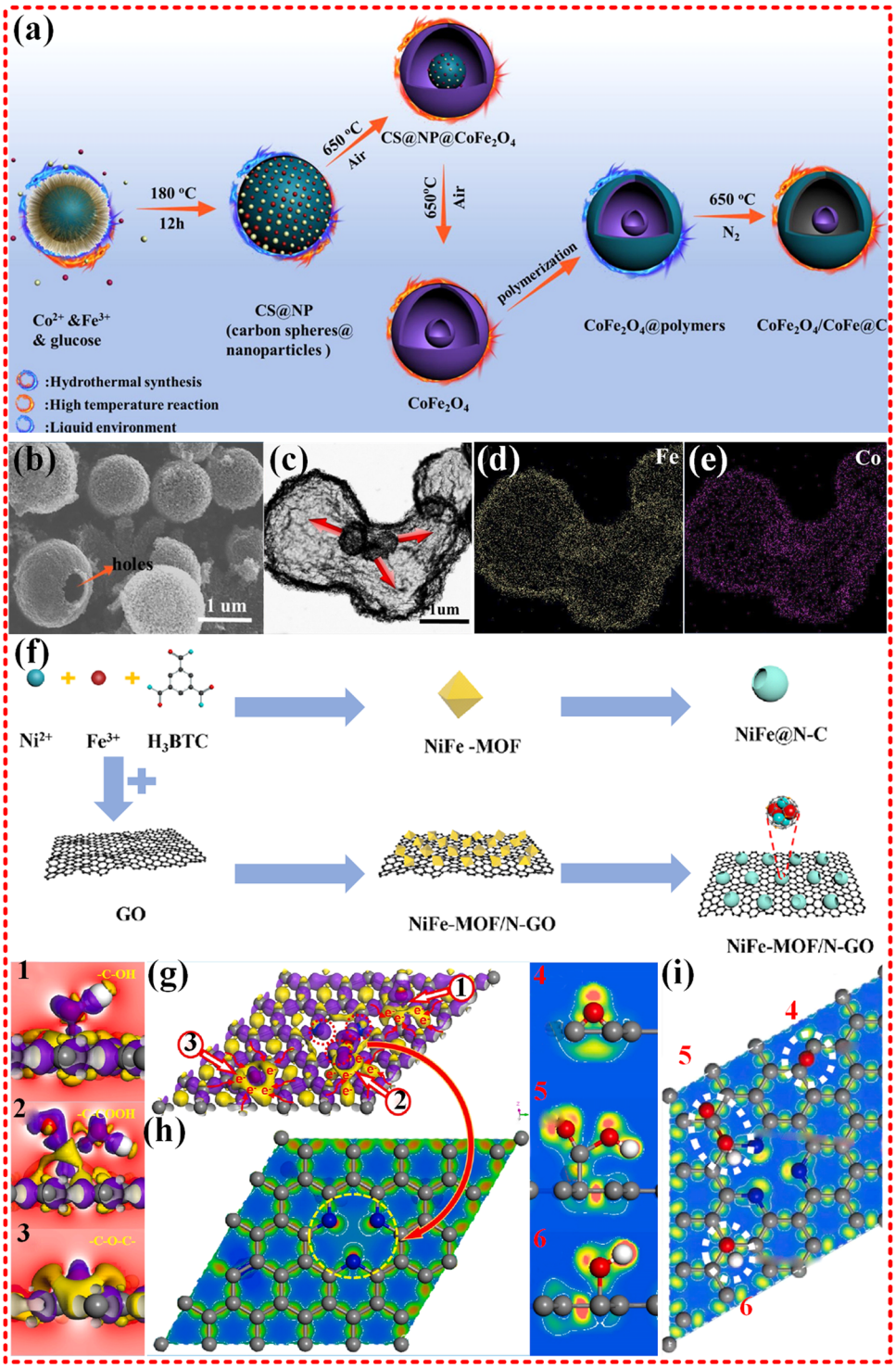

Fig. 10 (a)–(e) Schematic diagrams of the fabrication processes of $CoFe_2O_4$/CoFe@C composites, SEM and elemental mapping images of hollow $CoFe_2O_4$ composites, hysteresis loops and 2D RL of as-prepared samples, the EMW absorption mechanisms of the $CoFe_2O_4$/CoFe@C composites. Reproduced with permission from ref. 184, Copyright (2021) Elsevier. (f)–(i) The schematic diagram of fabricating NiFe@N–C and NiFe@N–C/rGO, SEM images of NiFe-MOF and NiFe@N–C, RL values of NiFe@N–C/rGO-30, magnetic hysteresis loops of as-prepared samples, electron density difference of pyridinic N-rGO structure, rGO functional group EDD details: (1) hydroxyl group; (2) carboxyl group; (3) planar oxygen doping. Electronic localization function of pyridinic N-rGO structure: (4) planar oxygen doping; (5) carboxyl group; (6) hydroxyl group. Reproduced with permission from ref. 185, Copyright (2022) Elsevier.

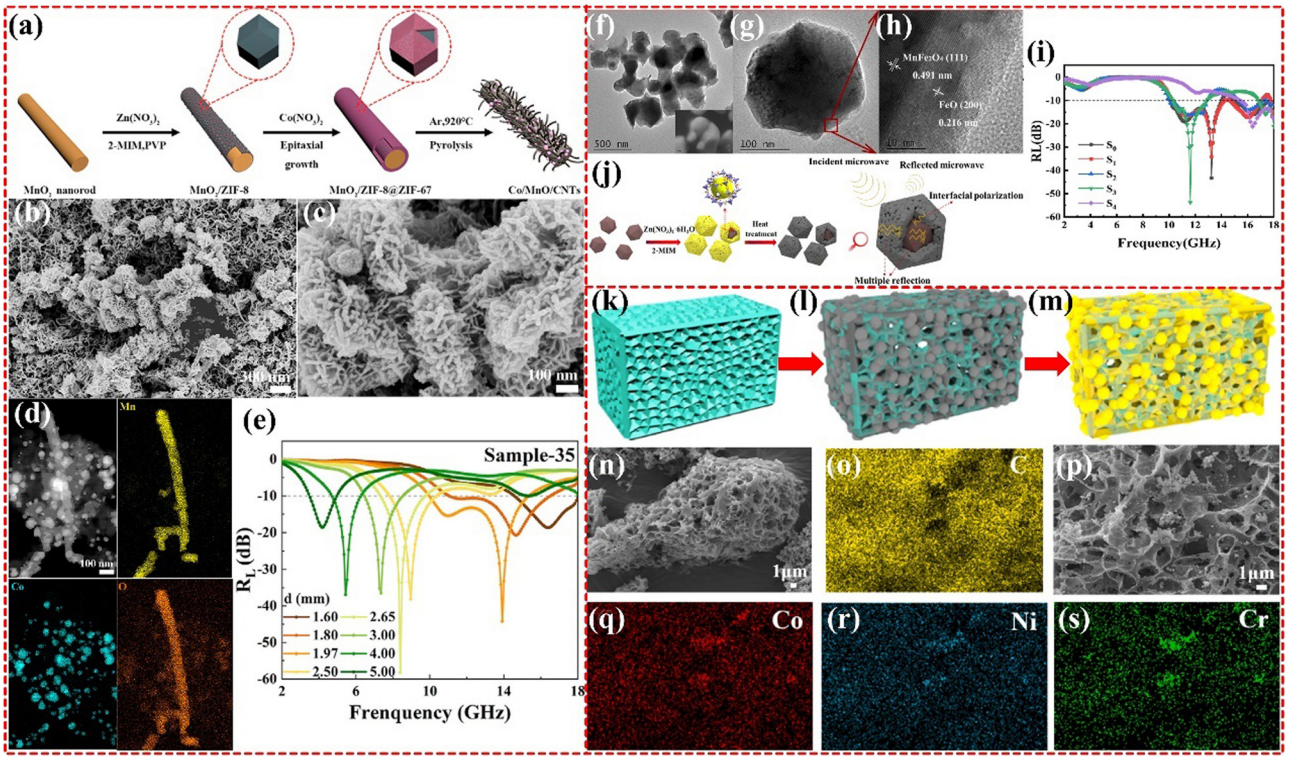

Fig. 11 (a)–(e) Schematic diagram of the growth process of Co/MnO/CNTs, SEM images of Co/MnO/CNTs, EDS mapping images and frequency-dependent RL of the as-obtained Co/MnO/CNTs. Reproduced with permission from ref. 187, Copyright (2020) Elsevier. (f)–(j) TEM and HRTEM of S3 sample, reflection loss of all samples at d = 1.8 mm; the schematic diagram of the microwave absorption mechanism of sample S3. Reproduced with permission from ref. 188, Copyright (2022) Elsevier. (k)–(s) The schematic synthesis process of $NiCo_{2-0.5x}Cr_2O_3$@C, SEM images of $NiCO_{2-0.5x}Cr_2O_3$@C Cr_0 and $Cr_{0.5}$, the EDS mapping of $Cr_{0.5}$. Reproduced with permission from ref. 189, Copyright (2021) Elsevier.

structures and energy level distributions. This variability influences the consumption of electric field energy in EMWs. Lower electronegativity corresponds to improved characteristics in the motion of free electrons. These free electrons can effectively interact with incident EMWs, causing their excitation and the generation of EMWs in the opposite direction. Consequently, this phenomenon reduces the penetration and propagation of the EMWs.

Furthermore, the distinct size and arrangement of various metals within MOFs result in diverse pore structures, specific surface areas, and crystalline arrangements. This diversity increases the propagation paths of EMWs within MOFs, creating more interfaces for interaction between EMWs and MOF-based composites. Consequently, this facilitates the absorption or scattering of electromagnetic waves at specific frequencies. Monometallic MOFs generally exhibit highly ordered and regular pore structures that contribute to their high specific surface area, enhancing their ability to absorb electromagnetic waves. The increased surface area allows for effective interaction with EMWs, thereby improving shielding efficiency. Additionally, metal ions present in monometallic MOFs, such as those found in Cu-based or Co-based MOFs, can provide conductive pathways, exhibiting good electrical conductivity.

However, monometallic MOFs often have lower mechanical strength and are susceptible to physical damage, which limits their application in EMWA scenarios requiring high mechanical resilience. Furthermore, certain monometallic MOFs may lack stability in humid or corrosive environments, potentially leading to decomposition or loss of functionality over time, thereby restricting their long-term utility in harsh environmental conditions. Additionally, some monometallic MOFs may excel in EMWA within specific frequency bands but exhibit reduced effectiveness in other frequency ranges.

Bimetallic MOFs leverage the synergistic interaction between two different metal ions to establish enhanced conductive pathways, thereby improving overall conductivity and EMWA properties. For instance, the inclusion of copper and nickel as heterogeneous metals in monometallic MOFs enhances both conductivity and EMWA capabilities. The introduction of bimetallic centers also enhances mechanical strength and stability, increasing durability in practical applications. Some bimetallic MOFs exhibit exceptional thermal stability, maintaining structural integrity and performance in high-temperature environments. For example, combinations like Co and Ni maintain robust electrical conductivity and EMWA performance at elevated temperatures.

However, interactions between different metal ions can sometimes impact material performance. Certain metals may preferentially form coordination structures, potentially weakening the properties of the other metal within the MOF. To

Table 2 MOF-based composites with mono-, bi- and multi-metallic centers for EMWA

Categories	Center metal	Filler	Loading (wt%)	RL_{min} (dB)	EAB (GHz)	Thickness (mm)	Ref.
Mono-	Co	Co/C-500	40	−35.3	5.8	2.5	78
		Co–C-800	30	−62.12	4.6	2.4	77
		Co@NCPs	30	−49.8	4.8	2.98	18
		Co@CNTs	20	−11.8	1.96	3.3	144
		Co/C-650	33	−47.6	5.11	2.0	79
	Ni	Ni/C	40	−23.4	4.68	1.9	150
		Ni@C	30	−55.7	6.0	1.85	152
		Ni/C	30	−57.25	5.1	1.8	151
		Ni/C@graphene foam	15	−63	5.4	2.1	22
		Ni@C-ZIF	40	−86.8	7.4	2.7	156
	Fe	Fe/C	25	−56.94	6.73	3.1	194
		Fe/C-600	40	−22.6	5.3	2.0	159
		Fe/C-650	30	−39.43	5.36	2.0	195
		Fe/Fe_3C@NC	30	−70.8	5.15	2.5	196
		Fe/Fe_3O_4/FeN/NC	30	−60.08	5.06	1.64	162
	Mn	MnO_2@NPC-800	50	−63.21	4.04	2.05	169
	Zr	ZrO_2/C	50	−58.7	5.5	1.7	170
	Zn	ZnO/NC-700	15	−51.2	4	3.1	171
		ZnO/C@PPy	15	−76.31	6.38	2.17	172
	Cu	CuO/C	50	−57.5	4.7	1.55	173
		$Cu_2S/Cu_{31}S_{16}$	20	−15.1	6.2	2.3	174
	Ti	TiO_2/C	40	−49.6	4.6	1.6	175
Bi-	CoCd	CoCd@CNTs	20	76.6	6.2	2.0	144
	CoZn	CoZn@CNTs	20	−28.3	3.0	1.8	144
	CoZn	Co@NC-ZnO	25	−69.6	6.8	2.4	176
	CoAl	CoAl-LDO@Co-C	30	−38.18	8.48	2.6	177
	MnCo	MnO/Co/C	50	−68.89	5.3	2.64	178
	CoZr	Co/ZrO_2/C	50	−57.2	6.9	3.3	179
	NiCu	Ni/NiO/Cu@C	10	−38.1	NA	3.2	180
	ZrTi	$TiO_2/ZrTiO_4$@C	35	−67.8	5.9	2.7	181
	CoNi	CoNi@NCPs	30	−55.4	4.92	1.74	18
	CoNi	$CNT/CoO/Ni_2O_3$	—	−49.6	3.87	2.0	182
	CoNi	$NiCo_2S_4$/PC	—	−67.81	6.16	2.1	183
	CoFe	$CoFe_2O_4$/CoFe@C	30	−51	5.9	2.17	184
	NiFe	NiFe@N–C/rGO-90	20	−55.34	7.14	2.04	185
	CoTi	$CoO/Ti_3C_2T_x$MXene-15	5	−52.23	4.88	1.9	191
Multi-	CoNiMn	CoNi/MnO@C	—	−55.2	8.0	2.1	197
	CoMnZn	MnO_2/ZIF-8@ZIF-67	35	−58.0	5.36	1.97	187
	NiCoCr	$NiCo_{2-0.5x}Cr_2O_3$@C	—	−52.71	5.28	1.89	189
	CoNiMo	H-CoNi@MoC/NC	15	−60.05	3.52	2.5	190
	FeCoNi	FeCo/FeCoNi@NPC	30	−67	6.24	1.91	192
	CoZnMo	$CoZn/C@MoS_2$@PPy	30	−49.18	4.56	1.5	193
	CoNiTi	$CoO/NiCo_2O_4/Ti_3C_2T_x$	10	−58.37	4.24	1.5	191

optimize electromagnetic properties, multiple metal centers can be strategically introduced, enabling precise tuning of electrical conductivity, magnetism, and dielectric constants for efficient EMWA. Multi-metal centers provide diverse active sites that enhance a material's capacity to absorb, reflect, and scatter EMWs across various frequency bands. Popular combinations such as Fe, Ni, and Co exemplify this approach, offering both high electrical conductivity and magnetic properties.

It is noteworthy that MOF-based composites utilized in EMWA applications often feature predominantly magnetic metals, contributing to superior EMWA properties. When the central metal of MOFs is magnetic, as seen with metals such as Co, Ni, and Fe, it typically contains metal ions with unpaired electrons. This characteristic leads to the manifestation of spin magnetic moments in the metal ions, and these moments interact with incident EMWs, influencing their propagation and absorption. Therefore, the deliberate modulation of magnetic metal species in MOF-based composites holds the potential for achieving selective shielding of EMWs.

2.3 Water remediation and air treatment

2.3.1 Water and air pollution. Water is a vital component for all forms of life, and its significance cannot be overstated. However, as the global population increases and industrialization continues to advance, the environment is being subjected to unprecedented levels of pollution.[198–202] Despite the importance of economic and social progress, negative consequences have emerged, and the contamination of water has become one of the most complex and critical challenges facing humanity. Various contaminants such as chemical dyes, biopharmaceuticals, personal care products, heavy metal ions, and fluoride are regularly detected in water sources. The effects of light pollutants are manageable and can be addressed. However, heavy pollutants, including toxic and carcinogenic substances,

have a devastating and uncontrollable impact on the environment and human health.[203–205] Among the organic pollutants, causing water pollution are methylene blue (MB), methyl orange (MO), congo red (CR), rhodamine B (RhB), sulfamethoxazole (SMZ), rose red (RR), and the heavy metal ion Cr(VI).[206]

Air pollution is a pressing issue that affects the health of living organisms, including humans. The rise of industrialization has resulted in a decline in air quality globally. Industrial emissions that are not effectively treated, as well as pollutants emitted from vehicles, trains, planes and ships, including carbon monoxide, nitrogen oxides, hydrocarbons, and lead, contribute significantly to air pollution. Additionally, secondhand smoke, oil smoke, refrigerators, and air conditioners also contribute this issue. Currently, the main source of air pollution is highly toxic gases and particulate matter (PM), among all air pollutants, volatile organic compounds (VOCs) are the most significant indoor and outdoor pollutants, accounting for 68% of the research conducted on photocatalytic air pollutant treatment. Other hazardous gases, such as H_2S, SO_x, NH_3, NO_x, CO, comprise 10% of the research, while particulate matter (PM) accounts for 22%. The air we breathe is vital for our survival, and it is crucial to address the issue of air pollution by mitigating emissions and developing effective treatment methods.[206,207]

The challenges posed by water and air pollution require a comprehensive and effective approach. Despite numerous methods and techniques having been developed, their success has been limited, and new problems continue to arise. To tackle these complex and evolving issues, it is crucial prioritize methods that are efficient, environmentally friendly, simple and cost-effective. Among these, photocatalytic degradation or reduction of pollutants has gained widespread acceptance due to its reliance on sunlight, a free and abundant energy source.

2.3.2 Introduction of MOF-based photocatalysis. The use of TiO_2 as the first catalysts in photocatalysis was a significant breakthrough in the field, which produced electron–hole pairs under UV light, prompting oxidation and reduction reactions.[208] Thus, the discovery gives a strategic orientation: the problem of pollutants can be solved as soon as a material, like TiO_2 is irradiated by UV light, then a large number of electron–hole pairs are produced to induce rapid oxidation and reduction reactions. However, TiO_2 is only sensitive to UV light, which accounts for less than 5% of sunlight, limiting its utilization for sunlight, in which the visible light accounts for nearly 45%. Thus, alternative photocatalysts are explored.[209–214] Among them, MOF materials have gained popularity due to the following properties: high specific surface area (over 6000 $m^2\ g^{-1}$) providing abundant reaction sites;[215] rich topology and tunable porous structure; electron leap platform provided by the metal centers facilitating the separation of electrons and holes in the reaction and thus accelerating the reaction; large-scale expansion and application in industry due to customizable structures. Moreover, MOF-based composites offer a broad range of central metals units and organic linkers that make them a promising option for various photocatalysis production conditions. MOFs act both as solar energy harvesting centers and as organic linkers are irradiated by sunlight, electrons are transferred to the metal centers, which makes MOFs typical semiconductor photocatalyst materials,[216,217] making full use of the sunlight in all wavelengths. MOF-based composites have dispersed conduction and valence bands, and can be identified as molecules in a crystalline lattice, which facilitates the leap of electrons from the top of the valence band to the bottom of the conduction band, thus generating holes, and these active species are involved in oxidation and reduction reactions. Zn-, Zr- and Ti-MOF-based composites exhibit semiconductor-like behavior and are particularly useful for photocatalytic performance. In particular, the Zr-MOF-based composites, such as UiO-66 family, are considered attractive for wastewater treatment applications.[75] Despite their various advantages presented in the field of photocatalysis, MOFs face challenges in maintaining long-term chemical stability in water, except in acidic or alkaline environments. A review of the performance of monometallic, bimetallic, and multi-metallic MOF-based photocatalysts in the field of photocatalysis is provided.

2.3.3 Water remediation

2.3.3.1 Monometallic MOF-based composites. Since the first application of Zn-MOF (MOF-5) to treat phenol in water in 2007,[74] there has been increasing interest in the use of monometallic MOFs for catalytic degradation of contaminants in water. Monometallic MOF-based composites such as those based on Zn, Fe, Co, Ni, Bi, Cu and Zr have all been employed for this purpose.[71–73,218–227] One such example is the Zn-based pillared-layer MOF, NNU-36, which was designed (as shown in Fig. 12a–c) for photocatalytic remediation of water for Cr(VI) reduction and dye degradation under visible light irradiation.[71] This unique MOF structure is constructed using Zn–N bonds, with organic linkers playing the main role in absorbing sunlight. Upon absorption of light energy, the catalyst generates a large number of photogenerated electron and hole pairs. These pairs are then transferred through the Zn–N bonds bridge, formed between metals and ligands, to achieve an effective separation of electrons and holes. The separated electrons accumulate at the bottom of the conduction band, while the positively charged holes gather at the top of the valence band, participating in the photocatalytic oxidation and reduction reactions, respectively. As a result of the concentration difference, a continuous flow of electrons and holes are produced, which rapidly move and participate in the photocatalytic reaction (as depicted in Fig. 12c). Despite the effective separation of electrons and holes, their attraction to positive and negative charges leads to recombination, which in turn hampers the photocatalytic efficiency of the system. To address this issue, researchers have developed methods to trap electrons and holes separately, which greatly enhances the photocatalytic efficiency of the system. For example, the Shun Li group synthesized porous ZnO nanocages/rGO/carbon sponge derived from Zn-MOF (ZIF-8) (as illustrated in Fig. 12d–f) for degradation of organic pollutants in the water.[72] In this system, the porous nanocages MOF-derived ZnO materials are band-aligned on the rGO surface, where the electrons generated

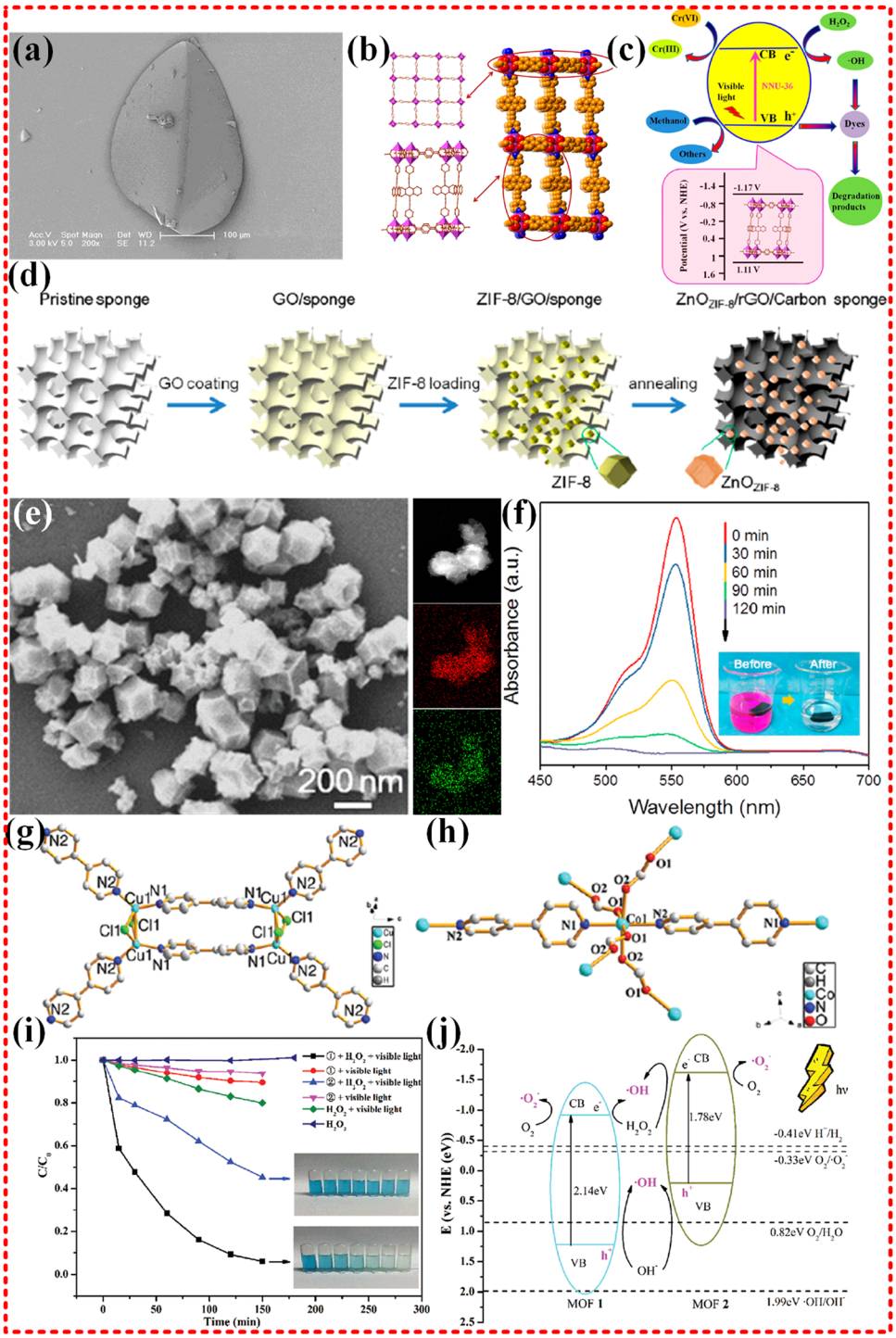

Fig. 12 (a)–(c) FESEM images of as-prepared NNU-36 photocatalysts. Pillared-layer structure of NNU-36, control experiments for the reduction of Cr(VI) under different conditions, control experiments for the photocatalytic degradation of RhB over NNU-36, schematic illustration of photocatalytic reduction Cr(VI) and degradation of dyes over NNU-36 under visible light irradiation, reproduced with permission from ref. 71, Copyright (2017) American Chemical Society. (d)–(f) Schematic illustration of the fabrication process, the SEM and element mapping images of ZnO_{ZIF-8}, changes of the characteristic absorption of RhB under different irradiation time using ZRCs, schematic illustration of photocatalytic reaction in ZRCs-based microreactor. Reproduced with permission from ref. 72, Copyright (2018) American Chemical Society. (g)–(j) Perspective view of the complex cation of 1 and 2, the MB degradation under different photocatalytic conditions, a schematic illustration of the energy position and MB degradation over two complexes. Reproduced with permission from ref. 218, Copyright (2021) Elsevier.

under solar irradiation are injected into the rGO, preventing recombination of electrons and holes left behind. Additionally, the porous structure and high specific surface area increase contact with the reaction target, while the open transport

channels promote the transport of electrons and ions and speed up the reaction. Furthermore, the carbon-based materials enhance the absorption of sunlight by the reaction system. These factors contribute to the superior photocatalytic performance exhibited by Zn-MOF derivatives. The zinc-based MOF ZIF-8 was utilized by Sujit K. Ghosh's group to protect hybrid bromide perovskites (HBP) nanocrystals in the degradation of toxic organic pollutants in water, yielding good photocatalytic performance. The sodium-like salt topology of the Zn-based MOF prevented nanoparticles from aggregating or escaping from the framework. The hbp@ZIF-8 composites possess a narrow band gap (2.26–3.1 eV), which indicates good light absorption properties.[73] In another study, Co- and Cu-based MOFs were synthesized and utilized for the degradation of MB under visible light (as shown in Fig. 12g–j).[218] These MOFs had different metal centers and ligands, leading to varying band gaps. The band gap of the Co-MOF was significantly smaller than that of the Cu-based MOF, suggesting that electrons could more easily leap to the conduction band bottom and achieve effective electron–hole separation. Notably, the photocatalytic process primarily occurred on the surface of the catalyst rather than inside, which is attributed to the larger particle size of MB relative to the pore size of Cu- and Co-MOF.

2.3.3.2 Bimetallic MOF-based composites. Bimetallic MOF-based composites have been demonstrated to possess more metal sites for ligands than monometallic MOF-based composites. This characteristic gives rise to a multidimensional stereospecific structure that promotes the production of active substances and good conduction channels for enhanced reaction rates. The Fe–Zr-based bimetallic MOF, derived from NH_2-UiO-66 MOF (as shown in Fig. 13a–e), was synthesized by Majid Masteri-Farahani's group for water remediation. This MOF-based composite has shown to effectively degrade organic dyes, such as methyl violet 2B, rhodamine B, malachite green, and MB, as well as tetracycline (TC). The dye and TC removal rates were up to 92% and 85%, respectively. The efficient separation of electron–hole carriers is obviously observed after the introduction of Fe into the Zr-MOF, with photogenerated electrons being transferred to Fe–Cr-MOF. This transfer leads to the reduction of Fe^{3+} to Fe^{2+}, which accelerates the photocatalytic process.[228]

Indeed, bimetallic MOFs have been found to enhance the efficiency of photocatalytic remediation of water compared to monometallic MOFs. For instance, Zn–Co-based bimetallic nanocages MOF (shown in Fig. 13f–i) were utilized in the photocatalytic removal of organic pollutants, including MB and crystal violet (CV), from water. The nanocages structure of the MOFs provides a large specific surface and reactive sites for superoxide group generation. This in turn, traps photogenerated electrons under visible light and inhibits electron and hole recombination, thereby boosting the photocatalytic performance. The Zn–Co-based nanocages MOF exhibited the 84.3%, 87.9%, and 89.5% of removal of CV, MB, and RhB dye pollutants, respectively.[229] A Fe–Sn-based MOF with a core–shell structure was synthesized and its photocatalytic ability was demonstrated by degrading acid red 3R (AR3R) dye in water with 100% degradation efficiency of AR3R within 30 minutes. The effective charge separation, strong photo-response, and rich active sites make a significant contribution the high photocatalytic efficiency of the material. it is also noteworthy that Fe and its oxides possess good ferromagnetism, which facilitates the catalyst's recovery rate, with over 90% after five cycles.[230] These findings suggest that the performance of monometallic MOFs with good structural stability and high recovery rates can be enhanced by introducing appropriate metals into the MOF. In addition to these representative bimetallic MOFs, several proliferating MOFs have been widely employed in photocatalysis for water remediation of pollutants in water.[231–235] While bimetallic MOFs offer numerous benefits for catalytic reactions, not all metals are suitable for their realization. Catalytic reactions require appropriate reaction sites and effective guiding channels for electron transfer and ion diffusion. Although a bimetallic center creates more metals sites for organic linkers to form ligands, it often comes at the expense of porous structures or guide channels, resulting in the generation of a large amount of reactive material that cannot be quickly transported to participate in the reaction. This not only fails to facilitate the reaction but also inhibits this process.

2.3.3.3 Multi-metallic MOF-based composites. Multi-metal MOF-based composites combine many advantages over mono- and bi-metal ones, including a larger specific surface area, diverse and controllable porous structures, good electron transport properties, and channeling by multiple metals. Bi-based materials are classical photocatalysts in the field of photocatalysis, owing to their unique electronic structure, good light absorption properties, strong redox ability, easily tunable structure, and richer active groups. A novel Zn–Bi–Co based multi-metallic MOFs were synthesized and applied for the treatment of textile wastewater, with CR dye being the primary pollutant. The introduction of Bi and Co metals into the Zn-MOF resulted in better photocatalytic activity (99.6%) for the degradation of CR dye, owing to the newly established interfaces and electron transfer channels that facilitated the transfer of photogenerated electrons while effectively separating them from holes (as shown in Fig. 14a). Furthermore, the introduction of metals into MOFs not only alters their surface morphology, but also increases surface area and the number of active sites, which are all inevitable factors leading to high performance. The superoxide and hydroxyl radicals, which directly depend on the number and separation efficiency of photogenerated electrons and holes, are considered to be the main reactive groups involved in photocatalytic reactions.[236] To explore the potential of multi-metallic MOFs in photocatalytic applications, the Vahid Safarifard group synthesized Zr–Ni–Fe based multi-metallic MOFs derived from Zr-MOF (MOF-808) (shown in Fig. 14b–d) focus on meropenem degradation and Cr(VI) reduction. The study investigated the influence of various factors, such as the amount of catalyst, pH, type of scavenger, drug dose on the catalytic performance. The results showed that the highest efficiency of 100% was achieved within

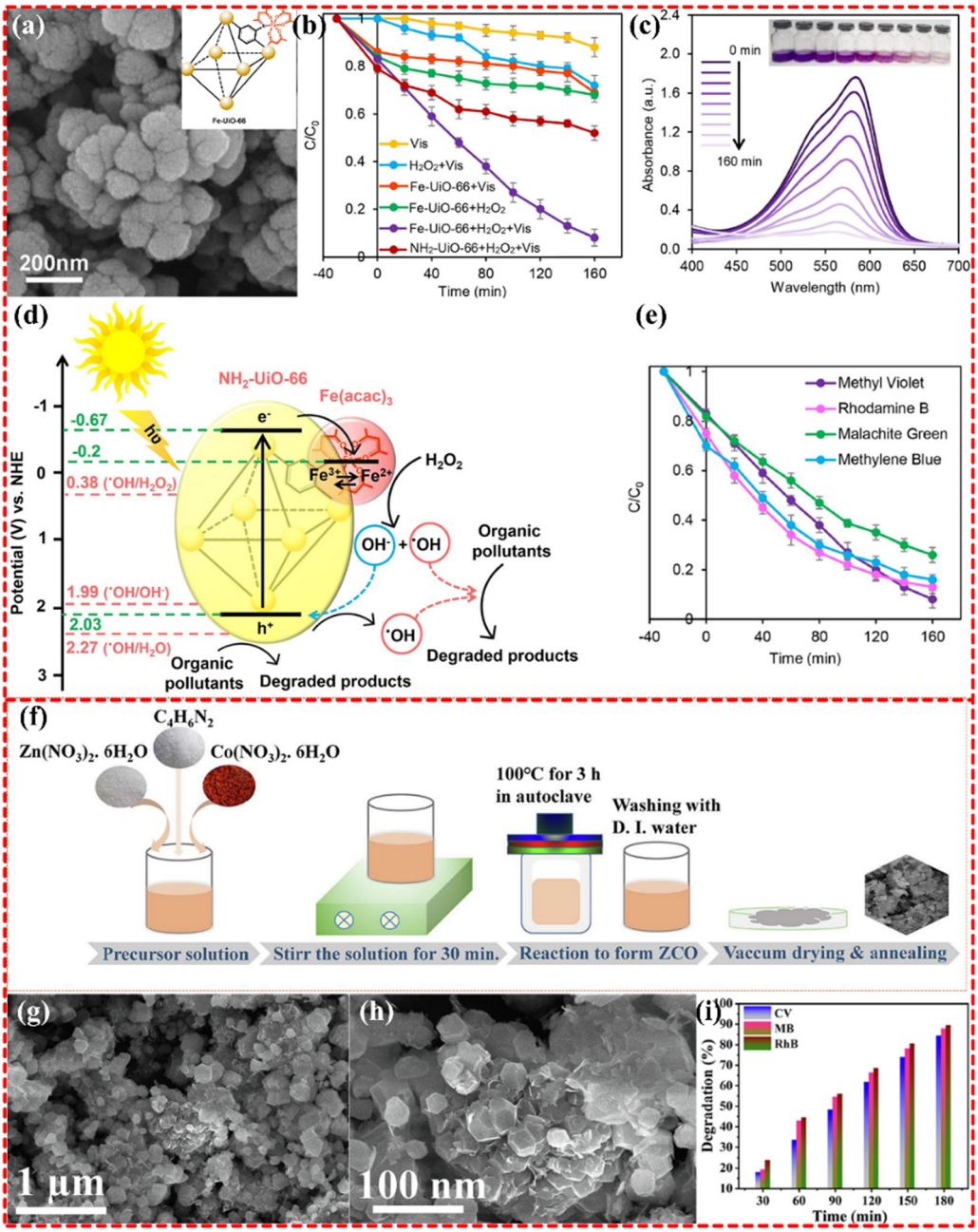

Fig. 13 (a)–(e) FE-SEM images of Fe-UiO-66, photocatalytic degradation of MV in various systems, UV-vis absorption spectra for Fe-UiO-66 + H_2O_2 + Vis system, photo-Fenton degradation of different organic dyes in the presence of Fe-UiO-66, the possible photocatalytic route for degradation of organic pollutants over Fe-UiO-66 photocatalyst. Reproduced with permission from ref. 228, Copyright (2021) Elsevier. (f)–(i) Schematic representation of the formation of ZnCo-MOF derived ZCO nanocages, FESEM image of ZCO at (a) low magnification, and (b) high magnification, histogram of dye degradation percentage estimated for photo catalytically degraded CV, MB, and RhB dyes in the existence of 50 mg of ZCO nanocages at several illumination times. Reproduced with permission from ref. 229, Copyright (2022) Elsevier.

60 minutes at pH = 2 for Cr(VI) reduction and 100% in 60 min for meropenem degradation. Moreover, the catalyst maintained the same degradation efficiency after eight cycles. It is worth noting that Ni and Fe are magnetic metals with a lower bandgap, which facilitates electron transfer, but also easy electron–hole *r* recombination, thereby inhibiting photocatalytic performance. It was found that the best performance was obtained at a ferrite: MOF ratio was 1 : 2, and the introduction of magnetic metals also enhanced the catalyst recovery rate.[237]

Pure TiO_2 is known for its limited photocatalytic performance and low utilisation of sunlight. Recently, X. Sahaya Shajan's group synthesized Zn–Ti–Cd based multi-metallic MOF nanocomposite aerogels and evaluated their photocatalytic performance in the degradation of methyl orange (MO) and

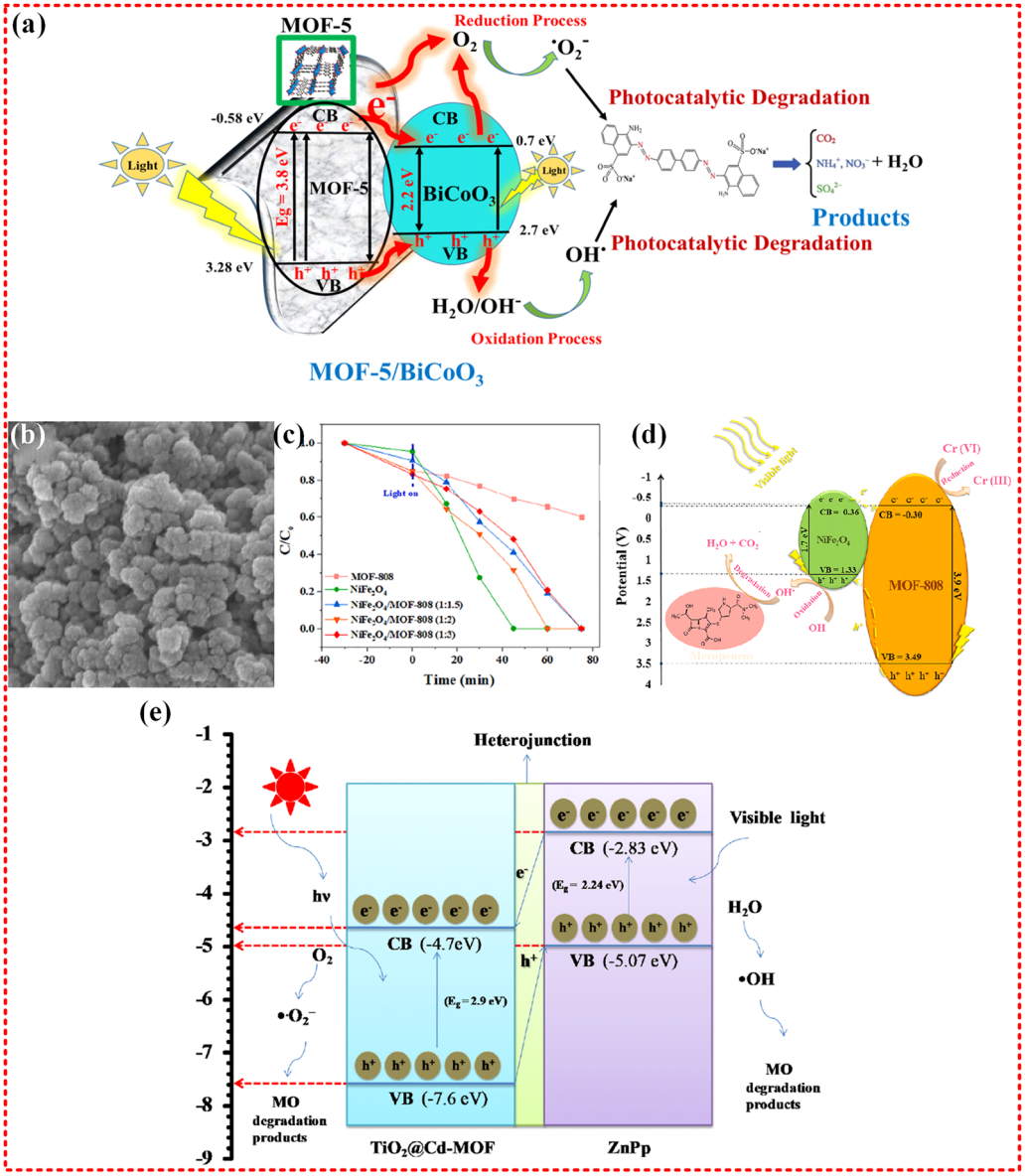

Fig. 14 (a) Photocatalytic mechanism of MOF-5/$BiCoO_3$ composite under light irradiation. Reproduced from ref. 236. (b)–(d) FE-SEM images of samples $NiFe_2O_4$/MOF-808, time-dependent plot for $NiFe_2O_4$, MOF-808, $NiFe_2O_4$/MOF-808 (1 : 1.5, 1 : 2 and, 1 : 3), Proposed mechanism of photocatalytic performance by $NiFe_2O_4$/MOF-808 composite, reproduced with permission from ref. 237, Copyright (2022) Elsevier. (e) Plausible photocatalytic mechanism of MO degradation by porphyrin-sensitized TiO_2@Cd-MOF nanocomposite aerogel heterogenous photocatalyst, reproduced with permission from ref. 238, Copyright (2022) Elsevier.

2-mercaptobenzothiazole (MBT) dye, with maximum degradation efficiency of 94.1% for MO dye. The enhanced performance of the nanocomposite aerogels can be attributed to the generation of multiple interfaces, enhanced light utilization, and efficient electron injection (shown in Fig. 14e).[238] The construction of polymetallic MOF-based composites by introducing magnetic or non-magnetic metals to improve photocatalytic performance has been tried from the past to the present,[239,240] but the development of new MOF-based composites is limited, and it is therefore essential to optimize the use of the existing ones.

The use of MOF-based composites as photocatalysts for water remediation holds great promise. Their multi-void and high specific surface area properties provide numerous reactive sites for photocatalytic reactions. Notably, the customizable nature of MOF-based composites, with various metal centers and tunable photo responsiveness, renders them highly prospective as photocatalysts. Table 3 presents a concise overview of the photocatalytic water remediation performance of monometallic, bimetallic, and multi-metallic MOF-based composites. The table includes key parameters such as the type and concentration of pollutants, catalyst amount, catalytic time, and photocatalytic efficiency. Monometallic MOFs typically exhibit high specific surface area and a well-defined pore structure, facilitating efficient pollutant adsorption and exposure of photocatalytic active sites, thereby enhancing

Table 3 MOF-based composites with mono-, bi- and multi-metallic centers for photocatalysis (water)

Categories	Center metal	Catalyst	Pollutant	$C_{pollutant}$ (mg/L)	$M_{catalyst}$ (mg)	Time (min)	η (%)	Ref.
Mono-	Zn	MOF-5	Phenols	40	80	25	50	74
		NNU-36	Cr(VI)	10	15	60	95.3	71
			RhB			70	96.2	
			MB			80	94.2	
			R6G			90	93.5	
		ZnO/C	RhB	10	50	120	89	72
		ZIF-8	Methyl orange (MO)	0.3	2	100	<10	73
		ZnO@ZIF-8	MB	10	10	240	94.1	241
	Cu	$[Cu_3(L)_2(4,4'\text{-bipy})]$	MB	10	40	100	81.17	222
		$[Cu(4,4'\text{-bipy})Cl]_n$		10	4	150	93.93	218
	Co	$[Co(4,4'\text{-bipy})\cdot(HCOO)_2]_n$		10			54.7	
	Ce	Ce-MOF	RhB	10	30	12	99	220
	Tb	Tb-MOF		10	30	24	95	
	Dy	Dy-MOF		10	30	60	90	
	Cr	MIL-53	MB	0.13	1	60	32	226
	Al					60	30	
	Fe					20	20	
		Fe_3O_4@MIL-100		10	10	180	93.93	242
	Ti	NH_2-MIL-125	MB		—	120	56	224
			Sodium fluorescein (SF)				60	
			RhB				33	
Bi-	FeZr	Fe/NH_2-UiO-66	Tetracycline (TC)	20	10	60	85	228
			Methyl violet 2B			160	87.1	
			RhB				87	
			Malachite green				74	
			MB				84	
	ZnCo	$ZnCo_2O_4$	Crystal violet (CV)	10	50	180	84.3	229
			MB				87.9	
			RhB				89.5	
	FeSn	Fe_3O_4@Sn-MOF	AR3R	—	—	30	100	230
	BiCu	Bi_2O_3/MOF/GO	RhB	10	50	60	85	234
	CuCr	$CuCr_2O_4$/CuO	MB	10	20	35	90	233
			TC			120	95	
	CoFe	Fe/MIL-53-NH_2	Bisphenol A (BPA)	50	5	150	100	232
	CoFe	$CoFe_2O_4$/Fe_2O_3	TC	30	10	80	99.7	231
			BPA				98.1	
			SMX				94.8	
			DFC				97	
			IBP				96.1	
			OFX				96.5	
	CuFe	MIL 53(Fe–Cu)	Ciprofloxacin	15	25	70	57.88	235
Multi-	ZnBiCo	MOF-5/$BiCoO_3$	Congo-red (CR)	25	10	90	99.6	236
	NiFeZr	$NiFe_2O_4$/MOF-808	Cr(VI)	10	15	60	100	237
	ZnTiCd	Zn/TiO_2@Cd-MOF	Methyl orange (MO)	10	10	60	97.4	238
	CoNiCuW	MOF/$CuWO_4$	MB	—	10	135	98	240
			4-NP			105	81	
	ZnBiFe	MOF/$BiFeO_3$	MB	20	30	100	93	239

photocatalytic efficiency. Metals such as Ti, Zn, and Fe within these MOFs demonstrate robust photocatalytic activity under UV irradiation, generating sufficient electron–hole pairs to initiate pollutant degradation in water. Furthermore, mono-metallic MOFs generally possess favorable chemical stability that persists throughout the photocatalytic process, while their structures and properties are relatively straightforward to manipulate and optimize. Nonetheless, their limited light absorption and increased propensity for electron–hole pair recombination highlight the rationale for exploring multi-metal MOFs.

MOF-based composites with diverse metal centers exhibit distinct electronic structures and light-absorbing abilities, resulting in a broad and effective light-absorbing range encompassing both visible and UV regions—a critical characteristic for effective photocatalysis. Multi-metallic MOFs feature multiple active sites capable of simultaneously providing photocatalytic, catalytic, and adsorption capacities, expanding their applicability across various water pollutant types. However, the synthesis of multi-metallic MOFs is inherently complex, and interactions between different metal ions within these frameworks can potentially hinder overall material performance and stability. Therefore, rigorous optimization and control are essential during the design and synthesis phases to ensure optimal functionality and durability of the materials. Furthermore, the efficiency of photocatalysis in water remediation is influenced by the lifetime of the excited state after the photoexcited catalytic reaction. The judicious selection and

modulation of metal centers in MOF-based composites can extend the excited state lifetime, significantly enhancing catalytic performance. The energy levels of catalytically active sites are intricately linked to the electronic energy levels of metal centers, and an optimal alignment between the two facilitates more facile electron transfer. The selection of metal centers, in general, plays a significant role in determining the stability of MOF-based composites catalysts. Certain metals exhibit heightened sensitivity to light and chemical environments, making them more susceptible to degradation. For sustained efficacy in photocatalytic water remediation applications, the development of MOF-based composites with long-term stability is crucial.

2.3.4 Atmosphere purification

2.3.4.1 Monometallic MOF-based composites. Recently, Yun Hu's group synthesized a Fe-based monometallic MOF (MIL-100) photocatalyst (as shown in Fig. 15a–e) for the degradation of a toxic VOC (acetaldehyde) and for bacteriostasis against *Escherichia coli* in indoor applications. The abundant exposure of unsaturated Fe^{2+} active sites lead to high catalytic performance by promoting the separation of photogenerated electrons and holes, thus participating in redox reactions. Superoxide groups are generated by the reaction of adsorbed oxygen with photogenerated electrons, while Fe^{2+} ions act as a mere bridge for electron transport, rather than as a beneficiary, as evidenced by the absence of reduced Fe^{+}. This abundant Fe^{2+} active sites could reduce O_2 to H_2O through a 4-electron pathway.[67] The conversion between Fe^{3+} and Fe^{2+} plays a crucial role in the separation of photogenerated electron-holes, which makes Fe-based MOFs unique. This property was also exploited by Xiao Wang's group to achieve effective treatment (over 80% for degradation of xylenes and styrene) of gaseous BTXS (benzene, toluene, xylenes and styrene) pollutants with large molecular sizes using a photocatalyst based on Fe MOF (MIL-100). In addition to the properties of Fe ions, the micro- and mesopores (2–10 nm) in Fe-based MOFs yield a large number of active sites for catalytic reactions, and the unsaturated acidic Fe_3–O sites facilitated the capture of BTXS

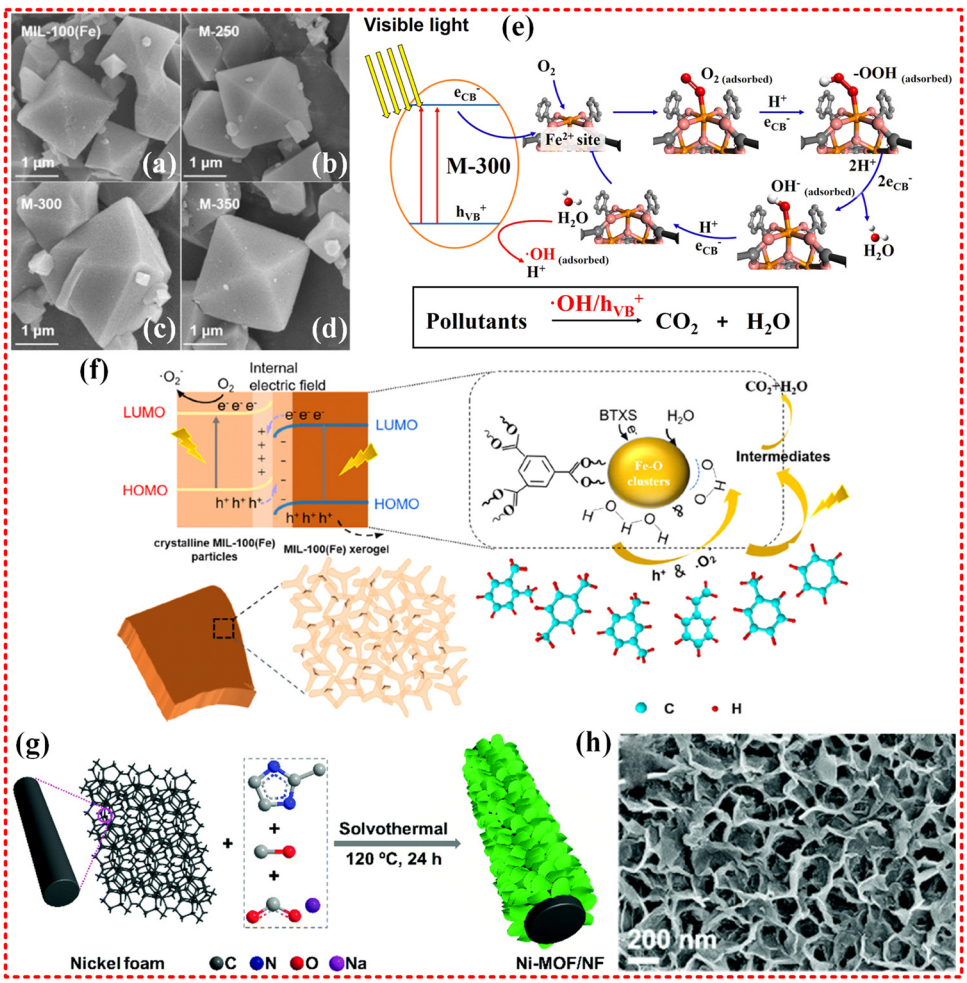

Fig. 15 (a)–(e) SEM images, and the mechanism for photocatalytic oxidation on M-300 catalyst under visible light, *E. coli* removal rate under the visible light and photocatalytic performance of acetaldehyde degradation under the sunlight, reproduced with permission from ref. 67, Copyright (2023) Elsevier. (f) The mechanism of photocatalytic degradation of BTXS on the MIL-100(Fe) MOF/MOX homojunctions. Reproduced with permission from ref. 70, Copyright (2021) Elsevier. (g) and (h) Illustration of the *in situ* preparation of Ni-MOF/NF, SEM images of Ni-MOF/NF, reproduced with permission from ref. 69, Copyright (2020) RSC Pub.

molecules (as shown in Fig. 15f).[70] A novel synthetic strategy for the synthesis of an acidic Ti-based MOF (MIL-125) for the degradation of chlorobenzene and toluene under visible light irradiation, which exhibited excellent photocatalytic properties by mineralizing 80% of pollutants in a shorter period of time, with a still impressive efficiency of over 90% after four cycles. Superoxide groups and hydroxyl radicals were identified as the main reactive oxygen radicals during photocatalytic reactions.[66] Another notable study by Taicheng An's group focused on the synthesis of a novel porous nickel foam (Ni-MOF/NF) (as shown in Fig. 15g–h), for the degradation of ethyl acetate, which achieved a remarkable removal efficiency of 98.1% and a mineralization efficiency of 86.6%. The high exposure of active sites, strong light absorption centers, and fast electron and mass transport channels and pathways in the Ni-based MOF foam were attributed to its excellent photocatalytic removal efficiencies for typical VOCs emitted from the paint spray industry.[69] The Zn-based MOF (ZIF-8) has also shown promising results, exhibiting >99.99% photocatalytic killing efficiency against airborne bacteria in 30 min and 97% particulate matter (PM) removal under visible light.[68] Additionally, Fe-, Zr-, and Re-MOF-based composites have been highly effective for the removal of toluene, ozone, 2-chloroethyl ethyl sulfide (CEES), carbon dioxide (CO_2, CO *etc.*), which are common polluting gases in everyday life.[243–247]

2.3.4.2 Bimetallic MOF-based composites. MOFs with bimetallic centers have been found to perform better than those with monometallic centers in response to airborne contaminants. This is due to a fundamental increase in electron channeling and faster movement. Toluene diisocyanate (TDI) and methylene diphenyl diisocyanate (MDI) are semi-volatile organic compounds and account for more than 90% of the isocyanate family in the world's total consumption. In recent research conducted by Majid Kermani's group, Bi–Ti-based bimetallic MOF-based composites were synthesized for degradation of TDI and MDI in the air. The results of this study showed that the bimetallic MOF-based composites were able to degrade more than 90% of isocyanates with synergistic effect coefficient of 2.03 and 2.34 for TDI and MDI, respectively. Interestingly, the removal rate using air as a carrier was found to be 61.7%, while in pure oxygen it was 80.8%.[248] Vahid Safarifard and colleagues synthesized a Co–Zn-based MOF for enhancing the photocatalytic aerobic oxidation of benzyl alcohol. The bimetallic MOF-based composites were prepared through metal ion exchange and effectively improved the photocatalytic performance for benzyl alcohol oxidation. The introduction of new metal ions increases the energy level in the conduction band of the original catalyst and facilitates the jump of electrons from the top of the valence band to the conduction band. Co acts as electron traps and immobilizes photogenerated electrons, which are then rapidly transferred to react with oxygen to produce super-positive groups.[249] In the same year, Vahid Safarifard's group also demonstrated that the Co–Zn-based bimetallic MOF-based composites exhibit good photocatalytic properties in aerobic oxidation of benzyl alcohol to benzaldehyde (as shown in Fig. 16a–e). The effective separation of photogenerated electron–hole pairs and good light absorption are considered to be the main factors, which of course cannot be achieved without the role of Co and Zn bimetallic centers. The electrons and holes serve as the main reactive species.[250] Moreover, the Co–Fe-based bimetallic MOF-based composites with dye-sensitized were synthesized by Zhengquan Li and coworkers for photocatalytic CO_2 reduction (as shown in Fig. 16f–i). The introduction of Ru metals facilitated the injection of photogenerated electrons into Fe-MOF, resulting in a negative shift of −0.15 V (*vs.* RHE) in its LUMO potential. This bimetallic MOF-based composites showed excellent photocatalytic performance with CO_2-to-CO activity of 1120 μmol g^{-1} h^{-1}. Additionally, Co metal ions were used to adapt the electronic structure of Fe-MOF, resulting in a remarkable photocatalytic activity of 1637 μmol g^{-1} h^{-1}.[251] In another study, the Fe–Ni MOF (as shown in Fig. 16j–o) was used for removal of hazardous indoor VOCs, achieving average adsorption and removal rates of 94.25% and 75.95%.[252] There are numerous examples of improved catalytic performance of MOF-based composites catalysts through the introduction of different metals. These improvements can be attributed to various factors, such as changes in electronic structure, electron transport channels, absorbance, and multivalent metal ion conversion for electron transfer.[252–259]

2.3.4.3 Multi-metallic MOF-based composites. Taicheng An and colleagues synthesized Z-scheme Au–Ti–Zr based multimetallic MOF-based composites for photocatalytic degradation of ethylacetate (as shown in Fig. 17a–e). The incorporation of Au directly broadens the light absorption range from the UV to the visible region, which is attributed to Au's excellent localized surface plasmon resonance properties. Moreover, the ultrafine Au species serve as an electron mediator, facilitating the transfer of photogenerated electrons and thereby enhancing the separation efficiency of photogenerated electron pairs. This efficient separation process accelerates the generation of reactive groups, such as superoxide, hydroxyl radicals, reaching 85%VOCs mineralization and 94.6% ethyl acetate degradation efficiency.[260] Au–Ti–Zn-MOF-based composites were synthesized by Wenxin Dai and colleagues for the catalytic oxidation of CO at room temperature (as shown in Fig. 17f–l). Notably, while the base MOF was substituted, it is reasonable to expect that the resulting catalyst structures would be distinct from aforementioned multi-metal MOF-based composites catalysts with using of Au and Ti. Particularly, ZIF-8 MOF is known to enhance the roughness of this composite catalyst, thereby preventing Au migration and aggregation. Additionally, ZIF-8 with abundant delocalized electrons of π bond could act as an electron donor and provide multiple electron transport channels that accelerate the transport of photogenerated electrons, and these behaviors together contribute to good photocatalytic performance.[261] Multi-metallic MOF-based composites applications are relatively limited due to the constraints posed by the synthesis and use of these catalysts in the air-catalyzed reactions. Specifically, only a limited number of species can be

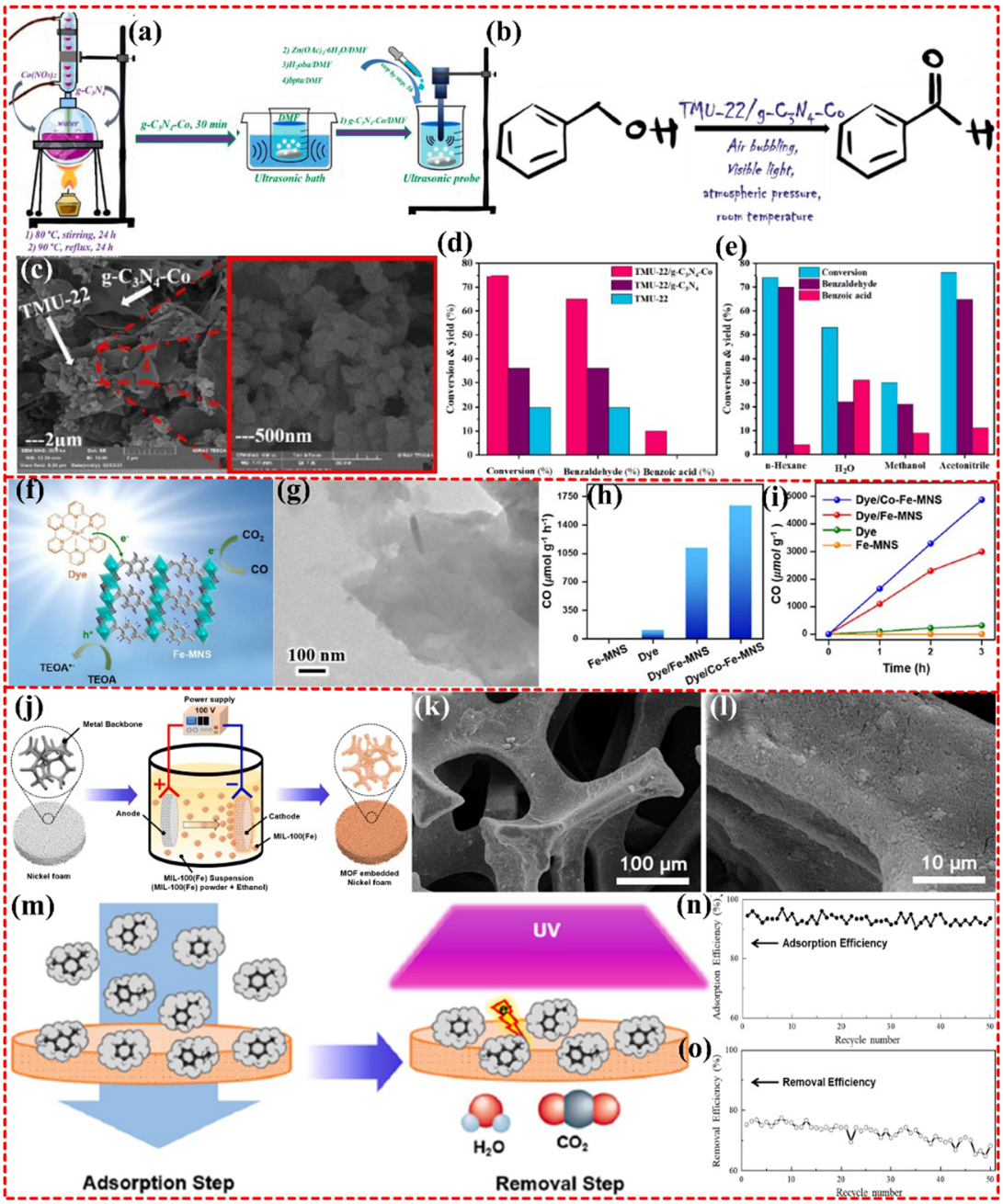

Fig. 16 (a)–(e) The schematic diagram for the synthesis of g-C_3N_4-Co, and (b) fabrication of TMU-22/g-C_3N_4-Co composite, the model reaction for photocatalytic aerobic oxidation of benzyl alcohol to benzaldehyde, SEM of TMU-22/g-C_3N_4-Co composite, checking the effect of composite composition and solvent. Reproduced with permission from ref. 250, Copyright (2022) Elsevier. (f)–(i) TEM image of the Co–Fe-MNS catalyst, photocatalytic CO production of 2D Fe-MNS, Dye, Dye/Fe-MNS, and dye/Co–Fe-MNS, time-dependent photocatalytic activities over different samples. Reproduced with permission from ref. 251, Copyright (2021) Elsevier. (j)–(o) A schematic of the electrophoretic deposition setup, the fabricated MIL-100(Fe)-based PMF, a scheme showing the photocatalytic decomposition of VOCs on to the PMF, the adsorption cycling test (top) and the removal performance (bottom) for 50 cycles. Reproduced with permission from ref. 252, Copyright (2021) Elsevier.

synthesized and used for catalytic reactions in air. Furthermore, metal ions have to be protected from oxidation to ensure an abundance of reaction sites, which becomes an increasingly challenging achievement as the number of metal species in MOFs increases. Precious metals are often favored to meet these conditions, but this comes at a high cost.

For photocatalytic degradation of hazardous gases in air, in addition to a large specific surface area providing sufficient reactive sites for the generation and effective separation of electron–hole pairs, additional features are necessary such as: (a) a highly tailored pore structure to improve adsorption efficiency, (b) faster electron transport, (c) sufficiently high

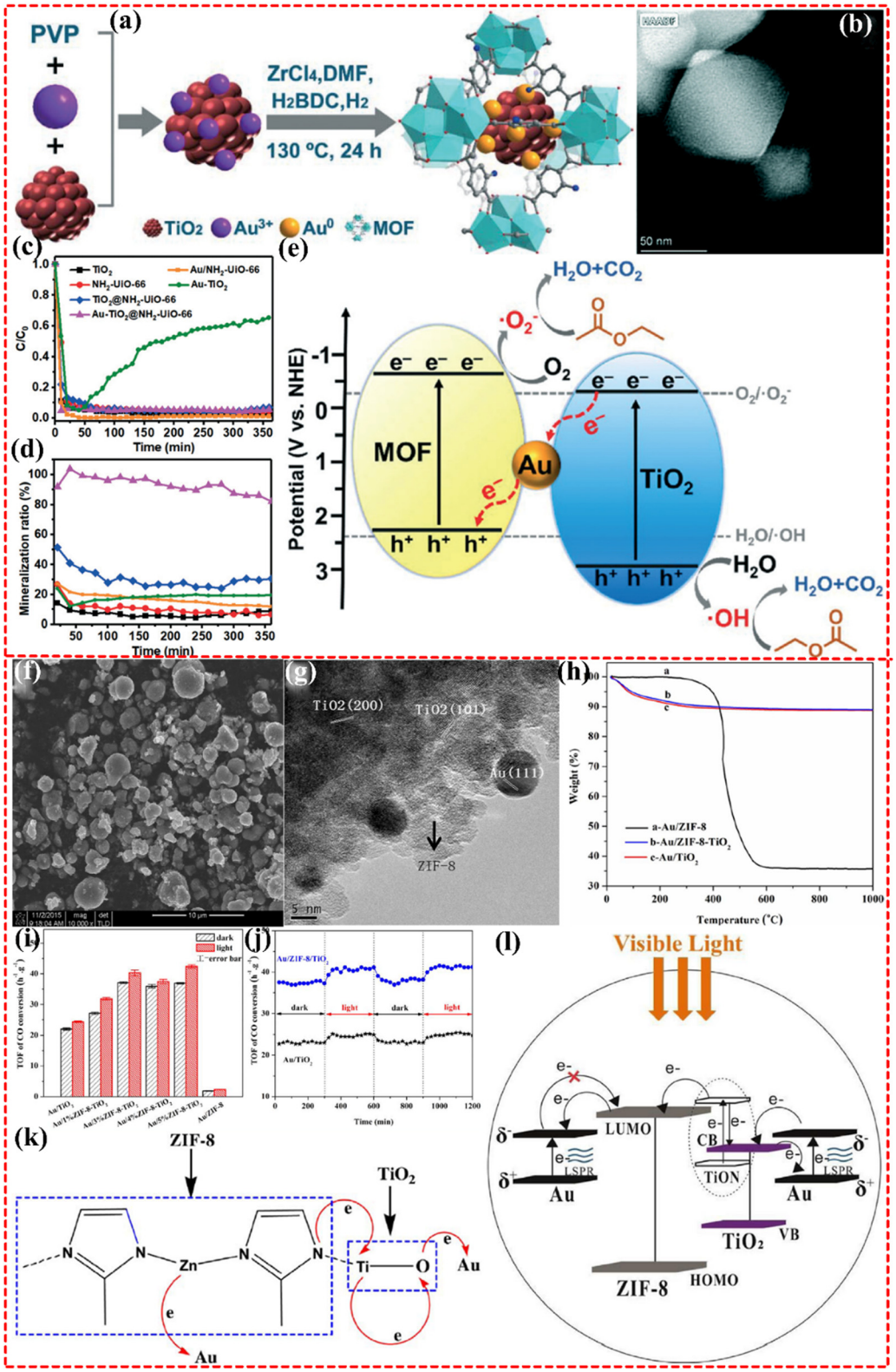

Fig. 17 (a)–(e) Illustration of the preparation of the Au–TiO_2@NH_2-UiO-66 nanocomposite, HAADF-STEM images, removal efficiencies (a) and mineralization efficiencies (b) of ethyl acetate during photocatalytic oxidation, possible reaction mechanism for the photocatalytic oxidation of ethyl acetate over Au–TiO_2@NH_2-UiO-66 under visible light irradiation. Reproduced with permission from ref. 260, Copyright (2021) Royal Society of Chemistry. (f)–(l) SEM and TEM images of Au/ZIF-8-TiO_2, thermogravimetry pattern of samples, the possible charge transfer behavior among Au, TiO_2 and ZIF-8 during the process of forming Au/ZIF-8-TiO_2 structure, proposed schematic of electron transfer among Au, TiO_2 and ZIF-8 sites over Au/ZIF-8-TiO_2 under visible light irradiation. Reproduced with permission from ref. 261, Copyright (2017) Elsevier.

Table 4 MOF-based composites with mono-, bi- and multi-metallic centers for photocatalysis (air)

Categories	Center metal	Catalyst	Pollutant	$C_{pollutant}$ (ppm)	$M_{catalyst}$ (mg)	Time (h)	η (%)	Ref.
Mono-	Fe	M-300	VOCs (acetaldehyde, acetone)	1	25	360	>90	67
		MIL-100(Fe) MOF/MOX	Benzene	25	50	140	23	70
			Toluene				41	
			Xylenes				83.1	
			Styrene				83	
		NH_2-MIL 101(Fe)	Gaseous toluene	4	20	600	79.4	243
		MIL-100(Fe)	Ozone	45	30	6000	100	245
	Ti	P-NH_2-MIL-125	Chlorobenzene	1	10	60	100	66
			Toluene			20	96	
	Ni	Ni-MOF/NF	Ethyl acetate	70	—	360	98.1	69
	Zn	Zn-MOF	PM	—	50	30	97	68
	Zr	NH_2-UiO-66	Ethyl acetate	70	100	360	95.3	260
Bi-	CoZn	TMU-22(Zn/Co)	Benzyl alcohol	0.5	60	250	73	249
		TMU-22/g-C_3N_4-Co	Benzyl alcohol	1	20	300	75	250
	TiBi	BiOI@MOF/zeolite	Toluene-diisocyante	10	—	180	98.7	248
			Methylene diphenyl diisocyanate				95.6	
	TiZn	ZIF-8 derived carbon-TiO_2	Toluene	25	—	—	76	262
	TiCr	TiO_2/MIL-101(Cr)	Formaldehyde	8	—	200	80	258
			o-Xylene	0.2	—		82	
		5.0-TMCr-60	Toluene	—	25	480	91.4	254
	TiZr	TiO_2@ NH_2-UiO-66 (Zr)	Gaseous styrene	30	—	80	90	255
		TiO_2@NH_2-UiO-66	Ethyl acetate	70	100	360	93.2	260
Multi-	AuTiZr	Au–TiO_2@NH_2-UiO-66	Ethyl acetate	70	100	360	94.6	260
	ZnAuTi	Au/ZIF-8-TiO_2	CO	2.5	50	—	—	261

stability against humidity, temperature, and gas influencing factors, attributing to the different environments in which the reaction occurs, with gases having a large free diffusivity as well as the presence of lower concentrations of hazardous gases. A brief overview of performance of monometallic, bimetallic, and multi-metallic MOF-based composites in the photocatalytic degradation of hazardous atmospheric gases is reported in Table 4. Pollutant type and concentration, amount of catalyst, reaction time and photocatalytic efficiency are listed into it.

The overall performance of monometallic MOF-based composite photocatalysts for the degradation of hazardous gas molecules in air is significantly weaker than that of bimetallic MOF-based composites. Many single-metal-centered MOFs exhibit significant photocatalytic activity primarily in the ultraviolet spectrum, which comprises a minor portion of sunlight. This restricts their utility in the visible spectrum, necessitating material modifications to broaden their light absorption capabilities. While the metal ions within monometallic MOFs serve as active sites, effectively capturing light energy and initiating electron–hole pair generation, the propensity for electron–hole recombination during photocatalysis diminishes their efficiency. Therefore, strategic material design and modification are imperative to mitigate electron–hole complexation and bolster photocatalytic efficacy. In particular, the lower catalytic efficiency of Fe based monometallic MOF-based composites may be attributed to the fact that metal Fe has lower common oxidation states, *i.e.*, +2 and +3 valence states, and usually higher oxidation states imply easier electron transfer phenomena. Whereas monometallic MOF-based composites with higher common oxidation states such as those with Ti (+2 and +4) and Zr (+4) exhibited higher photocatalytic performance under lower pollutant concentrations. This is attributed to the fact that monometallic MOF-based composites have only one metal center, which implies limited light absorption, electron generation and transfer capability.

On the contrary, bimetallic MOF-based composites have two different metal centers, the synergistic effect between them can improve the ability of light absorption, electron transfer and generation of reaction intermediates, thus achieving higher photocatalytic performance. In addition, the two heterogeneous metal centers slow down the compounding rate of electron–hole pairs, attributing to that the introduction of multi metals can create different electronic energy levels, thus facilitating the separation of photogenerated electrons and holes, furtherly increasing the lifetime of photogenerated electrons and holes, and improve the photocatalytic efficiency. Various metal centers offer diverse active sites that can augment the capture and degradation of pollutants. For instance, the combination of Pt and Au can yield exceptional catalytic activity, whereas iron and cobalt can improve magnetic separation capabilities.

Therefore, Ti elements with higher oxidation states are mostly used in bi- and multi-metallic MOF-based composites to form a synergistic effect to achieve better photocatalytic efficiency at low concentrations of pollutants. The few research works on MOF-based composites photocatalysts with multi-metal centers have shown that more metal centers are often accompanied by more complex structures, thus complicating the generation of multiple effects, which can further limit practical applications.

3. Conclusions and perspectives

This review provides a critical assessment of the recent advancements in MOF-based composites featuring monometallic, bimetallic, and multi-metallic centers, with a focus on their applications in detecting, absorbing, and degrading environmental pollutants. The components tunability of MOF-based composites by selecting and tailoring metal centers allows them to meet the needs of specific applications. Specifically, the discussion centers on their efficacy in hazardous gases sensing, EMWA, and the degradation of pollutants in both aqueous and atmospheric environments. Among them, the molecular sieve effect being considered unique in MOF-based composites with network structure of large and small pores are employed for hazardous gases sensing applications. The multi-channel structures are designed in the MOF-based composites by changing the chosen metals and post-treatment processes to enhance conductive and magnetic properties for EMWA, and rich active site and electron transport properties for degradation of pollutants in both aqueous and atmospheric environments.

In the following points, more specific conclusions and perspectives are provided:

(1) Employing only one type of metal may result in relatively low selectivity, limiting the material's capability to discern and detect specific gases. The incorporation of certain additional metal ions into MOFs evidently enhances their performance in hazardous gases sensing. However, challenges related to structural instability arise from mismatches between the incorporated metals. Relatively intricate synthesis processes lead to high production costs, restricting further applications.

(2) Multi-metallic MOF-based composites are very limited in hazardous gases sensing applications. Different factors limit sensor applications, such as the stability of multi-metallic MOFs, especially in high temperature or humidity environments for gas sensing, the structural damage or inactivation of the active sites of polymetallic MOFs. Moreover, no study has yet been able to demonstrate that the multi-metallic MOFs exhibit obvious advantages in terms of hazardous gas sensing compared to mono- and bi-metallic MOFs. The latter are highly favored due to easier synthesis methods and better structural stability.

(3) The material prerequisites for MOFs in EMWA encompass two main aspects. Firstly, the central metal must possess magnetic properties to effectively absorb the magnetic component of the EMWs. Secondly, the adoption of a multi-channel design is essential to enhance conductivity characteristics. Consequently, the design focus shifts towards the incorporation of multiple metals, with emphasis on magnetic metals, such as Co, Ni, and Fe. This strategic utilization of multi-metal MOFs, particularly those endowed with magnetic properties, holds considerable promise in advancing the performance of EMW absorbers.

(4) Relying solely on dielectric losses or magnetic losses would be unwise, but combination of magnetic and dielectric-based MOFs could potentially overcome the limitations of a lack of magnetism and make it the best option in the EMWA field. Furthermore, multi-metallic MOFs are capable of covering a broader range of EMW frequencies. This is attributed to the unique electronic structures and magnetic properties of the various metals involved, which enable these materials to absorb both low and high-frequency EMWs. The presence of multiple metal in MOFs enhances both dielectric loss and magnetic loss through the synergistic interactions among the different metals. Dielectric loss results from the energy dissipation during the polarization process within the material, while magnetic loss arises from the magnetization process of the magnetic metals. The integration of these two mechanisms significantly enhances the EMWA performance.

(5) Multi-metallic MOFs can absorb EMWs through various mechanisms, including conductive loss, magnetic loss, dielectric loss, and multiple scattering. The combination of different metal centers and organic ligands generates multiple absorption mechanisms, further enhancing the materials' absorption efficiency. For instance, the presence of heterogeneous atoms and interfaces provided interfacial polarization centers and defective polarization centers, driving polarization losses into action, resulting in enhancing impedance matching properties.

(6) By adjusting the types and ratios of metal ions and organic ligands, the physical and chemical properties of MOFs—such as electrical conductivity, magnetic permeability, and dielectric constant—can be precisely tuned to optimize their EMWA properties. However, structural stability and durability pose significant challenges for multi-metallic MOFs, particularly at high temperatures or under strong electromagnetic field environments. Ensuring the consistency and reproducibility of the performance of multi-metallic MOFs in large-scale production remains a difficult task, confining their application largely to experimental research stages.

(7) MOFs with diverse metal centers result in a broad and effective light-absorbing range encompassing both visible and UV regions—a critical characteristic for effective photocatalysis. Furthermore, the efficiency of photocatalysis in water remediation is influenced by the lifetime of the excited state after the photoexcited catalytic reaction. The judicious selection and modulation of metal centers in MOFs can extend the excited state lifetime, significantly enhancing catalytic performance, attributing to different metal centers exhibit different electron affinities and conductivities.

(8) A highly tailored pore structure to improve adsorption efficiency, faster electron transport, and a sufficiently high stability to against humidity, temperature, and gas influencing factors are necessary as MOF materials under different environments in which the reaction occurs, with gases having a large free diffusivity as well as the presence of lower concentrations of hazardous gases.

(9) Multi-metallic MOF applications are relatively limited due to the constraints posed by the synthesis and use of these catalysts in the air-catalyzed reactions. The synthesis of multi-metallic MOFs is complex and not ideal when strict microstructural and phase homogeneity are required. Additionally, multi-metallic MOFs may experience dissolution or

reorganization of metal ions during the reaction process, resulting in partial structural collapse or reduced activity. The use of multiple metal precursors in the synthesis further increases material costs and process complexity. Furthermore, metal ions have to be protected from oxidation to ensure an abundance of reaction sites, which becomes increasingly challenging as the number of metal species in MOFs increases. Precious metals are often favored to meet these conditions, but this comes at a high cost.

Data availability

Data sharing is not applicable to this review manuscript ''Multi-Metallic MOFs based Composites for Environmental Applications: Synergizing Metal Centers and Interactions'' as no datasets were generated or analysed during the current review work.

Conflicts of interest

The authors declare that they have no known competing financial interests or personal relationships.

Acknowledgements

The authors acknowledge the funding support from the financial support by China Scholarship Council (202106970006). The authors also acknowledge the 6G-life project (project no. 16KISK001K), VolkswagenStiftung project (grant no. 96632, 9B396), EU project ''SMELLODI'' (grant no. 101046369), the SAB project ''KoMMet'' funded by the State Ministry of Science and Cultural Affairs of Saxony, Germany (grant agreement ID: 100715133), and Cluster of Excellence ''Centre for Tactile Internet with Human-in-the-Loop'' (CeTI, project ID 390696704) of TUD Dresden University of Technology for support.

References

1 I. Abdalla, A. Elhassan, J. Yu, Z. Li and B. Ding, A hybrid comprised of porous carbon nanofibers and rGO for efficient electromagnetic wave absorption, *Carbon*, 2020, **157**, 703–713.
2 Y. Zhang, J. Zhang, X. Wang, Z.-H. Liu, S. Bi and Z.-L. Hou, *et al.*, Metal–organic frameworks derived carbon nanotube and carbonyl iron composite materials for broadband microwave absorbers with a wide filling range, *J. Magn. Magn. Mater.*, 2022, **555**, 169391.
3 M. Chong, B. Jin, C. Chow and C. Saint, New developments in photocatalytic water treatment technology: a review, *Water Res.*, 2010, **44**, 2997–3027.
4 J. Schneider, M. Matsuoka, M. Takeuchi, J. Zhang, Y. Horiuchi and M. Anpo, *et al.*, Understanding TiO_2 photocatalysis: mechanisms and materials, *Chem. Rev.*, 2014, **114**, 9919–9986.
5 J. L. C. Rowsell and O. M. Yaghi, Metal–organic frameworks: a new class of porous materials, *Microporous Mesoporous Mater.*, 2004, **73**, 3–14.
6 K. S. Park, Z. Ni, A. P. Côté, J. Y. Choi, R. Huang and F. J. Uribe-Romo, *et al.*, Exceptional chemical and thermal stability of zeolitic imidazolate frameworks, *Proc. Natl. Acad. Sci. U. S. A.*, 2006, **103**, 10186–10191.
7 G. S. Papaefstathiou and L. R. MacGillivray, Inverted metal–organic frameworks: solid-state hosts with modular functionality, *Coord. Chem. Rev.*, 2003, **246**, 169–184.
8 A. Mantion, L. Massüger, P. Rabu, C. Palivan, L. B. McCusker and A. Taubert, Metal−Peptide Frameworks (MPFs): ''Bioinspired'' Metal Organic Frameworks, *J. Am. Chem. Soc.*, 2008, **130**, 2517–2526.
9 S. Ma and H.-C. Zhou, A Metal−Organic Framework with Entatic Metal Centers Exhibiting High Gas Adsorption Affinity, *J. Am. Chem. Soc.*, 2006, **128**, 11734–11735.
10 Y. Liu, V. Kravtsov, R. Larsen and M. Eddaoudi, Molecular building blocks approach to the assembly of zeolite-like metal–organic frameworks (ZMOFs) with extra-large cavities, *Chem. Commun.*, 2006, 1488–1490.
11 S. Kitagawa, R. Kitaura and S. Noro, Functional porous coordination polymers, *Angew. Chem., Int. Ed.*, 2004, **43**, 2334–2375.
12 S. L. James, Metal–organic frameworks, *Chem. Soc. Rev.*, 2003, **32**, 276–288.
13 G. Ferey, Hybrid porous solids: past, present, future, *Chem. Soc. Rev.*, 2008, **37**, 191–214.
14 K. A. Cychosz, A. G. Wong-Foy and A. J. Matzger, Liquid Phase Adsorption by Microporous Coordination Polymers: Removal of Organosulfur Compounds, *J. Am. Chem. Soc.*, 2008, **130**, 6938–6939.
15 B. F. Hoskins and R. Robson, Design and construction of a new class of scaffolding-like materials comprising infinite polymeric frameworks of 3D-linked molecular rods. A reappraisal of the zinc cyanide and cadmium cyanide structures and the synthesis and structure of the diamond-related frameworks $[N(CH_3)_4][Cu_IZn_{II}(CN)_4]$ and Cu_I[4,4′,4″,4‴-tetracyanotetraphenylmethane]$BF_4 \cdot x C_6H_5NO_2$, *J. Am. Chem. Soc.*, 1990, **112**, 1546–1554.
16 H. Li, M. Eddaoudi, M. O'Keeffe and O. M. Yaghi, Design and synthesis of an exceptionally stable and highly porous metal–organic framework, *Nature*, 1999, **402**, 276–279.
17 Y. Zhao, W. Wang, Q. Wang, H. Zhao, P. Li and J. Yan, *et al.*, Construction of excellent electromagnetic wave absorber from multi-heterostructure materials derived from $ZnCo_2O_4$ and ZIF-67 composite, *Carbon*, 2021, **185**, 514–525.
18 Y. Zhao, W. Wang, J. Wang, J. Zhai, X. Lei and W. Zhao, *et al.*, Constructing multiple heterogeneous interfaces in the composite of bimetallic MOF-derivatives and rGO for excellent microwave absorption performance, *Carbon*, 2021, **173**, 1059–1072.
19 N. Zhai, J. Luo, M. Xiao, Y. Zhang, W. Yan and Y. Xu, In situ construction of Co@nitrogen-doped carbon/Ni nanocomposite for broadband electromagnetic wave absorption, *Carbon*, 2023, **203**, 416–425.

20 Z. Wu, W. Li, L. Hou, Q. Wei, H. Yang and Y. Jiang, *et al.*, A novel Sunflower-like MOF@COF for improved photocatalytic CO_2 reduction, *Sep. Purif. Technol.*, 2023, **311**, 123322.
21 W. Wang, H. Zhang, Y. Zhao, J. Wang, H. Zhao and P. Li, *et al.*, A novel MOF-drived self-decomposition strategy for CoO@N/C–Co/Ni–$NiCo_2O_4$ multi-heterostructure composite as high-performance electromagnetic wave absorbing materials, *Chem. Eng. J.*, 2021, **426**, 131667.
22 J. Wang, Q. Wang, W. Wang, P. Li, Y. Zhao and J. Zhai, *et al.*, Hollow Ni/C microsphere@graphene foam with dual-spatial and porous structure on the microwave absorbing performance, *J. Alloys Compd.*, 2021, **873**, 159811.
23 W. Ren, Y. Wang, J. Wang and R. Sun, Hydrothermally synthesized Mo/Zr-MOF photocatalyst for promoting the removal of Cr^{6+} under visible light, *Green Mater.*, 2023, **40**, 1–8.
24 T. Mageto, F. M. de Souza, J. Kaur, A. Kumar and R. K. Gupta, Chemistry and potential candidature of metal–organic frameworks for electrochemical energy storage devices, *Fuel Process. Technol.*, 2023, **242**, 107659.
25 J. Liang, H. Yu, J. Shi, B. Li, L. Wu and M. Wang, Dislocated Bilayer MOF Enables High-Selectivity Photocatalytic Reduction of CO_2 to CO, *Adv. Mater.*, 2023, **35**, 2209814.
26 M. Z. Iqbal, M. Shaheen, M. W. Khan, S. Siddique, S. Aftab and S. M. Wabaidur, *et al.*, Exploring MOF-199 composites as redox-active materials for hybrid battery-supercapacitor devices, *RSC Adv.*, 2023, **13**, 2860–2870.
27 Y. Gao, X.-H. Yi, C.-C. Wang, F. Wang and P. Wang, Effective Cr(VI) reduction over high throughput Bi-BDC MOF photocatalyst, *Mater. Res. Bull.*, 2023, **158**, 112072.
28 J. Zhang, G. Zhou, H. I. Un, F. Zheng, K. Jastrzembski and M. Wang, *et al.*, Wavy Two-Dimensional Conjugated Metal–Organic Framework with Metallic Charge Transport, *J. Am. Chem. Soc.*, 2023, **145**, 23630–23638.
29 M. Wang, Z. Zhang, H. Zhong, X. Huang, W. Li and M. Hambsch, *et al.*, Surface-Modified Phthalocyanine-Based Two-Dimensional Conjugated Metal–Organic Framework Films for Polarity-Selective Chemiresistive Sensing, *Angew. Chem., Int. Ed.*, 2021, **60**, 18666–18672.
30 J. Wang, N. Licciardello, M. Sgarzi and G. Cuniberti, Multifunctional polymer-based nanocomposites for synergistic adsorption and photocatalytic degradation of mixed pollutants in water, *Nanoscale Adv.*, 2024, **6**, 1653–1660.
31 J. Timpel, S. Klinghammer, L. Riemenschneider, B. Ibarlucea, G. Cuniberti and C. Hannig, *et al.*, Sensors for in situ monitoring of oral and dental health parameters in saliva, *Clin. Oral Investig.*, 2023, **27**, 5719–5736.
32 T. Thiele, B. Ibarlucea, T. F. Akbar, C. Werner and G. Cuniberti, StarPEG–heparin biosensors for rapid and portable diagnostics in complex biofluids, *Sens. Diagnostics*, 2022, **1**, 558–565.
33 V. Sessi, B. Ibarlucea, F. Seichepine, S. Klinghammer, I. Ibrahim and A. Heinzig, *et al.*, Multisite Dopamine Sensing With Femtomolar Resolution Using a CMOS Enabled Aptasensor Chip, *Front. Neurosci.*, 2022, **16**, 875656.
34 A. Pérez Roig, B. Ibarlucea, C. Amaro and G. Cuniberti, Vibrio vulnificus marine pathogen detection with thin-film impedance biosensors, *Biosens. Bioelectron.: X*, 2024, **17**, 100454.
35 F. M. Pennisi, A. L. Pellegrino, N. Licciardello, C. Mezzalira, M. Sgarzi and A. Speghini, *et al.*, Synthesis, characterization and photocatalytic properties of nanostructured lanthanide doped beta-$NaYF_4$/TiO_2 composite films, *Sci. Rep.*, 2022, **12**, 13748.
36 L. A. Panes-Ruiz, L. Riemenschneider, M. M. Al Chawa, M. Loffler, B. Rellinghaus and R. Tetzlaff, *et al.*, Selective and self-validating breath-level detection of hydrogen sulfide in humid air by gold nanoparticle-functionalized nanotube arrays, *Nano Res.*, 2022, **15**, 2512–2521.
37 S. Laleh, B. Ibarlucea, M. Stadtmuller, G. Cuniberti and M. Medina-Sanchez, Portable microfluidic impedance biosensor for SARS-CoV-2 detection, *Biosens. Bioelectron.*, 2023, **236**, 115362.
38 B. Ibarlucea, E. E. Yildirim, R. Tetzlaff, A. Ascoli, L.-A. Panes-Ruiz and G. Cuniberti, Nanoscale Mem-Devices for Chemical Sensing, 2023 30th IEEE International Conference on Electronics, Circuits and Systems (ICECS), 2023, pp. 1–5.
39 S. Huang, L. Riemenschneider, L. A. Panes-Ruiz, B. Ibarlucea and G. Cuniberti, Discrimination of Complex Mixtures Using Carbon Nanotubes-based Multichannel Electronic Nose: Coffee Aromas, 2023 IEEE Nanotechnology Materials and Devices Conference (NMDC), 2023, pp. 124–128.
40 S. Huang, B. Ibarlucea, L. A. Panes-Ruiz and G. Cuniberti Rapid Detection of SARS-CoV-2 Antigen Utilizing Machine Learning-Enabled Graphene-Based Smart Gas Sensors, 2023 IEEE International Conference on Metrology for eXtended Reality, Artificial Intelligence and Neural Engineering (MetroXRAINE), 2023, pp. 995–999.
41 S. Huang, A. Croy, L. A. Panes-Ruiz, V. Khavrus, V. Bezugly and B. Ibarlucea, *et al.*, Machine Learning-Enabled Smart Gas Sensing Platform for Identification of Industrial Gases, *Adv. Intelligent Systems*, 2022, **4**, 2200016.
42 S. Huang, A. Croy, A. L. Bierling, V. Khavrus, L. A. Panes-Ruiz and A. Dianat, *et al.*, Machine learning-enabled graphene-based electronic olfaction sensors and their olfactory performance assessment, *Appl. Phys. Rev.*, 2023, **10**, 021406.
43 C. Huang, W. Sun, Y. Jin, Q. Guo, D. Mucke and X. Chu, *et al.*, A General Synthesis of Nanostructured Conductive Metal–Organic Frameworks from Insulating MOF Precursors for Supercapacitors and Chemiresistive Sensors, *Angew. Chem., Int. Ed.*, 2024, **63**, 202313591.
44 C. Huang, X. Shang, X. Zhou, Z. Zhang, X. Huang and Y. Lu, *et al.*, Hierarchical conductive metal–organic framework films enabling efficient interfacial mass transfer, *Nat. Commun.*, 2023, **14**, 3850.
45 S. Fan, J. E. Inkumsah Jnr, E. Trave, M. Gigli, T. Joshi and N. Licciardello, *et al.*, Solar-driven photodegradation of ciprofloxacin and E. coli growth inhibition using a Tm^{3+}

upconverting nanoparticle-based polymer composite, *Chem. Eng. J.*, 2023, **476**, 146877.
46 W. Dargie, J. Wen, L. A. Panes-Ruiz, L. Riemenschneider, B. Ibarlucea and G. Cuniberti, Monitoring Toxic Gases Using Nanotechnology and Wireless Sensor Networks, *IEEE Sens. J.*, 2023, **23**, 12274–12283.
47 X. Ren, Z. Xu, D. Liu, Y. Li, Z. Zhang and Z. Tang, Conductometric NO_2 gas sensors based on MOF-derived porous ZnO nanoparticles, *Sens. Actuators, B*, 2022, **357**, 131384.
48 H. Liu, J. Kong, Z. Dong, Y. Zhao, B. An and J. Dong, *et al.*, Preparation of MOF-derived ZnO/Co_3O_4 nanocages and their sensing performance toward H_2S, *Phys. Chem. Chem. Phys.*, 2023, **25**, 17850–17859.
49 H. C. Zhou, J. R. Long and O. M. Yaghi, Introduction to metal–organic frameworks, *Chem. Rev.*, 2012, **112**, 673–674.
50 H. C. Zhou and S. Kitagawa, Metal–organic frameworks (MOFs), *Chem. Soc. Rev.*, 2014, **43**, 5415–5418.
51 O. Yassine, O. Shekhah, A. H. Assen, Y. Belmabkhout, K. N. Salama and M. Eddaoudi, H_2S Sensors: Fumarate-Based fcu-MOF Thin Film Grown on a Capacitive Interdigitated Electrode, *Angew. Chem.*, 2016, **128**, 16111–16115.
52 M. S. Yao, J. J. Zheng, A. Q. Wu, G. Xu, S. S. Nagarkar and G. Zhang, *et al.*, A Dual-Ligand Porous Coordination Polymer Chemiresistor with Modulated Conductivity and Porosity, *Angew. Chem., Int. Ed.*, 2020, **59**, 172–176.
53 L. S. Xie, G. Skorupskii and M. Dinca, Electrically Conductive Metal–Organic Frameworks, *Chem. Rev.*, 2020, **120**, 8536–8580.
54 L. Sun, C. H. Hendon, S. S. Park, Y. Tulchinsky, R. Wan and F. Wang, *et al.*, Is iron unique in promoting electrical conductivity in MOFs?, *Chem. Sci.*, 2017, **8**, 4450–4457.
55 L. Sun, M. G. Campbell and M. Dinca, Electrically Conductive Porous Metal–Organic Frameworks, *Angew. Chem., Int. Ed.*, 2016, **55**, 3566–3579.
56 M. S. Shah, M. Tsapatsis and J. I. Siepmann, Hydrogen Sulfide Capture: From Absorption in Polar Liquids to Oxide, Zeolite, and Metal–Organic Framework Adsorbents and Membranes, *Chem. Rev.*, 2017, **117**, 9755–9803.
57 W. Niu, K. Kang, Y. Ou, Y. Ding, B. Du and X. Guo, *et al.*, Cobalt ions induced morphology control of metal–organic framework-derived indium oxide nanostructures for high performance hydrogen sulfide gas sensors, *Sens. Actuators, B*, 2023, **381**, 133347.
58 Z. Meng, A. Aykanat and K. A. Mirica, Welding Metallophthalocyanines into Bimetallic Molecular Meshes for Ultrasensitive, Low-Power Chemiresistive Detection of Gases, *J. Am. Chem. Soc.*, 2019, **141**, 2046–2053.
59 G. Maurin, C. Serre, A. Cooper and G. Ferey, The new age of MOFs and of their porous-related solids, *Chem. Soc. Rev.*, 2017, **46**, 3104–3107.
60 J. Liu, W. Wang, G. Li, X. Bian, Y. Liu and J. Zhang, *et al.*, Metal–organic framework-derived CuO tube-like nanofibers with high surface area and abundant porosities for enhanced room-temperature NO_2 sensing properties, *J. Alloys Compd.*, 2023, **934**, 167950.
61 Y. Q. Lan, H. L. Jiang, S. L. Li and Q. Xu, Mesoporous metal–organic frameworks with size-tunable cages: selective CO_2 uptake, encapsulation of Ln^{3+} cations for luminescence, and column-chromatographic dye separation, *Adv. Mater.*, 2011, **23**, 5015–5020.
62 K. Guo, L. Zhao, S. Yu, W. Zhou, Z. Li and G. Li, A Water-Stable Proton-Conductive Barium(II)-Organic Framework for Ammonia Sensing at High Humidity, *Inorg. Chem.*, 2018, **57**, 7104–7112.
63 S. K. Bhardwaj, G. C. Mohanta, A. L. Sharma, K. H. Kim and A. Deep, A three-phase copper MOF-graphene-polyaniline composite for effective sensing of ammonia, *Anal. Chim. Acta*, 2018, **1043**, 89–97.
64 A. Ali, H. H. D. AlTakroori, Y. E. Greish, A. Alzamly, L. A. Siddig and N. Qamhieh, *et al.*, Flexible $Cu_3(HHTP)_2$ MOF Membranes for Gas Sensing Application at Room Temperature, *Nanomaterials*, 2022, **12**, 913.
65 M. Weber, J. H. Kim, J. H. Lee, J. Y. Kim, I. Iatsunskyi and E. Coy, *et al.*, High-Performance Nanowire Hydrogen Sensors by Exploiting the Synergistic Effect of Pd Nanoparticles and Metal–Organic Framework Membranes, *ACS Appl. Mater. Interfaces*, 2018, **10**, 34765–34773.
66 X. Zhang, K. Yue, R. Rao, J. Chen, Q. Liu and Y. Yang, *et al.*, Synthesis of acidic MIL-125 from plastic waste: Significant contribution of N orbital for efficient photocatalytic degradation of chlorobenzene and toluene, *Appl. Catal., B*, 2022, **310**, 121300.
67 J. Qin, Y. Pei, Y. Zheng, D. Ye and Y. Hu, Fe-MOF derivative photocatalyst with advanced oxygen reduction capacity for indoor pollutants removal, *Appl. Catal., B*, 2023, **325**, 122346.
68 P. Li, J. Li, X. Feng, J. Li, Y. Hao and J. Zhang, *et al.*, Metal–organic frameworks with photocatalytic bactericidal activity for integrated air cleaning, *Nat. Commun.*, 2019, **10**, 2177.
69 X. Ding, H. Liu, J. Chen, M. Wen, G. Li and T. An, *et al.*, In situ growth of well-aligned Ni-MOF nanosheets on nickel foam for enhanced photocatalytic degradation of typical volatile organic compounds, *Nanoscale*, 2020, **12**, 9462–9470.
70 L. Chen, X. Wang, Z. Rao, Z. Tang, G. Shi and Y. Wang, *et al.*, One-pot Synthesis of the MIL-100 (Fe) MOF/MOX Homojunctions with Tunable Hierarchical Pores for the Photocatalytic Removal of BTXS, *Appl. Catal., B*, 2022, **303**, 120885.
71 H. Zhao, Q. Xia, H. Xing, D. Chen and H. Wang, Construction of Pillared-Layer MOF as Efficient Visible-Light Photocatalysts for Aqueous Cr(VI) Reduction and Dye Degradation, *ACS Sustainable Chem. Eng.*, 2017, **5**, 4449–4456.
72 Y. Su, S. Li, D. He, D. Yu, F. Liu and N. Shao, *et al.*, MOF-Derived Porous ZnO Nanocages/rGO/Carbon Sponge-Based Photocatalytic Microreactor for Efficient Degradation of Water Pollutants and Hydrogen Evolution, *ACS Sustainable Chem. Eng.*, 2018, **6**, 11989–11998.
73 S. Mollick, T. N. Mandal, A. Jana, S. Fajal, A. V. Desai and S. K. Ghosh, Ultrastable Luminescent Hybrid Bromide

Perovskite@MOF Nanocomposites for the Degradation of Organic Pollutants in Water, *ACS Appl. Nano Mater.*, 2019, **2**, 1333–1340.
74 F. X. Llabrés i Xamena, A. Corma and H. Garcia, Applications for Metal−Organic Frameworks (MOFs) as Quantum Dot Semiconductors, *J. Phys. Chem. C*, 2007, **111**, 80–85.
75 F. Ahmadijokani, H. Molavi, M. Rezakazemi, S. Tajahmadi, A. Bahi and F. Ko, *et al.*, UiO-66 metal–organic frameworks in water treatment: a critical review, *Prog. Mater. Sci.*, 2022, **125**, 100904.
76 B. Wen, H. Yang, Y. Lin, Y. Qiu, Y. Cheng and L. Jin, Novel bimetallic MOF derived hierarchical Co@C composites modified with carbon nanotubes and its excellent electromagnetic wave absorption properties, *J. Colloid Interface Sci.*, 2022, **605**, 657–666.
77 K. Wang, Y. Chen, R. Tian, H. Li, Y. Zhou and H. Duan, *et al.*, Porous Co–C Core–Shell Nanocomposites Derived from Co-MOF-74 with Enhanced Electromagnetic Wave Absorption Performance, *ACS Appl. Mater. Interfaces*, 2018, **10**, 11333–11342.
78 Y. Lu, Y. Wang, H. Li, Y. Lin, Z. Jiang and Z. Xie, *et al.*, MOF-Derived Porous Co/C Nanocomposites with Excellent Electromagnetic Wave Absorption Properties, *ACS Appl. Mater. Interfaces*, 2015, **7**, 13604–13611.
79 J. Li, P. Miao, K.-J. Chen, J.-W. Cao, J. Liang and Y. Tang, *et al.*, Highly effective electromagnetic wave absorbing Prismatic Co/C nanocomposites derived from cubic metal–organic framework, *Composites, Part B*, 2020, **182**, 107613.
80 Z. Zhang, Z. Cai, Z. Wang, Y. Peng, L. Xia and S. Ma, *et al.*, A Review on Metal–Organic Framework-Derived Porous Carbon-Based Novel Microwave Absorption Materials, *Nanomicro Lett.*, 2021, **13**, 56.
81 Q. Yang, Q. Xu and H. L. Jiang, Metal–organic frameworks meet metal nanoparticles: synergistic effect for enhanced catalysis, *Chem. Soc. Rev.*, 2017, **46**, 4774–4808.
82 X. Xu, D. Li, L. Li, Z. Yang, Z. Lei and Y. Xu, Architectural Design and Microstructural Engineering of Metal–Organic Framework-Derived Nanomaterials for Electromagnetic Wave Absorption, *Small Struct.*, 2023, **4**, 2200219.
83 Q. Wang, Q. Gao, A. M. Al-Enizi, A. Nafady and S. Ma, Recent advances in MOF-based photocatalysis: environmental remediation under visible light, *Inorg. Chem. Front.*, 2020, **7**, 300–339.
84 Q. Wang and D. Astruc, State of the Art and Prospects in Metal–Organic Framework (MOF)-Based and MOF-Derived Nanocatalysis, *Chem. Rev.*, 2020, **120**, 1438–1511.
85 Z. Meng, R. M. Stolz, L. Mendecki and K. A. Mirica, Electrically-Transduced Chemical Sensors Based on Two-Dimensional Nanomaterials, *Chem. Rev.*, 2019, **119**, 478–598.
86 Y. M. Jo, Y. K. Jo, J. H. Lee, H. W. Jang, I. S. Hwang and D. J. Yoo, MOF-Based Chemiresistive Gas Sensors: Toward New Functionalities, *Adv. Mater.*, 2022, **35**, 2206842.
87 H. Yuan, N. Li, W. Fan, H. Cai and D. Zhao, Metal–Organic Framework Based Gas Sensors, *Adv. Sci.*, 2022, **9**, 2104374.
88 H. Wei, H. Zhang, B. Song, K. Yuan, H. Xiao and Y. Cao, *et al.*, Metal–Organic Framework (MOF) Derivatives as Promising Chemiresistive Gas Sensing Materials: A Review, *Int. J. Environ. Res. Public Health*, 2023, **20**, 4388.
89 H. Sohrabi, S. Ghasemzadeh, Z. Ghoreishi, M. R. Majidi, Y. Yoon and N. Dizge, *et al.*, Metal–organic frameworks (MOF)-based sensors for detection of toxic gases: A review of current status and future prospects, *Mater. Chem. Phys.*, 2023, **299**, 127512.
90 M. Rezki, N. L. W. Septiani, M. Iqbal, D. R. Adhika, I. G. Wenten and B. Yuliarto, Review—Recent Advance in Multi-Metallic Metal Organic Frameworks (MM-MOFs) and Their Derivatives for Electrochemical Biosensor Application, *J. Electrochem. Soc.*, 2022, **169**, 017504.
91 L. Chen, H. F. Wang, C. Li and Q. Xu, Bimetallic metal–organic frameworks and their derivatives, *Chem. Sci.*, 2020, **11**, 5369–5403.
92 M. Ahmed, Recent advancement in bimetallic metal organic frameworks (M′MOFs): synthetic challenges and applications, *Inorg. Chem. Front.*, 2022, **9**, 3003–3033.
93 Y. Zhou, R. Abazari, J. Chen, M. Tahir, A. Kumar and R. R. Ikreedeegh, *et al.*, Bimetallic metal–organic frameworks and MOF-derived composites: Recent progress on electro- and photoelectrocatalytic applications, *Coord. Chem. Rev.*, 2022, **451**, 214264.
94 S. Abednatanzi, P. Gohari Derakhshandeh, H. Depauw, F. X. Coudert, H. Vrielinck and P. Van Der Voort, *et al.*, Mixed-metal metal–organic frameworks, *Chem. Soc. Rev.*, 2019, **48**, 2535–2565.
95 X. Luo, R. Abazari, M. Tahir, W. K. Fan, A. Kumar and T. Kalhorizadeh, *et al.*, Trimetallic metal–organic frameworks and derived materials for environmental remediation and electrochemical energy storage and conversion, *Coord. Chem. Rev.*, 2022, **461**, 214505.
96 <Review 4.pdf>.
97 C. Z. Wang, J. Chen, Q. H. Li, G. E. Wang, X. L. Ye and J. Lv, *et al.*, Pore Size Modulation in Flexible Metal–Organic Framework Enabling High Performance Gas Sensing, *Angew. Chem., Int. Ed.*, 2023, **62**, 202302996.
98 N. Roney and F. Llados, *Toxicological profile for ammonia*, 2004.
99 S. L. M. Rubright, L. L. Pearce and J. Peterson, chemistry, *Environ. Toxicol. Hydrogen Sulfide*, 2017, **71**, 1.
100 T. Nagano, Practical methods for detection of nitric oxide, *Luminescence*, 1999, **14**, 283–290.
101 Y. Takimoto, A. Monkawa, K. Nagata, T. Gessei, M. Kobayashi and M. Kinoshita, *et al.*, Localized surface plasmon resonance sensing of SO_2 and H_2S using zeolitic imidazolate framework-8, *Sens. Actuators, B*, 2023, **383**, 133585.
102 S. Cao, T. Zhou, X. Xu, Y. Bing, N. Sui and J. Wang, *et al.*, Metal–organic frameworks derived inverse/normal bimetallic spinel oxides toward the selective VOCs and H_2S sensing, *J. Hazard. Mater.*, 2023, **457**, 131734.
103 Y. Zhang, S. Lv, L. Jiang, F. Liu, J. Wang and Z. Yang, *et al.*, Room-Temperature Mixed-Potential Type ppb-Level NO

Sensors Based on $K_2Fe_4O_7$ Electrolyte and Ni/Fe-MOF Sensing Electrodes, *ACS Sens.*, 2021, **6**, 4435–4442.

104 N. Kajal, V. Singh, R. Gupta and S. Gautam, Metal organic frameworks for electrochemical sensor applications: a review, *Environ. Res.*, 2022, **204**, 112320.

105 C. Gao, T. Wang and X. Wang, A NH_3 Gas Sensor Based on Flexible Copper(II) isonicotinate MOF /Reduced Graphene Oxide Composite Modified Interdigital Electrode, *Int. J. Electrochem. Sci.*, 2022, **17**, 220763.

106 P. Thawany, A. Khanna, U. Tiwari, A. Deep, M. Wuilpart and C. Caucheteur, A gold/MXene/MOF composite based optical fiber biosensor for haemoglobin detection, *Eur. Workshop Optical Fibre Sensors (EWOFS 2023)*, 2023, **12643**, 225–230.

107 P. Nizamidin, Q. Yang, X. Du and C. Guo, Optical gas sensing and kinetics of azobenzene modified niobium metal–organic framework film composite optical waveguides, *Opt. Laser Technol.*, 2023, **167**, 109708.

108 D. Y. Nadargi, A. Umar, J. D. Nadargi, S. A. Lokare, S. Akbar and I. S. Mulla, *et al.*, Gas sensors and factors influencing sensing mechanism with a special focus on MOS sensors, *J. Mater. Sci.*, 2023, **58**, 559–582.

109 B. Li, C. Feng, H. Wu, S. Jia and L. Dong, Calibration-free mid-infrared exhaled breath sensor based on BF-QEPAS for real-time ammonia measurements at ppb level, *Sens. Actuators, B*, 2022, **358**, 131510.

110 J. Yanez, E. Ledesma, A. Uranga and N. Barniol, AlN-based HBAR ultrasonic sensor for fluid detection in microchannels with multi-frequency operation capability over the GHz range, 2021 IEEE International Ultrasonics Symposium (IUS), 2021, pp. 1–4.

111 A. Coppola, K. Smettem, A. Ajeel, A. Saeed, G. Dragonetti and A. Comegna, *et al.*, Calibration of an electromagnetic induction sensor with time-domain reflectometry data to monitor rootzone electrical conductivity under saline water irrigation, *Eur. J. Soil Sci.*, 2016, **67**, 737–748.

112 X. Wang, J. Lu, W. Han, J. Yang, B. Jiang and Y. Sun, *et al.*, Co-PBA MOF-derived hierarchical hollow 4@NiO microcubes functionalized with Pt for superior H_2S sensing, *Sens. Actuators, B*, 2021, **342**, 130028.

113 X. Zhang, Z. Zhai, J. Wang, X. Hao, Y. Sun and S. Yu, *et al.*, Zr-MOF Combined with Nanofibers as an Efficient and Flexible Capacitive Sensor for Detecting SO_2, *ChemNanoMat*, 2021, **7**, 1117–1124.

114 M. Wang, L. Guo and D. Cao, Amino-Functionalized Luminescent Metal–Organic Framework Test Paper for Rapid and Selective Sensing of SO_2 Gas and Its Derivatives by Luminescence Turn-On Effect, *Anal. Chem.*, 2018, **90**, 3608–3614.

115 B. Chocarro-Ruiz, J. Pérez-Carvajal, C. Avci, O. Calvo-Lozano, M. I. Alonso and D. Maspoch, *et al.*, A CO_2 optical sensor based on self-assembled metal–organic framework nanoparticles, *J. Mater. Chem. A*, 2018, **6**, 13171–13177.

116 S. Yang, J. Sun, L. Xu, Q. Zhou, X. Chen and S. Zhu, *et al.*, Au@ZnO functionalized three–dimensional macroporous WO_3: a application of selective H_2S gas sensor for exhaled breath biomarker detection, *Sens. Actuators, B*, 2020, **324**, 128725.

117 J. Tan, S. Hussain, C. Ge, M. Wang, S. Shah and G. Liu, *et al.*, ZIF-67 MOF-derived unique double-shelled Co_3O_4/$NiCo_2O_4$ nanocages for superior Gas-sensing performances, *Sens. Actuators, B*, 2020, **303**, 127251.

118 S. Hussain, J. N. Okai Amu-Darko, M. Wang, A. A. Alothman, M. Ouladsmane and S. A. Aldossari, *et al.*, CuO-decorated MOF derived ZnO polyhedral nanostructures for exceptional H_2S gas detection, *Chemosphere*, 2023, **317**, 137827.

119 X. Wu, S. Xiong, Y. Gong, Y. Gong, W. Wu and Z. Mao, *et al.*, MOF-SMO hybrids as a H_2S sensor with superior sensitivity and selectivity, *Sens. Actuators, B*, 2019, **292**, 32–39.

120 Z. Li, Y. Zhang, H. Zhang, Y. Jiang and J. Yi, Superior NO_2 Sensing of MOF-Derived Indium-Doped ZnO Porous Hollow Cages, *ACS Appl. Mater. Interfaces*, 2020, **12**, 37489–37498.

121 S. Li, L. Xie, M. He, X. Hu, G. Luo and C. Chen, *et al.*, Metal–Organic frameworks-derived bamboo-like CuO/In_2O_3 Heterostructure for high-performance H_2S gas sensor with Low operating temperature, *Sens. Actuators, B*, 2020, **310**, 127828.

122 S. J. Choi, H. J. Choi, W. T. Koo, D. Huh, H. Lee and I. D. Kim, Metal–Organic Framework-Templated PdO–Co_3O_4 Nanocubes Functionalized by SWCNTs: Improved NO_2 Reaction Kinetics on Flexible Heating Film, *ACS Appl. Mater. Interfaces*, 2017, **9**, 40593–40603.

123 X. Zhou, X. Lin, S. Yang, S. Zhu, X. Chen and B. Dong, *et al.*, Highly dispersed Metal–Organic-Framework-Derived Pt nanoparticles on three-dimensional macroporous ZnO for trace-level H_2S sensing, *Sens. Actuators, B*, 2020, **309**, 127802.

124 Z. Yang, D. Zhang and H. Chen, MOF-derived indium oxide hollow microtubes/MoS_2 nanoparticles for NO_2 gas sensing, *Sens. Actuators, B*, 2019, **300**, 127037.

125 S. G. Surya, S. Bhanoth, S. M. Majhi, Y. D. More, V. M. Teja and K. N. Chappanda, A silver nanoparticle-anchored UiO-66(Zr) metal–organic framework (MOF)-based capacitive H_2S gas sensor, *CrystEngComm*, 2019, **21**, 7303–7312.

126 W. Zhou, Z. Xue, Q. Liu, Y. Li, J. Hu and G. Li, Trimetallic MOF-74 Films Grown on Ni Foam as Bifunctional Electrocatalysts for Overall Water Splitting, *ChemSusChem*, 2020, **13**, 5647–5653.

127 W.-D. Zhang, H. Yu, T. Li, Q.-T. Hu, Y. Gong and D.-Y. Zhang, *et al.*, Hierarchical trimetallic layered double hydroxide nanosheets derived from 2D metal–organic frameworks for enhanced oxygen evolution reaction, *Appl. Catal., B*, 2020, **264**, 118532.

128 M. Zhang, W. Xu, T. Li, H. Zhu and Y. Zheng, In Situ Growth of Tetrametallic FeCoMnNi-MOF-74 on Nickel Foam as Efficient Bifunctional Electrocatalysts for the Evolution Reaction of Oxygen and Hydrogen, *Inorg. Chem.*, 2020, **59**, 15467–15477.

129 D. Yang, Y. Chen, Z. Su, X. Zhang, W. Zhang and K. Srinivas, Organic carboxylate-based MOFs and

derivatives for electrocatalytic water oxidation, *Coord. Chem. Rev.*, 2021, **428**, 213619.

130 D. Senthil Raja, C.-L. Huang, Y.-A. Chen, Y. Choi and S.-Y. Lu, Composition-balanced trimetallic MOFs as ultra-efficient electrocatalysts for oxygen evolution reaction at high current densities, *Appl. Catal., B*, 2020, **279**, 119375.

131 S. Ren, X. Duan, F. Ge, M. Zhang and H. Zheng, Trimetal-based N-doped carbon nanotubes arrays on Ni foams as self-supported electrodes for hydrogen/oxygen evolution reactions and water splitting, *J. Power Sources*, 2020, **480**, 228866.

132 N. Raza, T. Kumar, V. Singh and K.-H. Kim, Recent advances in bimetallic metal–organic framework as a potential candidate for supercapacitor electrode material, *Coord. Chem. Rev.*, 2021, **430**, 213660.

133 X. Liu, L. Zhang and J. Wang, Design strategies for MOF-derived porous functional materials: preserving surfaces and nurturing pores, *J. Materiomics*, 2021, **7**, 440–459.

134 S. Kim and A. Muthurasu, Metal–organic framework–assisted bimetallic Ni@Cu microsphere for enzyme-free electrochemical sensing of glucose, *J. Electroanal. Chem.*, 2020, **873**, 114356.

135 M. Ding, J. Chen, M. Jiang, X. Zhang and G. Wang, Ultrathin trimetallic metal–organic framework nanosheets for highly efficient oxygen evolution reaction, *J. Mater. Chem. A*, 2019, **7**, 14163–14168.

136 C.-C. Cheng, P.-Y. Cheng, C.-L. Huang, D. Senthil Raja, Y.-J. Wu and S.-Y. Lu, Gold nanocrystal decorated trimetallic metal organic frameworks as high performance electrocatalysts for oxygen evolution reaction, *Appl. Catal., B*, 2021, **286**, 119916.

137 N. K. Chaudhari, H. Jin, B. Kim and K. Lee, Nanostructured materials on 3D nickel foam as electrocatalysts for water splitting, *Nanoscale*, 2017, **9**, 12231–12247.

138 C. Castillo-Blas, N. Lopez-Salas, M. C. Gutierrez, I. Puente-Orench, E. Gutierrez-Puebla and M. L. Ferrer, *et al.*, Encoding Metal-Cation Arrangements in Metal–Organic Frameworks for Programming the Composition of Electrocatalytically Active Multimetal Oxides, *J. Am. Chem. Soc.*, 2019, **141**, 1766–1774.

139 M. Amirzehni, J. Hassanzadeh and B. Vahid, Surface imprinted CoZn-bimetalic MOFs as selective colorimetric probe: application for detection of dimethoate, *Sens. Actuators, B*, 2020, **325**, 128768.

140 L. Deng, R. Shu and J. Zhang, Fabrication of ultralight nitrogen-doped reduced graphene oxide/nickel ferrite composite foams with three-dimensional porous network structure as ultrathin and high-performance microwave absorbers, *J. Colloid Interface Sci.*, 2022, **614**, 110–119.

141 W. Chu, K. Wang, H. Li, Y. Chen and H. Liu, Harvesting yolk–shell nanocomposites from Fe-MIL-101 self-template in NaCl/KCl molten salt environment for high-performance microwave absorber, *Chem. Eng. J.*, 2022, **430**, 133112.

142 H. Cheng, Y. Pan, X. Wang, C. Liu, C. Shen and D. W. Schubert, *et al.*, Ni Flower/MXene-Melamine Foam Derived 3D Magnetic/Conductive Networks for Ultra-Efficient Microwave Absorption and Infrared Stealth, *Nano-micro Lett.*, 2022, **14**, 63.

143 Z. Cai, L. Su, H. Wang, M. Niu, L. Tao and D. Lu, *et al.*, Alternating Multilayered Si_3N_4/SiC Aerogels for Broadband and High-Temperature Electromagnetic Wave Absorption up to 1000 degrees C, *ACS Appl. Mater. Interfaces*, 2021, **13**, 16704–16712.

144 B. Wen, H. Yang, Y. Lin, Y. Qiu, Y. Cheng and L. Jin, Novel bimetallic MOF derived hierarchical Co@C composites modified with carbon nanotubes and its excellent electromagnetic wave absorption properties, *J. Colloid Interface Sci.*, 2022, **605**, 657–666.

145 B.-Y. Zhu, P. Miao, J. Kong, X.-L. Zhang, G.-Y. Wang and K.-J. Chen, Co/C Composite Derived from a Newly Constructed Metal–Organic Framework for Effective Microwave Absorption, *Cryst. Growth Des.*, 2019, **19**, 1518–1524.

146 K. Yang, G. Song, Y. Li, Q. An, S. Zhai and Z. Xiao, Transforming *in situ* grown chitosan/ZIF-67 aerogels into 3D N-doped Co/CoO/carbon composites for improved electromagnetic wave absorption, *J. Alloys Compd.*, 2023, **936**, 168195.

147 H. Wang, L. Xiang, W. Wei, J. An, J. He and C. Gong, *et al.*, Efficient and Lightweight Electromagnetic Wave Absorber Derived from Metal Organic Framework-Encapsulated Cobalt Nanoparticles, *ACS Appl. Mater. Interfaces*, 2017, **9**, 42102–42110.

148 R. Qiang, Y. Du, D. Chen, W. Ma, Y. Wang and P. Xu, *et al.*, Electromagnetic functionalized Co/C composites by in situ pyrolysis of metal–organic frameworks (ZIF-67), *J. Alloys Compd.*, 2016, **681**, 384–393.

149 Q. Li, J. Tan, Z. Wu, L. Wang, W. You and L. Wu, *et al.*, Hierarchical magnetic-dielectric synergistic Co/CoO/RGO microspheres with excellent microwave absorption performance covering the whole X band, *Carbon*, 2023, **201**, 150–160.

150 W. Liu, Q. Shao, G. Ji, X. Liang, Y. Cheng and B. Quan, *et al.*, Metal–organic-frameworks derived porous carbon-wrapped Ni composites with optimized impedance matching as excellent lightweight electromagnetic wave absorber, *Chem. Eng. J.*, 2017, **313**, 734–744.

151 Y. Qiu, Y. Lin, H. Yang, L. Wang, M. Wang and B. Wen, Hollow Ni/C microspheres derived from Ni-metal organic framework for electromagnetic wave absorption, *Chem. Eng. J.*, 2020, **383**, 123207.

152 Z. Zhang, Q. Zhu, X. Chen, Z. Wu, Y. He and Y. Lv, *et al.*, Ni@C composites derived from Ni-based metal organic frameworks with a lightweight, ultrathin, broadband and highly efficient microwave absorbing properties, *Appl. Phys. Express*, 2018, **12**, 011001.

153 X. Zhao, M. Bei, F. Liu, F. Bu, X. Jiang and L. Yu, Solvent-conditioned Ni-MOF-derived flower-like porous carbon composites for electromagnetic wave absorption, *Synth. Met.*, 2023, **293**, 117294.

154 Z. Yang, Y. Zhang, M. Li, L. Yang, J. Liu and Y. Hou, *et al.*, Surface Architecture of Ni-Based Metal Organic Framework

Hollow Spheres for Adjustable Microwave Absorption, *ACS Appl. Nano Mater.*, 2019, **2**, 7888–7897.

155 R. Yang, J. Yuan, C. Yu, K. Yan, Y. Fu and H. Xie, *et al.*, Efficient electromagnetic wave absorption by SiC/Ni/NiO/C nanocomposites, *J. Alloys Compd.*, 2020, **816**, 152519.

156 J. Yan, Y. Huang, Y. Yan, L. Ding and P. Liu, High-Performance Electromagnetic Wave Absorbers Based on Two Kinds of Nickel-Based MOF-Derived Ni@C Microspheres, *ACS Appl. Mater. Interfaces*, 2019, **11**, 40781–40792.

157 X. Liang, B. Quan, Y. Sun, G. Ji, Y. Zhang and J. Ma, *et al.*, Multiple Interfaces Structure Derived from Metal–Organic Frameworks for Excellent Electromagnetic Wave Absorption, *Part. Part. Syst. Charact.*, 2017, **34**, 1700006.

158 K. Cao, X. Yang, R. Zhao and W. Xue, Fabrication of an Ultralight Ni-MOF-rGO Aerogel with Both Dielectric and Magnetic Performances for Enhanced Microwave Absorption: Microspheres with Hollow Structure Grow onto the GO Nanosheets, *ACS Appl. Mater. Interfaces*, 2023, **15**, 9685–9696.

159 R. Qiang, Y. Du, H. Zhao, Y. Wang, C. Tian and Z. Li, *et al.*, Metal organic framework-derived Fe/C nanocubes toward efficient microwave absorption, *J. Mater. Chem. A*, 2015, **3**, 13426–13434.

160 S. Peng, S. Wang, G. Hao, C. Zhu, Y. Zhang and X. Lv, *et al.*, Preparation of magnetic flower-like carbon-matrix composites with efficient electromagnetic wave absorption properties by carbonization of MIL-101(Fe), *J. Magn. Magn. Mater.*, 2019, **487**, 165306.

161 Z. Li, J. Zhou, B. Wei, C. Zhou, M. Wang and Z. Chen, *et al.*, Fe/Fe_3C@ N-doped carbon composite materials derived from MOF with improved framework stability for strong microwave absorption, *Synth. Met.*, 2023, **293**, 117272.

162 M. Ma, Y. Bi, Z. Jiao, J. Yue, Z. Liao and Y. Wang, *et al.*, Facile fabrication of metal–organic framework derived Fe/Fe_3O_4/FeN/N-doped carbon composites coated with PPy for superior microwave absorption, *J. Colloid Interface Sci.*, 2022, **608**, 525–535.

163 Y. Yang, D. Xu, L. Lyu, F. Wang, Z. Wang and L. Wu, *et al.*, Synthesis of MOF-derived Fe_7S_8/C rod-like composites by controlled proportion of carbon for highly efficient electromagnetic wave absorption, *Composites, Part A*, 2021, **142**, 106246.

164 Z. Xiang, Y. Song, J. Xiong, Z. Pan, X. Wang and L. Liu, *et al.*, Enhanced electromagnetic wave absorption of nanoporous Fe_3O_4@carbon composites derived from metal–organic frameworks, *Carbon*, 2019, **142**, 20–31.

165 Y. Wang, W. Zhang, X. Wu, C. Luo, Q. Wang and J. Li, *et al.*, Conducting polymer coated metal–organic framework nanoparticles: facile synthesis and enhanced electromagnetic absorption properties, *Synth. Met.*, 2017, **228**, 18–24.

166 Y.-R. Li, Y.-M. Li, B.-B. Chen, W.-J. Hu and D.-Y. Wang, Highly efficient electromagnetic wave absorption Fe-MOF-rGO based composites with enhanced flame retardancy, *J. Alloys Compd.*, 2022, **918**, 165516.

167 X. Li, E. Cui, Z. Xiang, L. Yu, J. Xiong and F. Pan, *et al.*, Fe@NPC@CF nanocomposites derived from Fe-MOFs/biomass cotton for lightweight and high-performance electromagnetic wave absorption applications, *J. Alloys Compd.*, 2020, **819**, 152952.

168 Y. Cui, J. Ge, T. Ma, L. Liu, P. Ju and F. Meng, *et al.*, Enhanced electromagnetic wave absorption of Fe_3O_4@C derived from spindle-like MOF, *Mater. Lett.*, 2022, **316**, 132060.

169 H. Yang, Z. Shen, H. Peng, Z. Xiong, C. Liu and Y. Xie, 1D-3D mixed-dimensional MnO_2@nanoporous carbon composites derived from Mn-metal organic framework with full-band ultra-strong microwave absorption response, *Chem. Eng. J.*, 2021, **417**, 128087.

170 X. Zhang, J. Qiao, C. Liu, F. Wang, Y. Jiang and P. Cui, *et al.*, A MOF-derived ZrO_2/C nanocomposite for efficient electromagnetic wave absorption, *Inorg. Chem. Front.*, 2020, **7**, 385–393.

171 Z. Yu, R. Zhou, M. Ma, R. Zhu, P. Miao and P. Liu, *et al.*, ZnO/nitrogen-doped carbon nanocomplex with controlled morphology for highly efficient electromagnetic wave absorption, *J. Mater. Sci. Technol.*, 2022, **114**, 206–214.

172 H. Qiu, X. Zhu, P. Chen, Y. Chen, G. Chen and W. Min, Construction of core-shell structured ZnO/C@PPy composite as high-performance dielectric electromagnetic wave absorber, *J. Magn. Magn. Mater.*, 2022, **543**, 168604.

173 J. Ma, X. Zhang, W. Liu and G. Ji, Direct synthesis of MOF-derived nanoporous CuO/carbon composites for high impedance matching and advanced microwave absorption, *J. Mater. Chem. C*, 2016, **4**, 11419–11426.

174 W. Li, J. Chen and P. Gao, MOFs-derived hollow Copper-based sulfides for optimized electromagnetic behaviors, *J. Colloid Interface Sci.*, 2022, **606**, 719–727.

175 J. Ma, W. Liu, X. Liang, B. Quan, Y. Cheng and G. Ji, *et al.*, Nanoporous TiO_2/C composites synthesized from directly pyrolysis of a Ti-based MOFs MIL-125(Ti) for efficient microwave absorption, *J. Alloys Compd.*, 2017, **728**, 138–144.

176 L. Wang, M. Huang, X. Qian, L. Liu, W. You and J. Zhang, *et al.*, Confined Magnetic-Dielectric Balance Boosted Electromagnetic Wave Absorption, *Small*, 2021, **17**, 2100970.

177 X. Zhang, Z. Wang, L. Xu, K. Zuraiqi, T. Daeneke and Z. Yao, *et al.*, Liquid metal derived MOF functionalized nanoarrays with ultra-wideband electromagnetic absorption, *J. Colloid Interface Sci.*, 2022, **606**, 1852–1865.

178 X. Zhang, X. Tian, C. Liu, J. Qiao, W. Liu and J. Liu, *et al.*, MnCo-MOF-74 derived porous MnO/Co/C heterogeneous nanocomposites for high-efficiency electromagnetic wave absorption, *Carbon*, 2022, **194**, 257–266.

179 X. Zhang, J. Qiao, J. Zhao, D. Xu, F. Wang and C. Liu, *et al.*, High-efficiency electromagnetic wave absorption of cobalt-decorated NH_2-UIO-66-derived porous ZrO_2/C, *ACS Appl. Mater. Interfaces*, 2019, **11**, 35959–35968.

180 L. Huang, C. Chen, X. Huang, S. Ruan and Y.-J. Zeng, Enhanced electromagnetic absorbing performance of MOF-derived Ni/NiO/Cu@C composites, *Composites, Part B*, 2019, **164**, 583–589.

181 J. Qiao, X. Zhang, C. Liu, L. Lyu, Y. Yang and Z. Wang, *et al.*, Non-Magnetic Bimetallic MOF-Derived Porous

Carbon-Wrapped $TiO_2/ZrTiO_4$ Composites for Efficient Electromagnetic Wave Absorption, *Nanomicro Lett.*, 2021, **13**, 75.

182 W. Jinxiao, Y. Jianfeng, Y. Jun and Z. Hui, An Ni–Co bimetallic MOF-derived hierarchical CNT/CoO/Ni_2O_3 composite for electromagnetic wave absorption, *J. Alloys Compd.*, 2021, **876**, 160126.

183 Z. Jia, X. Zhang, Z. Gu and G. Wu, MOF-derived Ni-Co bimetal/porous carbon composites as electromagnetic wave absorber, *Adv. Compos. Hybrid Mater.*, 2022, **6**, 28.

184 J. Ge, S. Liu, L. Liu, Y. Cui, F. Meng and Y. Li, *et al.*, Optimizing the electromagnetic wave absorption performance of designed hollow $CoFe_2O_4$/CoFe@C microspheres, *J. Mater. Sci. Technol.*, 2021, **81**, 190–202.

185 H. Zhao, Q. Wang, H. Ma, Y. Zhao, L. Li and P. Li, *et al.*, Hollow spherical NiFe-MOF derivative and N-doped rGO composites towards the tunable wideband electromagnetic wave absorption: Experimental and theoretical study, *Carbon*, 2023, **201**, 347–361.

186 D. Ding, Y. Wang, X. Li, R. Qiang, P. Xu and W. Chu, *et al.*, Rational design of core-shell Co@C microspheres for high-performance microwave absorption, *Carbon*, 2017, **111**, 722–732.

187 W. Xue, G. Yang, S. Bi, J. Zhang and Z.-L. Hou, Construction of caterpillar-like hierarchically structured Co/MnO/CNTs derived from MnO_2/ZIF-8@ZIF-67 for electromagnetic wave absorption, *Carbon*, 2021, **173**, 521–527.

188 F. Long, L. Wang, S. U. Rehman, J. Zhang, S. Shen and B. Peng, *et al.*, Double shell structured $MnFe_2O_4$ @FeO/C derived from $MnFe_2O_4$@ZIF-8 for electromagnetic wave absorption, *J. Alloys Compd.*, 2022, **906**, 164197.

189 L. Sun, Z. Jia, S. Xu, M. Ling, D. Hu and X. Liu, *et al.*, Synthesis of $NiCo_{2-0.5x}Cr_2O_3$@C nanoparticles based on hydroxide with the heterogeneous interface for excellent electromagnetic wave absorption properties, *Compos. Commun.*, 2022, **29**, 100993.

190 X. Yang, W. Gao, J. Chen, X. Lu, D. Yang and Y. Kang, *et al.*, Co–Ni Electromagnetic Coupling in Hollow Mo_2C/NC Sphere for Enhancing Electromagnetic Wave Absorbing Performance, *Chin. J. Chem.*, 2022, **41**, 64–74.

191 H.-Y. Wang, X.-B. Sun and G.-S. Wang, A MXene-modulated 3D crosslinking network of hierarchical flower-like MOF derivatives towards ultra-efficient microwave absorption properties, *J. Mater. Chem. A*, 2021, **9**, 24571–24581.

192 P. Li, Y. Zhao, Y. Zhao, J. Yan, H. Zhao and W. Zhao, *et al.*, Trimetallic Prussian blue analogue derived FeCo/FeCo-Ni@NPC composites for highly efficient microwave absorption, *Composites, Part B*, 2022, **246**, 110268.

193 Y. Bi, M. Ma, Y. Liu, Z. Tong, R. Wang and K. L. Chung, *et al.*, Microwave absorption enhancement of 2-dimensional CoZn/C@MoS_2@PPy composites derived from metal–organic framework, *J. Colloid Interface Sci.*, 2021, **600**, 209–218.

194 J. Luo, S. Wang, S. Peng, T. Zhang, G. Hao and L. Xiao, *et al.*, High-performance electromagnetic wave absorbers based on Fe-based MOFs-derived Fe/C composites, *Synth. Met.*, 2021, **272**, 116663.

195 S. Peng, S. Wang, G. Hao, C. Zhu, Y. Zhang and X. Lv, *et al.*, Preparation of magnetic flower-like carbon-matrix composites with efficient electromagnetic wave absorption properties by carbonization of MIL-101(Fe), *J. Magn. Magn. Mater.*, 2019, **487**, 165306.

196 Z. Li, J. Zhou, B. Wei, C. Zhou, M. Wang and Z. Chen, *et al.*, Fe/Fe_3C@N-doped carbon composite materials derived from MOF with improved framework stability for strong microwave absorption, *Synth. Met.*, 2023, **293**, 117272.

197 Y. Liu, X. Zhou, Z. Jia, H. Wu and G. Wu, Oxygen Vacancy-Induced Dielectric Polarization Prevails in the Electromagnetic Wave-Absorbing Mechanism for Mn-Based MOFs-Derived Composites, *Adv. Funct. Mater.*, 2022, **32**, 2204499.

198 F. D. Owa, Water Pollution: Sources, Effects, Control and Management, *Mediterranean J. Soc. Sci.*, 2014, **3**, 1–6.

199 A. Karataş and E. Karataş, Environmental education as a solution tool for the prevention of water pollution, *J. Survey Fisheries Sci.*, 2016, **3**, 61–70.

200 L. J. J. E. S. Puckett, Technology. Identifying the major sources of nutrient water pollution, *Environ. Sci. Technol.*, 1995, **29**, 408A–414AA.

201 F. N. Chaudhry and M. F. Malik, Factors affecting water pollution: a review, *J. Ecosyst. Ecography*, 2017, **7**, 225–231.

202 B. Moss, Water pollution by agriculture, *Philos. Trans. R. Soc., B*, 2008, **363**, 659–666.

203 P. Sharma, J. Kherb, J. Prakash and R. Kaushal, A novel and facile green synthesis of SiO_2 nanoparticles for removal of toxic water pollutants, *Appl. Nanosci.*, 2021, **13**, 735–747.

204 S. Rawat and J. Singh, Fenton like oxidative degradation of toxic water pollutants by iron nanoparticles synthesized via facile green route using waste iron rust as the iron precursor, *Environ. Eng. Res.*, 2022, **28**, 210621.

205 M. Haseena, M. F. Malik, A. Javed, S. Arshad, N. Asif and S. Zulfiqar, *et al.*, Water pollution and human health. Environmental Risk Assessment and Remediation. Environmental risk assessment and remediation, *Environ. Risk Assess. Rem.*, 2017, **1**, 16–19.

206 H. Daglar, C. Altintas, I. Erucar, G. Heidari, E. N. Zare and O. Moradi, *et al.*, Metal–organic framework-based materials for the abatement of air pollution and decontamination of wastewater, *Chemosphere*, 2022, **303**, 135082.

207 R. Rao, S. Ma, B. Gao, F. Bi, Y. Chen and Y. Yang, *et al.*, Recent advances of metal–organic framework-based and derivative materials in the heterogeneous catalytic removal of volatile organic compounds, *J. Colloid Interface Sci.*, 2023, **636**, 55–72.

208 J. Schneider, M. Matsuoka, M. Takeuchi, J. Zhang, Y. Horiuchi and M. Anpo, *et al.*, Understanding TiO_2 photocatalysis: mechanisms and materials, *Chem. Rev.*, 2014, **114**, 9919–9986.

209 D. Xu, Y. Huang, Q. Ma, J. Qiao, X. Guo and Y. Wu, A 3D porous structured cellulose nanofibrils-based hydrogel with carbon dots-enhanced synergetic effects of adsorption

and photocatalysis for effective Cr(VI) removal, *Chem. Eng. J.*, 2023, **456**, 141104.

210 J. Kim, X. Sun, B. A. van der Worp and T. Ritter, Anti-Markovnikov hydrochlorination and hydronitrooxylation of α-olefins via visible-light photocatalysis, *Nat. Catal.*, 2023, **6**, 196–203.

211 M. Jing, H. Zhao, L. Jian, C. Pan, Y. Dong and Y. Zhu, Coral-like B-doped g-C_3N_4 with enhanced molecular dipole to boost photocatalysis-self-Fenton removal of persistent organic pollutants, *J. Hazard. Mater.*, 2023, **449**, 131017.

212 R. Ham, C. J. Nielsen, S. Pullen and J. N. H. Reek, Supramolecular Coordination Cages for Artificial Photosynthesis and Synthetic Photocatalysis, *Chem. Rev.*, 2023, **123**, 5225–5261.

213 Y.-N. Gong, X. Guan and H.-L. Jiang, Covalent organic frameworks for photocatalysis: Synthesis, structural features, fundamentals and performance, *Coord. Chem. Rev.*, 2023, **475**, 214889.

214 W. An, H. Wang, T. Yang, J. Xu, Y. Wang and D. Liu, *et al.*, Enriched photocatalysis-Fenton synergistic degradation of organic pollutants and coking wastewater via surface oxygen vacancies over Fe-BiOBr composites, *Chem. Eng. J.*, 2023, **451**, 138653.

215 H. Furukawa, N. Ko, Y. B. Go, N. Aratani, S. B. Choi and E. Choi, *et al.*, Ultrahigh porosity in metal–organic frameworks, *Science*, 2010, **329**, 424–428.

216 J. D. Xiao and H. L. Jiang, Metal–Organic Frameworks for Photocatalysis and Photothermal Catalysis, *Acc. Chem. Res.*, 2019, **52**, 356–366.

217 S. G. Khasevani and M. R. Gholami, Synthesis of BiOI/$ZnFe_2O_4$–Metal–Organic Framework and g-C_3N_4-Based Nanocomposites for Applications in Photocatalysis, *Ind. Eng. Chem. Res.*, 2019, **58**, 9806–9818.

218 M. Zhang, L. Wang, T. Zeng, Q. Shang, H. Zhou and Z. Pan, *et al.*, Two pure MOF-photocatalysts readily prepared for the degradation of methylene blue dye under visible light, *Dalton Trans.*, 2018, **47**, 4251–4258.

219 J. Xue, M. Xu, J. Gao, Y. Zong, M. Wang and S. Ma, Multifunctional porphyrinic Zr-MOF composite membrane for high-performance oil-in-water separation and organic dye adsorption/photocatalysis, *Colloids Surf., A*, 2021, **628**, 127288.

220 Q. Xia, X. Yu, H. Zhao, S. Wang, H. Wang and Z. Guo, *et al.*, Syntheses of Novel Lanthanide Metal–Organic Frameworks for Highly Efficient Visible-Light-Driven Dye Degradation, *Cryst. Growth Des.*, 2017, **17**, 4189–4195.

221 Z. Wang, M. He, H. Jiang, H. He, J. Qi and J. Ma, Photocatalytic MOF membranes with two-dimensional heterostructure for the enhanced removal of agricultural pollutants in water, *Chem. Eng. J.*, 2022, **435**, 133870.

222 C. Shi, X. Zhou, D. Liu, L. Li, M. Xu and H. Sakiyama, *et al.*, A new 3D high connection Cu-based MOF introducing a flexible tetracarboxylic acid linker: Photocatalytic dye degradation, *Polyhedron*, 2021, **208**, 115441.

223 S. A. Jasim, H. I. M. Amin, A. Rajabizadeh, M. A. L. Nobre, F. Borhani and A. T. Jalil, *et al.*, Synthesis characterization of Zn-based MOF and their application in degradation of water contaminants, *Water Sci. Technol.*, 2022, **86**, 2303–2335.

224 J. Huang, D. Huang, F. Zeng, L. Ma and Z. Wang, Photocatalytic MOF fibrous membranes for cyclic adsorption and degradation of dyes, *J. Mater. Sci.*, 2020, **56**, 3127–3139.

225 X. Guo, D. Yin, K. K. Khaing, J. Wang, Z. Luo and Y. Zhang, Construction of MOF/COF Hybrids for Boosting Sunlight-Induced Fenton-like Photocatalytic Removal of Organic Pollutants, *Inorg. Chem.*, 2021, **60**, 15557–15568.

226 J. J. Du, Y. P. Yuan, J. X. Sun, F. M. Peng, X. Jiang and L. G. Qiu, *et al.*, New photocatalysts based on MIL-53 metal–organic frameworks for the decolorization of methylene blue dye, *J. Hazard. Mater.*, 2011, **190**, 945–951.

227 P. Mahata, G. Madras and S. Natarajan, Novel Photocatalysts for the Decomposition of Organic Dyes Based on Metal–Organic Framework Compounds, *J. Phys. Chem. B*, 2006, **110**, 13759–13768.

228 M. S. Hosseini, A. Abbasi and M. Masteri-Farahani, Improving the photocatalytic activity of NH_2-UiO-66 by facile modification with $Fe(acac)_3$ complex for photocatalytic water remediation under visible light illumination, *J. Hazard. Mater.*, 2022, **425**, 127975.

229 N. Kitchamsetti, D. Narsimulu, A. Chinthakuntla, C. Shilpa Chakra and A. L. F. de Barros, Bimetallic MOF derived $ZnCo_2O_4$ nanocages as a novel class of high performance photocatalyst for the removal of organic pollutants, *Inorg. Chem. Commun.*, 2022, **144**, 109946.

230 L. Yue, Y. Cao, Y. Han, Z. Li, X. Luo and Y. Liu, Preparation of core-shell structured Fe_3O_4@Sn-MOF composite and photocatalytic performance, *J. Alloys Compd.*, 2021, **870**, 159339.

231 S.-W. Lv, J.-M. Liu, N. Zhao, C.-Y. Li, F.-E. Yang and Z.-H. Wang, *et al.*, MOF-derived $CoFe_2O_4/Fe_2O_3$ embedded in g-C_3N_4 as high-efficient Z-scheme photocatalysts for enhanced degradation of emerging organic pollutants in the presence of persulfate, *Sep. Purif. Technol.*, 2020, **253**, 117413.

232 S.-W. Lv, J.-M. Liu, N. Zhao, C.-Y. Li, Z.-H. Wang and S. Wang, A novel cobalt doped MOF-based photocatalyst with great applicability as an efficient mediator of peroxydisulfate activation for enhanced degradation of organic pollutants, *New J. Chem.*, 2020, **44**, 1245–1252.

233 S. Hariganesh, S. Vadivel, D. Maruthamani, M. Kumaravel, B. Paul and N. Balasubramanian, *et al.*, Facile large scale synthesis of $CuCr_2O_4$/CuO nanocomposite using MOF route for photocatalytic degradation of methylene blue and tetracycline under visible light, *Appl. Organomet. Chem.*, 2020, **34**, 5365.

234 Y. Chen, B. Zhai, Y. Liang and Y. Li, Hybrid photocatalysts using semiconductor/MOF/graphene oxide for superior photodegradation of organic pollutants under visible light, *Mater. Sci. Semicond. Process.*, 2020, **107**, 104838.

235 A. Chatterjee, A. K. Jana and J. K. Basu, A binary MOF of iron and copper for treating ciprofloxacin-contaminated

waste water by an integrated technique of adsorption and photocatalytic degradation, *New J. Chem.*, 2021, **45**, 17196–17210.

236 B. Sarwar, A. Khan, T. Fazal, M. Aslam, N. Qaisrani and A. Ahmed, Synthesis of Novel MOF-5 Based $BiCoO_3$ Photocatalyst for the Treatment of Textile Wastewater, *Sustainability*, 2022, **14**, 12885.

237 N. Khosroshahi, M. Bakhtian and V. Safarifard, Mechanochemical synthesis of ferrite/MOF nanocomposite: Efficient photocatalyst for the removal of meropenem and hexavalent chromium from water, *J. Photochem. Photobiol., A*, 2022, **431**, 114033.

238 V. Ramasubbu, P. Ram Kumar, T. Chellapandi, G. Madhumitha, E. M. Mothi and X. S. Shajan, Zn(II) porphyrin sensitized (TiO_2@Cd-MOF) nanocomposite aerogel as novel photocatalyst for the effective degradation of methyl orange (MO) dye, *Opt. Mater.*, 2022, **132**, 112558.

239 Y. Si, Y. Li, J. Zou, X. Xiong, X. Zeng and J. Zhou, Photocatalytic Performance of a Novel MOF/$BiFeO_3$ Composite, *Materials*, 2017, **10**, 1161.

240 H. Ramezanalizadeh and F. Manteghi, Synthesis of a novel MOF/$CuWO_4$ heterostructure for efficient photocatalytic degradation and removal of water pollutants, *J. Cleaner Prod.*, 2018, **172**, 2655–2666.

241 B. Yu, F. Wang, W. Dong, J. Hou, P. Lu and J. Gong, Self-template synthesis of core–shell ZnO@ZIF-8 nanospheres and the photocatalysis under UV irradiation, *Mater. Lett.*, 2015, **156**, 50–53.

242 C.-F. Zhang, L.-G. Qiu, F. Ke, Y.-J. Zhu, Y.-P. Yuan and G.-S. Xu, *et al.*, A novel magnetic recyclable photocatalyst based on a core–shell metal–organic framework Fe_3O_4@MIL-100(Fe) for the decolorization of methylene blue dye, *J. Mater. Chem. A*, 2013, **1**, 14329–14334.

243 Z. Zhang, X. Li, B. Liu, Q. Zhao and G. Chen, Hexagonal microspindle of NH2-MIL-101(Fe) metal–organic frameworks with visible-light-induced photocatalytic activity for the degradation of toluene, *RSC Adv.*, 2016, **6**, 4289–4295.

244 H. Q. Xu, J. Hu, D. Wang, Z. Li, Q. Zhang and Y. Luo, *et al.*, Visible-Light Photoreduction of CO_2 in a Metal–Organic Framework: Boosting Electron-Hole Separation via Electron Trap States, *J. Am. Chem. Soc.*, 2015, **137**, 13440–13443.

245 H. Wang, P. Rassu, X. Wang, H. Li, X. Wang and X. Wang, *et al.*, An Iron-Containing Metal–Organic Framework as a Highly Efficient Catalyst for Ozone Decomposition, *Angew. Chem., Int. Ed.*, 2018, **57**, 16416–16420.

246 Y. Liu, A. J. Howarth, J. T. Hupp and O. K. Farha, Selective Photooxidation of a Mustard-Gas Simulant Catalyzed by a Porphyrinic Metal–Organic Framework, *Angew. Chem., Int. Ed.*, 2015, **54**, 9001–9005.

247 R. Huang, Y. Peng, C. Wang, Z. Shi and W. Lin, A Rhenium-Functionalized Metal–Organic Framework as a Single-Site Catalyst for Photochemical Reduction of Carbon Dioxide, *Eur. J. Inorg. Chem.*, 2016, 4358–4362.

248 J. Mehralipour, A. Jonidi Jafari, M. Gholami, A. Esrafili and M. Kermani, Photocatalytic-proxone process application in the degradation of toluene-diisocyante, and methylene diphenyl diisocyanate from polluted air, *J. Photochem. Photobiol., A*, 2023, **438**, 114549.

249 S. M. Hosseini, H. Dehghan and V. Safarifard, Enhancement of photocatalytic aerobic oxidation of benzyl alcohol with the incorporation of cobalt in Zn-based MOF via post-synthetic metal exchange, *Polyhedron*, 2022, **212**, 115581.

250 A. Amini, M. Karimi, M. Rabbani and V. Safarifard, Cobalt-doped g-C_3N_4/MOF heterojunction composite with tunable band structures for photocatalysis aerobic oxidation of benzyl alcohol, *Polyhedron*, 2022, **216**, 115728.

251 A. Mahmoud Idris, X. Jiang, J. Tan, Z. Cai, X. Lou and J. Wang, *et al.*, Dye-Sensitized Fe-MOF nanosheets as Visible-Light driven photocatalyst for high efficient photocatalytic CO_2 reduction, *J. Colloid Interface Sci.*, 2022, **607**, 1180–1188.

252 J. Lee, J. Jang, J. Kim and S.-H. Lim, A recyclable indoor air filter system based on a photocatalytic metal–organic framework for the removal of harmful volatile organic compounds, *Chem. Eng. J.*, 2022, **430**, 132891.

253 W. Zhu, P. Liu, S. Xiao, W. Wang, D. Zhang and H. Li, Microwave-assisted synthesis of Ag-doped MOFs-like organotitanium polymer with high activity in visible-light driven photocatalytic NO oxidization, *Appl. Catal., B*, 2015, **172–173**, 46–51.

254 X. Zhang, Z. Zhu, R. Rao, J. Chen, X. Han and S. Jiang, *et al.*, Highly efficient visible-light-driven photocatalytic degradation of gaseous toluene by rutile-anatase TiO_2@MIL-101 composite with two heterojunctions, *J. Environ. Sci.*, 2022, **134**, 21–33.

255 P. Yao, H. Liu, D. Wang, J. Chen, G. Li and T. An, Enhanced visible-light photocatalytic activity to volatile organic compounds degradation and deactivation resistance mechanism of titania confined inside a metal–organic framework, *J. Colloid Interface Sci.*, 2018, **522**, 174–182.

256 H. Wang, T. Yu, X. Tan, H. Zhang, P. Li and H. Liu, *et al.*, Enhanced Photocatalytic Oxidation of Isopropanol by HKUST-1@TiO_2 Core–Shell Structure with Ultrathin Anatase Porous Shell: Toxic Intermediate Control, *Ind. Eng. Chem. Res.*, 2016, **55**, 8096–8103.

257 Q. Mu, Y. Su, Z. Wei, H. Sun, Y. Lian and Y. Dong, *et al.*, Dissecting the interfaces of MOF-coated CdS on synergized charge transfer for enhanced photocatalytic CO_2 reduction, *J. Catal.*, 2021, **397**, 128–136.

258 Y. Hu, Z. Huang, L. Zhou, D. Wang and G. Li, Synthesis of nanoscale titania embedded in MIL-101 for the adsorption and degradation of volatile pollutants with thermal desorption gas chromatography and mass spectrometry detection, *J. Sep. Sci.*, 2014, **37**, 1482–1488.

259 A. Crake, K. C. Christoforidis, A. Kafizas, S. Zafeiratos and C. Petit, CO_2 capture and photocatalytic reduction using bifunctional TiO_2 /MOF nanocomposites under UV-vis irradiation, *Appl. Catal., B*, 2017, **210**, 131–140.

260 H. Liu, X. Chang, X. Liu, G. Li, W. Zhang and T. An, Boosting the photocatalytic degradation of ethyl acetate

by a Z-scheme Au–TiO2@NH2-UiO-66 heterojunction with ultrafine Au as an electron mediator, *Environ. Sci.: Nano*, 2021, **8**, 2542–2553.

261 Y. Zhang, Q. Li, C. Liu, X. Shan, X. Chen and W. Dai, *et al.*, The promoted effect of a metal–organic frameworks (ZIF-8) on Au/TiO_2 for CO oxidation at room temperature both in dark and under visible light irradiation, *Appl. Catal., B*, 2018, **224**, 283–294.

262 J. Qin, J. Wang, J. Yang, Y. Hu, M. Fu and D. Ye, Metal organic framework derivative-TiO_2 composite as efficient and durable photocatalyst for the degradation of toluene, *Appl. Catal., B*, 2020, **267**, 118667.